General Review of Electrochemical and Corrosion Phenomena Under Conditions Associated with Supercritical Water Oxidation

by

Christopher R. Sydnor

B.S., Materials Science and Engineering
University of Pennsylvania, 1998

SUBMITTED TO THE DEPARTMENT OF MATERIALS SCIENCE AND ENGINEERING
IN PARTIAL FULFILLMENT OF THE REQUIREMENTS FOR THE DEGREE OF

MASTER OF SCIENCE IN MATERIALS SCIENCE AND ENGINEERING
AT THE
MASSACHUSETTS INSTITUTE OF TECHNOLOGY

SEPTEMBER 2002

© 2002 Massachusetts Institute of Technology
All rights reserved

Signature of Author.....
Department of Materials Science and Engineering

Certified by.....
Ronald M. Latanision
Professor of Materials Science and Engineering
Thesis Supervisor

Accepted by.....
Harry Tuller
Chairman, Committee on Graduate Students
Department of Materials Science and Engineering

SCIENCE

MASSACHUSETTS INSTITUTE OF TECHNOLOGY
OCT 1 8 2002
LIBRARIES

General Review of Electrochemical and Corrosion Phenomena Under Conditions Associated with Supercritical Water Oxidation

by

Christopher R. Sydnor

Submitted to the Department of Materials Science and Engineering
on August 30, 2002 in Partial Fulfillment of the
Requirements for the Degree of Master of Science in
Materials Science and Engineering

ABSTRACT

Supercritical Water Oxidation (SCWO) is a promising technology for destroying highly toxic organic compounds present in aqueous waste streams. Organic wastes that have been identified as possible targets for destruction by SCWO include EPA-regulated organic wastes, organic components of DOE mixed low-level radioactive wastes, and DOD chemical weapons stockpiles. SCWO capitalizes on the properties of water in the supercritical phase to affect spontaneous and rapid oxidation of hydrocarbons to form CO_2, H_2O, and, depending on the species of heteroatom present in the organic waste, one or more acids. HCl, H_2SO_4, and H_3PO_4 are the acids most frequently encountered in SCWO process streams. The formation of acids in SCWO feeds at high temperatures and pressures under highly oxidizing conditions leads to severe corrosion of the process unit for even the most corrosion resistant constructional alloys.

Currently, the existence of a constructional material that can withstand the extremely aggressive conditions present in all sections of the SCWO process stream for all candidate organic wastes is extremely unlikely. Previous attempts to identify such materials have proved unsuccessful. This has led to more fundamental research addressing physical chemistry, electrochemistry, and corrosion phenomena in aqueous systems under hydrothermal conditions. This review addresses this research as it pertains to SCWO technology, and based on these findings, discusses potential methodologies for reducing corrosion damage in SCWO systems. Currently, it appears that proper selection and/or development of construction materials in conjunction with precise control of feed stream chemistry may be a promising option for corrosion control in SCWO process environments.

Thesis Supervisor: Ronald M. Latanision
Title: Professor of Materials Science and Engineering

Contents

Acknowledgements

I would like to express my sincere gratitude to my parents, Russ and Chris, my advisor, Prof. Ronald M. Latanision, Dr. Bryce Mitton, my sister, Mary, and my brother, Phil for their generosity, support, and patience over the last year.

Chapter 1

Introduction – Corrosion in Supercritical Water Oxidation (SCWO) Systems

1.1 The Properties of Water

The properties of water change significantly as its temperature and pressure approach the critical point at 374°C and 22.1 MPa (221 bar). As the critical point is approached, density, viscosity, heat capacity, isothermal compressibility, dielectric constant, ionic dissociation constant, and solvation properties change drastically as a function of changes in either temperature or pressure. Under supercritical conditions, the density of water is approximately 100 kg m^{-3}. This density is intermediate between that of liquid water (1 g cm^{-3}) and low-pressure water vapor (<0.001 g cm^{-3}). Near the critical point, these drastic changes in the density of water correlate directly with drastic changes in its solvation properties. At 25 MPa (250 bar), the dielectric constant of water, which is a measure of its ability to shield charge, drops from approximately 80 at room temperature to 2 at 450°C, and the ionic dissociation constant decreases from 10^{-14} at room temperature to 10^{-23} at supercritical conditions. The result is that low-density supercritical water acts as a non-polar dense gas with solvation properties approaching those of a low-polarity organic. Thus, as a solvent, supercritical water exhibits high solubilities for non-polar organic compounds and non-condensable gases. For example, benzene above 300°C and 250 bar is completely miscible in water over all concentrations [1, 2]. Gases such as oxygen [3], nitrogen [4], carbon dioxide [5], and methane [6] are also completely miscible in supercritical water. Conversely, the solubility of inorganic compounds is very low in supercritical water: The solubility of NaCl in water, for example, drops from about 37 wt% at 300°C to only 120 ppm at 550°C, at a pressure of 250 bar. Figure 1-1 [7] graphically depicts the relative changes in density, organic solubility, and inorganic solubility as a function of temperature, in the vicinity of the critical point.

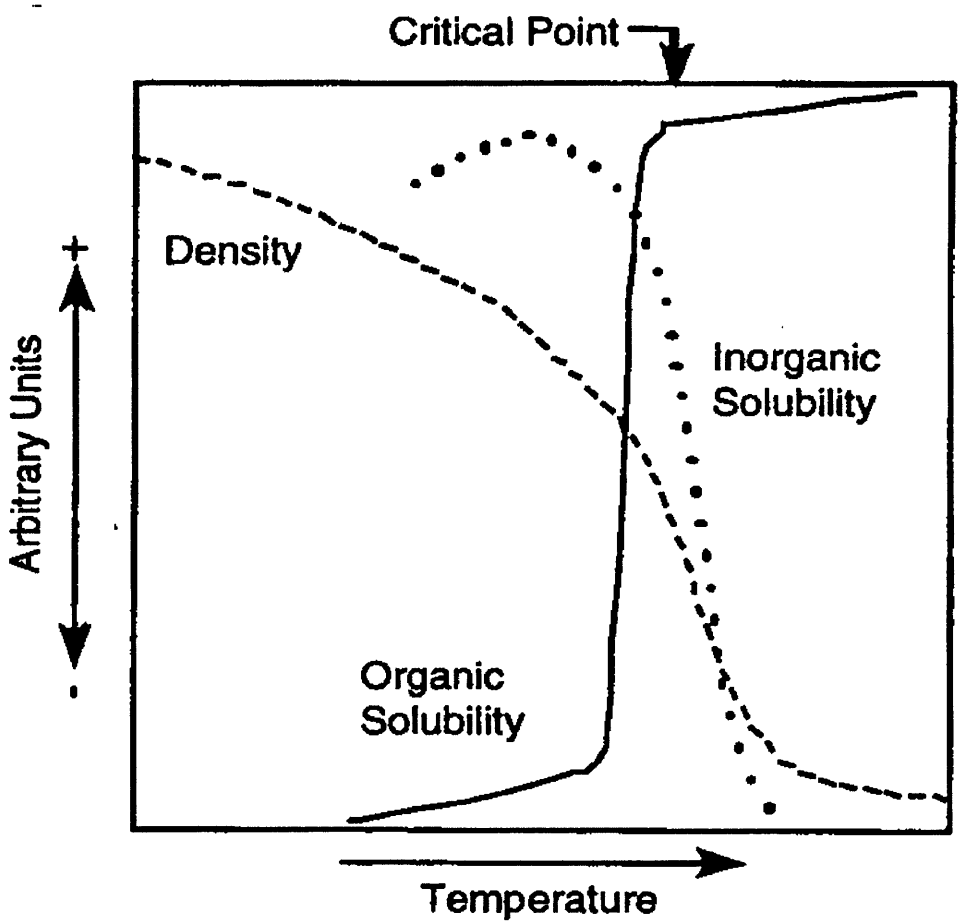

Figure 1-1: Relative changes in density, organic solubility, and inorganic solubility of water, as a function of temperature, in the vicinity of the critical point. From Mitton, *et al.* (2001), Reference [7].

This combination of solvation and physical properties make supercritical water an ideal aqueous medium for the oxidation of organics: Organic compounds and oxygen are dissolved spontaneously and rapidly in water above the critical point. The products of the spontaneous and rapid oxidation of organics (hydrocarbons) in supercritical aqueous systems are CO_2, H_2O, acids, solid inorganic salts or oxides, and thermal energy. CO_2 and H_2O are innocuous species, and are, therefore, of little concern. Acids and inorganic solids, however, present considerable engineering challenges to the widespread industrial application of technology related to the oxidation of organics in supercritical aqueous systems. This technology, known as Supercritical Water Oxidation, will be discussed in the next section.

1.2 Supercritical Water Oxidation

Over the last twenty years, supercritical water has found numerous applications as an aqueous medium for different processes, including chemical reactions, extractions, ceramic processing, analytical applications, biomass conversion, and the destruction of hazardous organic wastes. The last application, destruction of hazardous organic wastes, occurs in aqueous process streams under supercritical conditions and is the application that this review addresses. The chemical process that brings about the destruction of the organic waste is governed by oxidation reaction. Hence, the universally accepted name for the process, by which the destruction of hazardous organic waste in supercritical aqueous systems occurs, is Supercritical Water Oxidation (SCWO), and the systems used for this process are called SCWO systems. SCWO systems provide high destruction efficiencies for organics within short residence times: Typical destruction and removal efficiencies can exceed 99.999% for normal operating conditions of 250 bar and 600°C and residence times of 60 seconds or less. These efficiency levels meet requirements for the destruction of Environmental Protection Agency (EPA)-controlled substances and Department of Defense (DOD) chemical weapons stocks. The SCWO process is an entirely self-contained closed-cycle operation, precluding any exposure of hazardous materials to the surroundings and allowing for the capture and storage of reaction products for analysis and further treatment.

The SCWO process can be effectively used to treat organics present in dilute aqueous waste streams; the disposal of many these organic wastes is of great interest to the U.S. government: The destruction Environmental Protection Agency (EPA)-regulated wastes, Department of Energy (DOE), and Department of Defense (DOD) stockpiled wastes are all promising applications for SCWO. In the United States, specific wastes that have been identified as potential targets for destruction by the SCWO process include solid rocket propellants, explosives, organic components of mixed low-level liquid radioactive wastes, and chemical warfare agents [8]. NASA has also investigated SCWO for use in remediation of biomass and human metabolic waste for long-term space flight [9]. Germany and Japan have targeted various industrial aqueous toxic wastes for destruction by SCWO [10, 11]. The destruction of chemical warfare agents in the United States represents a particularly important and promising application for the SCWO process: The Chemical Weapons Convention (CWC), which was signed by 130 countries in January, 1993, seeks to eliminate chemical weapons and their production early in the new millennium [12, 13]. The successful elimination of chemical weapons requires a safe, clean, efficient, and economical waste disposal methodology. While a number of traditional destruction methodologies, such as landfill or incineration, do currently exist, they face significant public opposition, due to unacceptable environmental emissions and unfavorable economics [14]. SCWO represents a promising alternative for the destruction of these hazardous chemical agents and other organic wastes. However, in order for SCWO technology to be successfully implemented for widespread government/industrial applications, a number of scientific/engineering issues must be fully addressed.

The following is an overview of the process steps and equipment for SCWO [15]. Typically, an SCWO process begins with two or three aqueous feed streams: an oxidizer stream, the organic waste stream, and, in some cases, an auxiliary fuel stream. The SCWO feeds are initially pressurized from ambient conditions to the operating pressure of the reactor and then pumped

through a heat exchanger, where they are preheated to the desired supercritical temperature. Depending on the specific design of the system, these feed streams may be brought up to pressure and preheated before or after mixing. In either case, the combined reactant streams enter the main reactor in the supercritical state. The reactor may be either a vessel reactor or continuously fed stirred-tank reactor (CSTR), or a tubular, plug-flow type reactor (PFR). The vessel and continuous stirred-tank reactors are vertically oriented and employ two major temperature zones, which are designed to facilitate solids handling and mitigate corrosion. The top temperature zone is the hot reaction zone. This high temperature zone, which operates entirely under supercritical conditions during SCWO processing, is maintained at a nominally constant pressure, with temperatures ranging from 400–650°C. Most of the oxidation of the organic waste takes place in the top temperature zone, producing mainly CO_2 and H_2O, and depending on control of pH in the feed stream, acids and inorganic salts. The lower temperature zone is maintained within a lower subcritical temperature range, and a correspondingly higher fluid density. Vertical separation between the top temperature zone and the lower cooler zone are a result of buoyancy forces, which arise from a difference in fluid density between the top high temperature zone and the lower cooler zone. Mixing within the reactor is facilitated by buoyancy forces arising from large differences in the local fluid density within the top temperature zone. Low-density fluid phase products are carried upwards through an exhaust port. At higher feed stream pH values, the SCWO of organic compounds will produce inorganic salts. In the hot reaction zone these salts will precipitate out of the supercritical phase and settle into the lower, cooler zone, where the subcritical fluid redissolves the salt into dense liquid phase brine. The brine phase is continuously removed to prevent crystallization of salt on the reactor walls. Leaving the reactor, the supercritical fluid phase effluent is screened for solids, cooled in a heat exchanger, and depressurized. The cool-down heat exchanger recovers heat from the effluent, which can be used to preheat the feed, or potentially, to produce steam for electric power generation [16]. The spontaneous SCWO of the organic waste in the reactor can potentially produce heat in excess of that required to preheat the feed. Therefore, influent reactant streams may be used to cool the hot product effluent streams, through the use of one heat exchanger that integrates the steps of influent preheating and effluent cool-down. This process produces sufficient thermal energy in the influent to sustain the SCWO reaction without the need for preheating by an external source, and the SCWO process is capable of operating under self-sustaining conditions [17].

An actual schematic of the SCWO process originally developed by Modar, Inc. [18], is shown in Figure 1-2 [7]. Modar is now a division of General Atomics, Inc., Advanced Technologies Group – the organization that now owns all proprietary technology related to SCWO. In this process aqueous organic waste (1) may be treated with a neutralizing agent (2) or have fuel injected for startup (3). At the top of the reactor vessel (5), the feed is mixed with air or oxygen. This process incorporates a continuously fed stirred-tank reactor vessel, where spontaneous oxidation of the organic waste liberates heat and raises the upper hot reaction zone (6) to supercritical temperatures as high as 650°C. Inorganic salts precipitate out of the top zone and impinge on the lower cooler zone (7), which is at a temperature of about 200°C. The salts, which redissolve in the lower cooler zone, may be continuously taken off as brine (8), or periodically removed as solids. The primary effluent (9) passes out of the top of the reactor in the supercritical phase and enters a quench separator (10), where the gas (11) and liquid (12) are separated. The liquid effluent from the quench separator is sent through the heat exchanger (4),

which exchanges thermal energy between the hot effluent and the cool influent feeds. This results in simultaneous cooling of the liquid effluent (14) and preheating of the influent feeds utilizing the thermal energy of the effluent, thereby allowing SCWO process to operate under self-sustaining conditions.

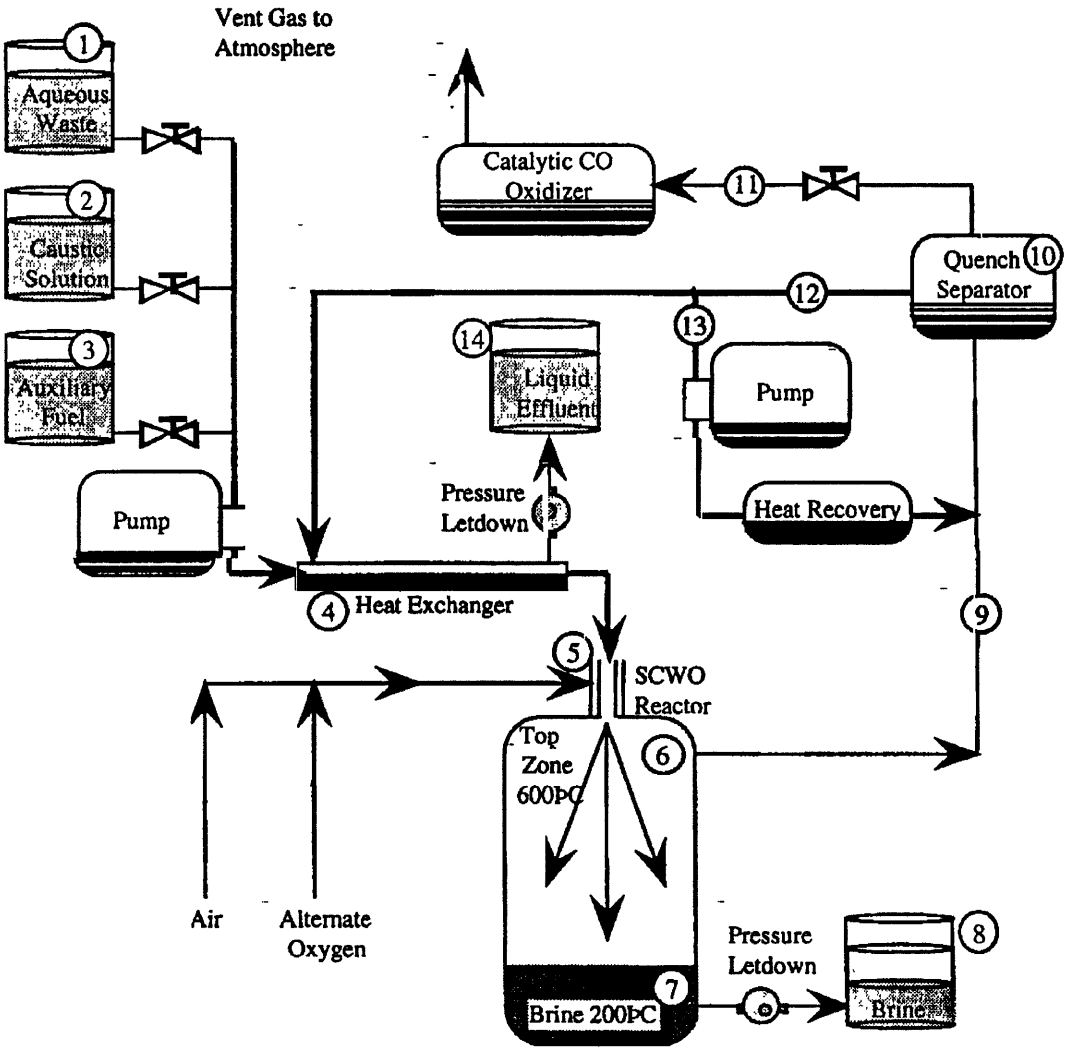

Figure 1-2: Schematic of the SCWO process developed by Modar, Inc. [18], now a division of General Atomics, Inc. From Mitton, *et al.* (2001), Reference [7].

1.3 Corrosion – A Major Obstacle to Implementation of SCWO Technology

The major disadvantages of SCWO revolve around high operating pressures (P > 23 MPa), potential inorganic solids handling problems, and for most waste streams, corrosion of the process unit. The corrosion issue represents the greatest obstacle to successful implementation of SCWO: Although, from a technological standpoint, SCWO has demonstrated remarkable success in efficiently destroying many hazardous organic wastes, the process must be carried out in a system capable of accommodating elevated temperatures, high pressures, and chemically aggressive environments. These chemically aggressive environments arise primarily as a result of the formation of acids under highly oxidizing conditions during the oxidation of hydrocarbons. Although the products of the hydrocarbon oxidation reaction include such innocuous species as CO_2 and H_2O, the formation of acids in the process stream also occurs for many organic wastes due to the existence of certain heteroatoms in the organic compounds. Moreover, the SCWO reactor utilizes a high partial pressure of oxygen in order to achieve rapid oxidation of the organic waste, giving rise to conditions that are highly oxidizing. Kriksunov and Macdonald [19] give an example of a typical reaction scheme for the oxidation of an organic compound in the SCWO process:

$$C_aH_bX_c + ([a + (b - c)]/2)O_2 \rightarrow \quad aCO_2 + [(b - c)/2]H_2O + cH^+ + cX^-$$

In the above reaction, $C_aH_bX_c$ represents a simple hydrocarbon, and X represents the heteroatom, which is taken, in this case, to be a halogen such as Fluorine (F) or Chlorine (Cl). When the hydrocarbon oxidation reaction takes place, the halogen, X, converts to halide, X^-, which can persist as an acid in the fluid phase. Thus, from a corrosion standpoint, the SCWO reaction results in the formation of innocuous byproducts, CO_2 and H_2O, as well as the potentially aggressive species, cH^+ and cX^-, which represent the dissociated generic acid, HX, in solution. The pH of the solution, a measure of acidity, is defined with respect to the concentration of the hydrogen ion, H^+, in solution. This definition of acidity applies regardless of the type of organic compound being oxidized because all acids are universally defined as H^+ donors. Quite often, low pH values, indicating high concentrations of H^+, result in greater susceptibility to general corrosion, and mass loss, given favorable thermodynamic conditions. Non-halogen heteroatoms, including Sulfur (S) and Phosphorous (P), can also be present in the organic waste compound. Thus, in actual SCWO applications, the anion, X^-, can be any number of species, including sulfate (SO_4^{2-}), phosphate (PO_4^{3-}), or the aforementioned halides. Unlike H^+, these anions may or may not behave independently as an aggressive species, and this depends entirely on the species of anion in the solution: Some halides, particularly chloride (Cl^-), are known to give rise to localized effects, including pitting and stress corrosion cracking (SCC). Whereas, localized attack traditionally has not been observed in aqueous solutions containing sulfates or phosphates.

Many of the organic wastes being considered for destruction by SCWO contain such potentially corrosive precursors: DOE wastes often contain solvents or oils that are high in chlorine or other potentially corrosive species (e.g. fluorine, sulfur, tributyl phosphate). The SCWO process results in oxidation of these compounds to form extremely aggressive acidic products. In the case of chemical warfare agents, the oxidation of Sarin (GB) produces a mix of hydrofluoric and phosphoric acids. The oxidation of VX is known to produce sulfuric and phosphoric acids.

Finally, the oxidation of mustard agent (HD) produces hydrochloric and sulfuric acids [20]. The presence of such acids in high-temperature process streams under highly oxidizing conditions will result in significant corrosion of the process unit. Hence, corrosion represents a major obstacle and may ultimately be the deciding factor in the implementation of this technology for widespread industrial/government applications [21-23].

1.4 Scope and Purpose of Thesis

This review presents a comprehensive treatment of electrochemical and corrosion phenomena under conditions associated with the Supercritical Water Oxidation (SCWO) process. This is accomplished by discussing the relevant aspects of electrochemistry, corrosion science, and corrosion performance as they pertain to high-temperature, high-pressure aqueous environments containing aggressive species, expected in various SCWO process streams. Each of the relevant scientific and engineering principles is discussed as it pertains to SCWO technology. For each of these principles, the relevant literature addressing the specific electrochemical and/or corrosion issue is cited.

In many instances, research may not specifically address the SCWO process, but one or more environmental characteristics associated with the SCWO process. The reason for this is that research specifically addressing corrosion mitigation in SCWO process environments, both real and simulated, has only been ongoing since 1990. However, research into the thermodynamics of metals in aqueous environments under hydrothermal conditions has been ongoing since 1970. Clearly, the former may be viewed as "engineering" research because it has sought to identify materials that can withstand the harsh conditions of SCWO. However, given the abysmal record of corrosion performance for candidate alloys in simulated SCWO feeds, much of this engineering research is of limited value without a clear connection to the later, which is representative of the formal "science" of metal-water systems under hydrothermal conditions.

Thus, the reader should keep the following in mind when examining the issue of corrosion in SCWO systems: Despite more than ten years of research, corrosion of the SCWO process unit remains as great a challenge to full-scale implementation as ever. Indeed, attempts by researchers to identify materials that can withstand the harsh oxidizing conditions that exist in the process stream have proved markedly unsuccessful. Hence, the only way that the SCWO corrosion challenge can be successfully met is by acquiring fundamental knowledge of physicochemical, electrochemical, and corrosion phenomena in SCWO environments. In recent years, a great deal of progress has been made in understanding these phenomena on a fundamental level. However, there are many questions that are still unanswered. Therefore the goal of this thesis is to provide a framework for additional research in this area by addressing the key scientific and engineering principals, as they pertain to corrosion in SCWO process environments.

REFERENCES – Chapter 1

1. C.J. Rebert and W.B. Kay, "The Phase Behavior and Solubility Relations of the Benzene-Water System," AIChE Journal, 5 (1959), p. 285.
2. J. Conolly, "Solubility of Hydrocarbons in Water Near the Critical Solution Temperature," J. Chem. Eng. Data, 11 (1) (1966), p. 13.
3. M.L. Japas and E.U. Franck, "High Pressure Phase Equilibria and PVT-Data of the Water-Oxygen System Including Water-Air to 673K and 250 MPa," Ber. Bunsenges Phys. Chem., 89 (1985), p. 1268
4. M.L. Japas and E.U. Franck, "High Pressure Phase Equilibria and PVT-Data of the Water-Nitrogen System to 673K and 250 MPa," Ber. Bunsenges Phys. Chem., 89 (1985), pp. 793-800
5. A.E. Mather and E.U. Franck, "Phase Equilibria in the System Carbon Dioxide-Water at Elevated Pressures," J. Phys. Chem., 96 (1) (1992), pp. 6-8.
6. T. Krader and E.U. Franck, "The Ternary Systems H_2O-CH_4-NaCl and H_2O-CH_4-$CaCl_2$ to 800K and 250 MPa," Ber. Bunsenges Phys. Chem., 91 (1987), pp. 627-634.
7. D.B. Mitton, *et al.*, "Assessing Degradation Mechanisms in Super Critical Water Oxidation Systems," *Corrosion 2001*, Houston, TX, 2001, paper #01352.
8. Hart, P. W., 1995. "Treatment of U.S. DOE Mixed Waste Using SCWO Technology," *Proceedings of the First International Workshop on Supercritical Water Oxidation*, Amelia Island, FL, 6-9 Feb. 1995, WCN Forums Lake Bluff IL.
9. P.A. Webley, *et al.*, "Oxidation Kinetics of Model Compounds of Metabolic Waste in Supercritical Water," (Paper presented at the 20th Inter-Society Conference on Environmental Systems, Williamsburg, VA, Warrendale, PA: Society of Automotive Engineers, 1990), paper #901333.
10. Ebert, K; Franck, E.U., 1995. "Potential & Needs of SCWO in Future Technologies in Europe," *Proceedings of the First International Workshop on Supercritical Water Oxidation*, Amelia Island, FL, 6-9 Feb. 1995.
11. Suzuki, A., 1995. "Construction of the First SCWO Pilot-Scale Plant in Japan," *Proceedings of the First International Workshop on Supercritical Water Oxidation*, Amelia Island, FL, 6-9 Feb. 1995.
12. L. Drake, "Selecting Technologies for Destruction of the Chemical Weapons Stockpile," MIT Energy Laboratory Seminar, February 9 (1993).
13. Aqua Fortis, US Army Research Office **2**, No. 1, (1993)
14. K.C. Swallow and D. Ham, The Nucleus, **11**, 11, (1993)
15. J.A. Cline, "Experimental and *Ab* Initio Investigations into the Fundamentals of Corrosion, in the Context of Supercritical Water Oxidation Systems," PhD thesis in Chemical Engineering, Massachusetts Institute of Technology, Cambridge, MA, (2000).
16. J.W. Tester, *et al.*, in Emerging Technologies for Hazardous Waste Management III, (Washington, DC: ACS 1993), pp. 35-76.
17. M.J. Cocero, E. Alonso, M.T. Sanz, F. Fdz-Polanco, "Supercritical water oxidation process under energetically self-sufficient operation," J. Supercritical Fluids, (2002).
18. M. Modell, Standard Handbook of Hazardous Waste Treatment and Disposal (New York, NY: McGraw Hill, 1989), pp. 8-153.

19. L.B. Kriksunov and D.D. Macdonald, "Corrosion in Supercritical Water Oxidation Systems: A Phenomenological Analysis," J. Electrochem. Soc., 142 (12) (1995), p. 4069.
20. K.W. Downey, R.H. Snow, D.A. Hazelbeck and A.J. Roberts, *Innovations in Supercritical Fluids*, ACS Symposium Series, 608, p.313, ACS, Washington, DC (1995).
21. R.M. Latanision and R.W. Shaw, Co-Chairs, *Corrosion in Supercritical Water Oxidation Systems* – Summary of a Workshop held at MIT May 6-7, 1993 Report No. MIT-EL 93-006, (1993).
22. D.B. Mitton, J.C. Orzalli and R.M. Latanision, *Proc. 3rd Int. Symp. On Supercritical Fluids*, Vol. 3, p. 43 (1994).
23. A.J. Thomas and E.F. Gloyna, "Corrosion Behavior of High Grade Alloys in the Supercritical Water Oxidation of Sludges," University of Texas at Austin Technical Report CRWR 229 (1991).

Chapter 2

The Physical Chemistry and Electrochemistry of Supercritical Water Oxidation Process Environments

2.1 Overview

By all objective standards, the SCWO process environment is the most aggressive aqueous service environment yet encountered, from a materials degradation standpoint. This is due to the formation of acids under highly oxidizing conditions in hydrothermal aqueous environments. These unprecedented environmental conditions are necessary for achieving complete, spontaneous, and rapid destruction of the most toxic and resilient organic wastes ever produced. However, these are also the same conditions that lead to rapid degradation of the most corrosion resistant constructional materials currently available. This corrosion challenge cannot be effectively met through design and/or materials selection alone: If corrosion in SCWO systems is to be effectively dealt with, it is absolutely necessary to have a fundamental understanding of physical chemistry and electrochemistry within the process environment and the manner in which environmental conditions affect corrosion phenomena.

As an example, consider the phase stability diagram for iron in water at 400°C and 500 bar. This diagram, given in Figure 2-1, depicts the regions in potential-pH space for thermodynamic stability of iron and its passive oxides in supercritical water. Macdonald, *et al.*, constructed this diagram as part of the ongoing research program to understand and affect thermodynamic corrosion conditions in SCWO process environments. pH represents the acidity of the solution, and potential represents the solution's oxidizing power. The two shaded regions indicate the regions in potential-pH space where supercritical thermal power plants and SCWO systems operate for the supercritical conditions given above. Before going into a detailed discussion of electrochemical thermodynamics, it is immediately clear that SCWO systems are far more susceptible to corrosion due to lower pH values and greater oxidizing potentials. Supercritical thermal power plants, on the other hand, are able to control corrosion because the chemical conditions are far less acidic and less oxidizing.

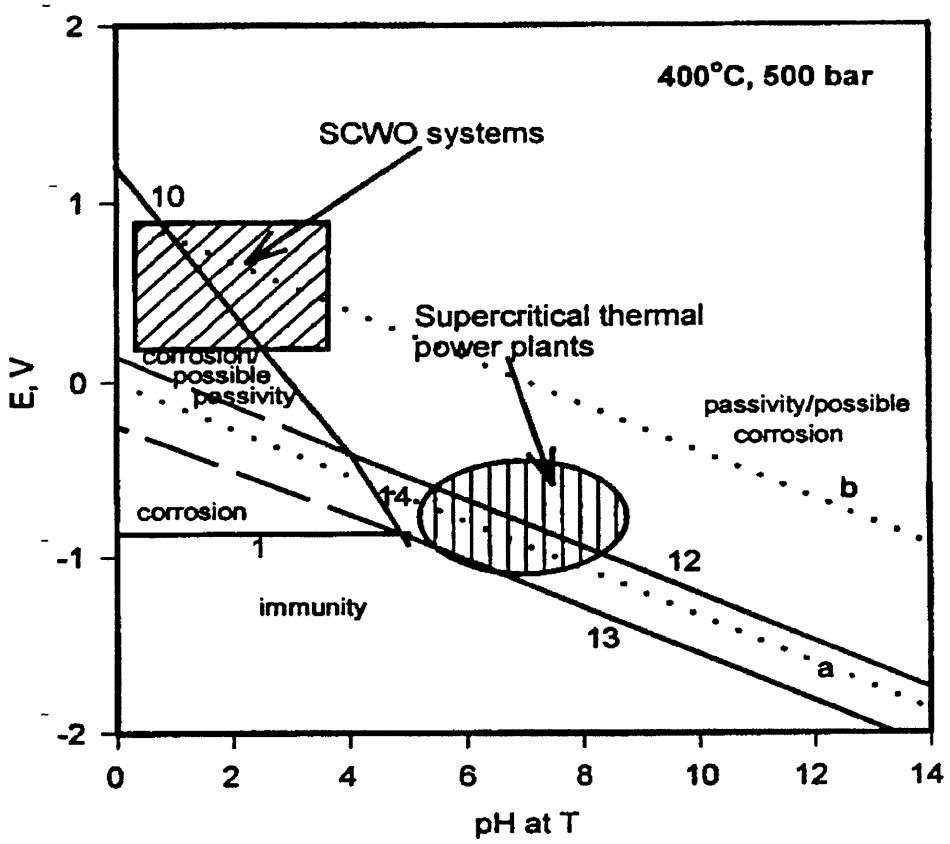

Figure 2-1: Potential-pH diagram for iron in supercritical water at 400°C and 500 bar. The regions, in potential-pH space, of operation for SCWO systems and supercritical thermal power plants are given for reference. From Macdonald, *et al.*, "Probing the Chemical and Electrochemical Properties of SCWO Systems," *Electrochimica Acta* 47 (2001), p. 775.

The following is a detailed review of physical chemistry and electrochemistry, as they relate to corrosion phenomena in the supercritical water oxidation environment. The key scientific principles include the development of potential-pH diagrams at elevated temperatures and pressures, measurement and standardization of electrochemical parameters in supercritical aqueous environments, electrochemical polarization studies, and theoretical modeling based upon the chemical kinetics of the corrosion reaction. The first two topics can be classified as thermodynamic issues, whereas the later two may be viewed as kinetic issues. All constitute an important scientific foundation for the development of effective corrosion engineering methods for SCWO systems.

These principles form a framework for the science of corrosion in the supercritical water oxidation environment, which includes aqueous solutions of aggressive species under oxidizing conditions at both subcritical and supercritical conditions. Much of this review of electrochemistry and corrosion science in the SCWO environment follows the work of Macdonald, *et al.* However, a majority of the earlier work dealing with the thermodynamics of corrosion at elevated temperatures and pressures was based on the thermodynamic models of

Criss and Coble and the model later established by Helgeson, *et al.* Townsend, Macdonald, and Lee initiated the application of these high temperature thermodynamic models to the construction of potential-pH diagrams at elevated temperatures. Macdonald, *et al.*, is responsible for the development of theoretical kinetic models of corrosion and the development of standards and techniques for the measurement of electrochemical parameters in supercritical aqueous environments. Huang, *et al.*, and subsequently, Macdonald, *et al*, carried out electrochemical polarization studies in supercritical aqueous environments.

2.2 Electrochemical Thermodynamics

The electrochemical thermodynamics of a metal immersed in a potentially corrosive aqueous environment are summarized graphically through the use of potential-pH diagrams, or Pourbaix diagrams [1]. Potential-pH diagrams graphically display the regions of thermodynamic stability for the various solid (metal or metal oxide/hydroxide) or aqueous ionic species that are known to exist over a range of oxidation-reduction (redox) potentials and pH values at a given temperature and pressure. Thus, potential-pH diagrams can be viewed as phase stability diagrams in potential-pH space for systems consisting of a metal (or possibly alloy) immersed in aqueous solution. Potential-pH diagrams indicate the potential-pH conditions where the metal is thermodynamically stable and hence immune to corrosion, the conditions that result in the dissolution (corrosion) of the metal in the form of aqueous ionic species, and the stability conditions for the formation of oxidized surface films that give rise to passivation.

Potential-pH diagrams are developed by first identifying the chemical equilibria that are known to exist for the system of interest, which generally involves a metal immersed in an aqueous environment. The set of reactions representing the equilibria for the system must then be identified. Each of these reactions is a half-cell electrochemical reaction, involving an exchange of electrons. The reactions in the reaction set may be written as either oxidation or reduction reactions, depending on whether the oxidized species is designated as the product or reactant. These half-cell reactions form the basis for determining boundary lines dividing the regions of stability for the various equilibria in potential-pH space. A reaction set for the Fe-H_2O system, as presented by Professor Marcel Pourbaix who pioneered the construction and use of potential-pH diagrams for pure metals, is shown below [1]:

$H_2 \rightarrow 2H^+ + 2e^-$
$2H_2O \rightarrow O_2 + 4H^+ + 4e^-$
$3Fe + 4H_2O \rightarrow Fe_3O_4 + 8H^+ + 8e^-$
$2Fe_3O_4 + H_2O \rightarrow 3Fe_2O_3 + 2H^+ + 2e^-$
$2Fe^{3+} + 3H_2O \rightarrow Fe_2O_3 + 6H^+$
$Fe \rightarrow Fe^{2+} + 2e^-$
$Fe + 2H_2O \rightarrow HFeO_2^- + 3H^+ + 2e^-$
$3Fe^{2+} + 4H_2O \rightarrow Fe_3O_4 + 8H^+ + 2e^-$
$3HFeO_2^- + H^+ \rightarrow Fe_3O_4 + 2H_2O + 2e^-$
$2Fe^{2+} + 3H_2O \rightarrow Fe_2O_3 + 6H^+ + 2e^-$

The diagrams can be constructed based upon the stoichiometry for each of the chemical reactions in the reaction set for the system and the free energy data for all the species involved at some standard state. For constructions at some designated temperature and pressure, the standard state is taken to be unit activity at that particular temperature and pressure. Ambient temperature potential-pH diagrams are constructed as follows: Thermodynamic data at the standard state for both solid and dissolved ionic species in aqueous solution at ambient temperature and pressure are readily available. The chemical equation for each reaction in the reaction set is balanced. The standard state free energy changes, ΔG°, for each of the half-cell reactions, are equal to the sum of the standard state free energies of the products minus the sum of the standard state free energies of the reactants. The standard state free-energy change is associated with a standard state electrochemical or electrode potential for each of the reactions shown above according to the fundamental relationship:

$$\Delta G = -nFE$$

Where n is the number of electrons exchanged in the oxidation-reduction reaction, as determined by the reaction stoichiometry and F is Faraday's constant 96500 coulombs per equivalent. However, it is impossible to measure the absolute value of the electrode potential for any half-cell reaction. Therefore standard state free energy changes for the half-cell reactions above are generally written as a potential relative to a reference half-cell reaction, which is designated as the reference electrode. The standard state requires that all reactants and products be at unit activity, and as concentrations of ionic species deviate from unit activity it is necessary to relate these variable activities to the non-standard state half-cell potentials, written as a full-cell potential, E, relative to the reference electrode. For deviations from unit activity, the half-cell electrochemical potential, e, for a half-cell reaction can be related to solution chemistry, or pH, by applying the Nernst equation:

$$e = e^{\circ} + \frac{2.3RT}{nF}\log\frac{(A)^{a}}{(B)^{b}} - \frac{m}{n}0.059\ pH$$

Where (A) represents the activity of some species, A, and $pH \equiv -\log (H^{+})$

For a general half-cell reaction given by:

$$aA + mH^{+} + ne^{-} = bB + dH_2O$$

A complete background on electrode potentials, along with the derivation of the Nernst equation, and examples of potential-pH diagram constructions is given in references [2, 3]. Boundary lines on the diagrams dividing the regions of equilibrium for each of the species involved represent the various electrochemical reactions in the above reaction set. For electrochemical reactions, these lines are plotted on potential-pH diagrams by expressing the electrochemical potential in terms of solution pH through the use of the Nernst equation. Pourbaix has constructed diagrams for pure elemental metals under ambient conditions by applying the above methodology. These

diagrams for pure metallic elements in aqueous solutions under ambient conditions are given in the "Atlas of Electrochemical Equilibria in Aqueous Solutions" [4].

Traditionally, potential-pH diagrams have been constructed at ambient temperature and pressure, and prior to 1970 constructions at elevated temperatures did not exist in the literature. The development of potential-pH diagrams for candidate alloys at high temperatures and pressures, both subcritical and supercritical, is necessary for the development of effective methodologies for corrosion mitigation in supercritical aqueous systems. The potential and pH conditions that result in metallic immunity or passivity at ambient temperature will not necessarily result in this behavior at elevated temperatures and pressures, either in the subcritical or supercritical temperature ranges. This is due to the dependence of thermodynamic state functions on temperature and pressure. The standard aqueous electrode potentials correspond directly to standard free energy changes at a given temperature and pressure. The standard free energies of products and reactants are temperature dependent. Hence standard free energy changes and electrode potentials are temperature dependent, and one could therefore conceive of a third temperature axis mutually orthogonal to the potential axis and the pH axis on a three-dimensional potential-pH-temperature phase stability diagram at a given pressure.

The construction of potential-pH diagrams for common metals and alloys in aqueous solutions at elevated temperatures started in the late 1960's and was facilitated by the development of methodologies for computing the necessary thermodynamic data at elevated temperatures. Townsend was the first researcher to apply this extrapolation technique for thermodynamic state functions, based upon the "entropy correspondence principal" of Criss and Coble [5], to the construction of the potential-pH diagram for the Fe-H_2O system at temperatures up to 200°C [6]. A 3-D potential-pH-temperature phase stability diagram for Fe-H_2O formed by combining individual 2-D potential pH diagrams at T = 25°, 60°, 100°, 150°, and 200°C is given in Figure 2-2. In the twenty years following this initial work, research in this area was expanded to include the construction of elevated temperature potential-pH diagrams for other important metal-water systems [7 - 16]. Several of the most notable references pertaining to the constructions of potential-pH diagrams at elevated subcritical temperatures for elemental metals in aqueous systems are briefly summarized: In 1972-1973 Macdonald, *et al.*, constructed elevated temperature potential-pH diagrams for the Cu-H_2O, Ni-H_2O, Co-H_2O, and Al-H_2O systems [10, 11]. In 1981 Lee, et al., constructed elevated temperature potential-pH diagrams for the Cr-H_2O, Ti-H_2O, Mo-H_2O, and Pt-H_2O systems [14]. Subsequently, Macdonald, *et al.*, constructed diagrams at elevated temperatures for Ta-H_2O [15]. In general, the elevated temperature constructions can differ drastically from those at ambient conditions. In virtually all of the elevated temperature constructions for individual metallic elements, the diagrams indicate that the region of metallic immunity is suppressed to lower oxidation-reduction potentials at higher subcritical temperatures. The regions of passivity may be suppressed to more limited ranges of potential, however passive film stability can often occur at lower pH values for elevated temperatures. Overall, the specific nature and extent of these changes in electrochemical phase equilibria, with respect to temperature and pressure, depends on the chemical thermodynamics of the metal, its soluble ionic species, and the insoluble oxides/hydroxides that can exist for the system of interest. For additional background on the subject, several reviews of the literature pertaining to the constructions of potential-pH diagrams at elevated subcritical temperatures ($T \leq 300$°C) for elemental metals in aqueous environments have been written [17-19].

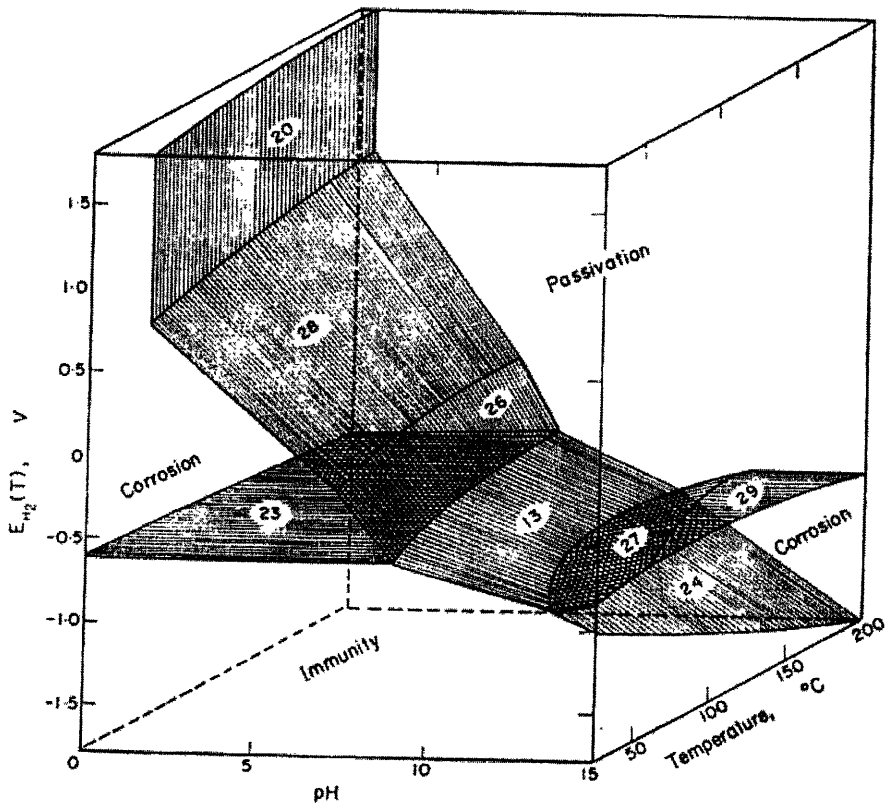

Figure 2-2: 3-D potential-pH-temperature phase stability diagram for Fe-H_2O formed by combining individual 2-D potential pH diagrams at T = 25°, 60°, 100°, 150°, and 200°C. From Townsend, (1970), Reference [6].

Diagrams for individual metallic elements at a given temperature and pressure may be superimposed to form a composite diagram for a group of metallic elements in aqueous solution. This method has often been used to assess the corrosion behavior of alloys. Thus, the superposition of the diagrams for iron, chromium, and nickel could provide limited insight into the corrosion behavior of stainless steel. This procedure is of limited effectiveness because it does not consider the possibility of the formation of solid oxides/hydroxides containing more than one metallic element. Such insoluble binary metallic oxides are known to exist for many alloy systems (e.g. stainless steels), and may exhibit fields of stability that cover larger ranges of potential and pH than the fields of stability for single metal oxides.

Cubicotti was the first researcher to address the construction of elevated temperature potential-pH diagrams specifically for alloy-H_2O systems [20-22]. These constructions dealt primarily with stainless steels (e.g. Fe-Cr-Ni alloys) at subcritical temperatures relevant to Boiling Water Reactor and Light Water Reactor systems. These constructions are still somewhat relevant to SCWO technology due to the ongoing investigations into the corrosion behavior of nickel-base alloys and stainless steels in SCWO process streams: The diagrams were constructed at elevated temperatures that were within the range of SCWO temperatures, where corrosion is a major concern. Also, Fe, Cr and Ni are elements that are present in virtually all candidate nickel alloys addressed as part of the SCWO corrosion research program. These elevated temperature constructions were particularly significant because they addressed the formation of "binary oxides" under certain potential-pH-temperature conditions. The phase stability fields for these binary oxides was computed to exist over significant ranges of potential and pH at elevated temperatures, and it was hypothesized that the stability of such binary oxides was a significant factor contributing to corrosion resistance in such Light Water Reactor systems. In particular, computations at 300°C revealed the existence of large passivity fields in potential-pH space, where such solid binary metallic oxides as $NiFe_2O_4$, $FeCr_2O_4$, and $NiCr_2O_4$ were determined to be stable. Roughly, the stability regions for these species existed over moderately acidic to moderately caustic ranges of pH (typically 3-9) and low to moderately high redox potentials (vs. SHE). Whether or not such oxides could play a roll in passive protection of SCWO constructional alloys is an issue that should be investigated further.

Mitton, *et al.*, constructed a composite potential-pH diagram for Ni, Fe, Cr, and Mo at 300°C [23]. This composite potential-pH diagram, given in Figure 2-3, is the only composite diagram prepared specifically as part of the research program addressing corrosion mitigation in SCWO systems. Although this diagram is a superposition of diagrams for individual metal-water systems at one subcritical temperature and does not address the formation of insoluble binary metallic oxides, it has helped to provide a thermodynamic explanation for certain corrosion phenomena in high subcritical temperature regions of the SCWO process stream. It is likely that this diagram, after being further developed, could play a roll in the mitigation of corrosion via feed stream modification [23]. The thermodynamic implications of this diagram on corrosion of the SCWO process unit are discussed in Chapter 3.

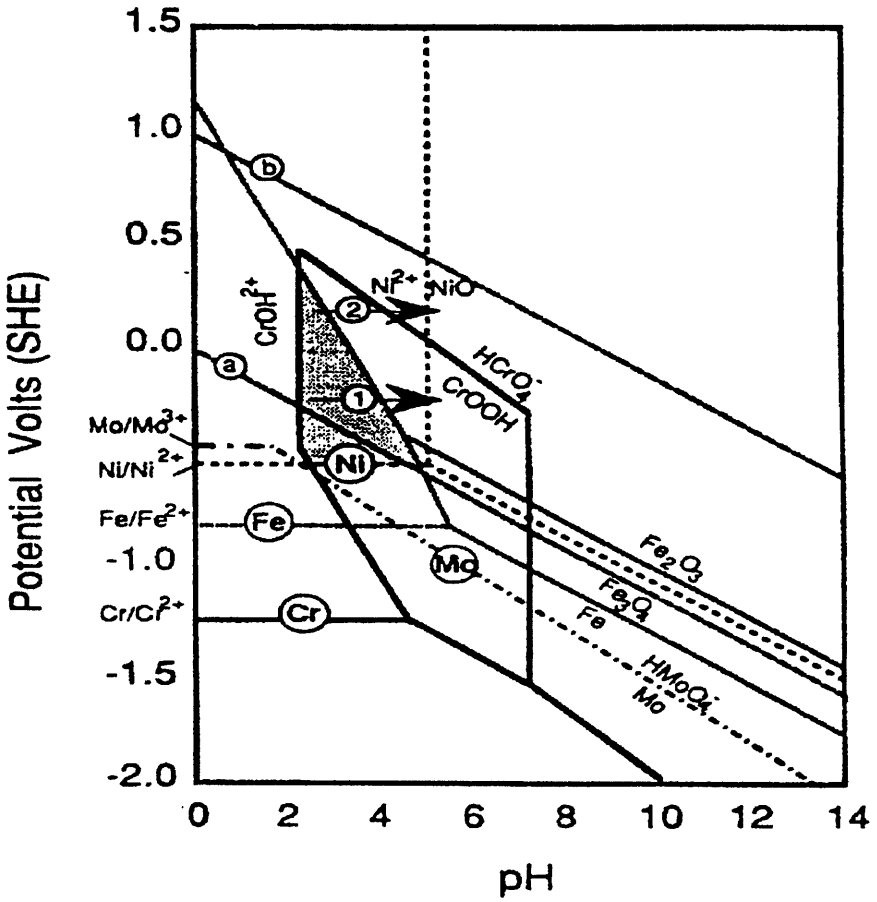

Figure 2-3: Composite potential-pH phase stability diagram for Ni, Fe, Cr, Mo at 300°C. From Mitton, *et al.* (1996), Reference [23].

At the present time, only a very limited amount of research has been carried out pertaining to the construction of potential-pH diagrams at near-critical or supercritical temperatures. Most of the earlier work pertaining to elevated temperature constructions was carried out before SCWO technology was sighted as viable alternative for organic waste destruction. Therefore, all of the earlier elevated temperature constructions discussed above are limited to the subcritical regime, usually for $T \leq 300^{\circ}C$. However these constructions are still highly relevant in light of the numerous observations of the most severe corrosion occurring in SCWO heat exchanger tubing, where temperatures are high, but subcritical. Indeed, the composite potential-pH diagram constructed by Mitton, *et al.*, for Ni, Fe, Cr, Mo at 300°C (Figure 2-3), was presented as a thermodynamic tool for mitigation of corrosion in the high subcritical temperature regime. This composite diagram was based on the elevated temperature thermodynamic data of Macdonald and Lee, whose elevated temperature constructions were published in 1972 and 1981, respectively, long before the SCWO of organics was discovered.

Potential-pH diagrams at temperatures and pressures in the vicinity of the critical point of water first appeared in 1989: Huang *et al.* presented potential-pH diagram constructions, for iron and chromium at a pressure and temperature corresponding to the critical point of water [24]. However these initial constructions under conditions corresponding to the critical point were carried out using the "entropy correspondence principal" of Criss and Coble [5], the use of which is absolutely not justified for near critical and supercritical conditions. This issue was not revisited until the mid 1990's when researchers, namely Macdonald, *et al.*, recognized the need for research into potential-pH diagram constructions that cover temperature ranges extending well into the supercritical regime. Kriksunov and Macdonald constructed potential-pH diagrams for the iron-water system for temperatures ranging from 100°C to 500°C [25]. A limited amount of work was also carried out for the Ni-H_2O system under supercritical conditions [26, 27]. A potential-pH diagram for Ni-H_2O under supercritical conditions is given below. These constructions were based upon a modern thermodynamic model for hydrothermal aqueous systems, capable of generating reliable thermodynamic data at both subcritical and supercritical temperatures. The construction of elevated temperature potential-pH diagrams for both subcritical and supercritical conditions is central to an understanding of electrochemistry and corrosion science in the SCWO process environment. Hence, a review of the thermodynamic principles behind elevated temperature constructions is presented.

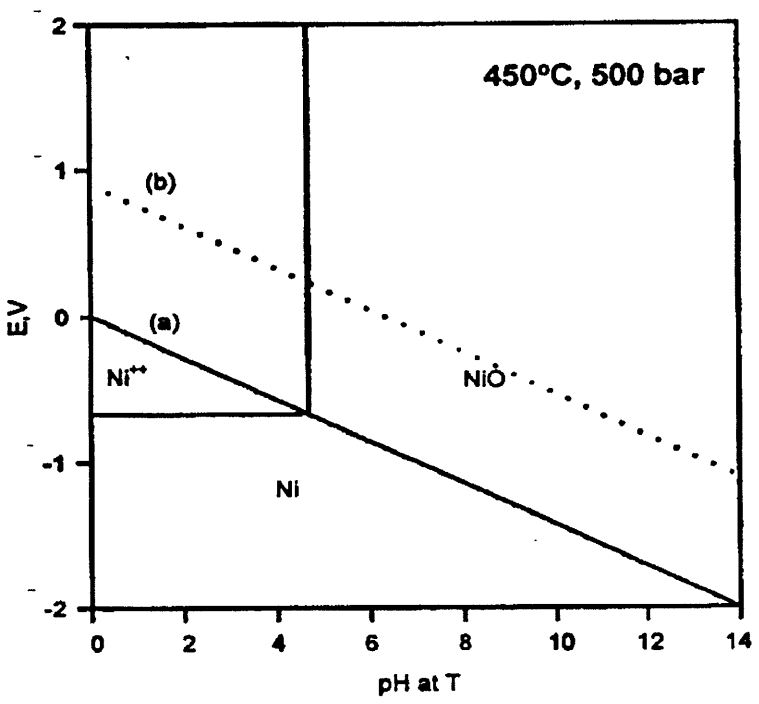

Figure 2-4: Potential-pH diagram for nickel in supercritical water. From Macdonald, *et al.*, (1995), References [26, 27].

2.3 Construction of Potential-pH Diagrams at Elevated Temperatures and Pressures ($T \leq 300^{\circ}C$)

In order to construct potential-pH diagrams at elevated temperatures and pressures, free energy data for all species participating in a reaction set, like the one given previously for Fe-H_2O, are required at the temperature of interest. In general, the standard state (e.g. unit activity) free energy of a substance at a higher temperature T_2 can be obtained by integrating thermodynamic state functions over the desired temperature range. This derivation follows the work of Townsend and Lee [6, 14] in extending potential-pH diagrams to high temperatures, where $T \leq 300^{\circ}C$.

The standard free energy changes for each of the reactions in the reaction set can be determined at ambient conditions by using values for the standard free energies of the species participating in the reaction, which can be obtained from literature data.

ΔG° is the standard Gibbs free energy change at temperature, $T = 25^{\circ}C$, and

$$\Delta G^{\circ}(T) = \Delta H^{\circ}(T) - T\Delta S^{\circ}(T)$$

ΔH° and ΔS° are the standard enthalpy and standard entropy changes at temperature, T, respectively, for each of the reactions in the reaction set.

For each of the species participating in a reaction, the standard enthalpy of that species at temperature, T_2, can be expressed in terms of the standard enthalpy of the species at temperature, T_1, using the following thermodynamic relationship:

$$H^{\circ}(T_2) \equiv \int_{T_1}^{T_2} \overline{C}_p^{\circ}(T)\, dT + H^{\circ}(T_1)$$

In a similar manner, there exists a thermodynamic relationship, relating the standard entropy of the species at temperature, T_2, to the standard entropy of the species at temperature, T_1.

$$S^{\circ}(T_2) \equiv \int_{T_1}^{T_2} \frac{\overline{C}_p^{\circ}(T)}{T}\, dT + S^{\circ}(T_1)$$

C_p° is the standard molar heat capacity. Thus, the Gibbs free energy of a substance at temperature, T_2, can be expressed as follows:

$$\overline{G}^{\circ}(T_2) \equiv \overline{G}^{\circ}(T_1) - \overline{S}^{\circ}(T_1)\cdot(T_2 - T_1) + \int_{T_1}^{T_2} \overline{C}_p^{\circ}(T)\, dT - T_2 \int_{T_1}^{T_2} \frac{\overline{C}_p^{\circ}(T)}{T}\, dT$$

From the equation above, it is clear that determining the Gibbs free energy for a species at temperature, T_2, requires knowledge of the Gibbs free energy for that species at temperature, T_1, the standard entropy at T_1, and the manner in which standard molar heat capacity varies as a function of temperature. For pure phases, including solids, liquids, and gases, accurate molar heat capacity functions are available from the literature data in the following form:

$$\overline{C}_p^{\circ}(T) = A + BT + CT^{-2}$$

By applying these equations the Gibbs free energy for a pure phase at temperature T_2 can be obtained in a relatively straightforward manner. For ionic species, however, the partial molar heat capacity functions are not available, and application of these equations for determining elevated temperature Gibbs free energies is not possible.

Criss and Cobble have demonstrated that reliable calculations of standard free energies for ionic species at elevated temperatures can be performed in the absence of high temperature data on the basis of a "correspondence principle" for ionic entropies [5]. The application of this correspondence principle is central to the development of elevated temperature potential-pH diagrams because of the central role of electrochemical reactions involving dissolved ionic species, namely, the reaction for active metallic corrosion. This principle is based upon the following observation: Absolute ionic entropies for a given class of ions at a given reference temperature, T_1, are linearly related to the absolute entropies of those ions at some other temperature, T_2, provided that the correct standard state is selected for the ionic entropies at the given reference temperature. This requires knowledge of the absolute entropy of the ionic species at the reference temperature, which must initially be taken as 25°C, given the absence of this data for ionic species at elevated temperatures. The absolute entropy of ionic species, i, at 25°C is determined by normalizing the conventional value for the ionic entropy to the absolute scale:

$$S_{25}^{\circ}(\text{i, abs.}) = S_{25}^{\circ}(\text{i, conventional}) - 5.0Z$$

In the above relationship, S_{25}°(i, abs.) is the absolute entropy of ionic species, i, at 25°C and, S_{25}°(i, conventional) is the conventional entropy for the ionic species, which is available from the literature, where the conventional entropy scale is based upon the value of $S^{\circ}(H^+, \text{conventional}) = 0$, at any temperature. Z is equal to the ionic charge, and –5.0eu is the absolute entropy of the hydrogen cation at 25°C. Criss and Coble show that the above relationship is valid at any other temperature, T_2, and there exists a linear relationship between the absolute entropy of the ionic species, i, at temperature T_2, and the absolute entropy at 25°C or any other reference temperature. This linear relationship has the following form:

$$S_{T2}^{\circ}(\text{i, abs.}) = a(T_2) + b(T_2)S_{25}^{\circ}(\text{i, abs.})$$

This is a semi-empirical equation based on Criss and Coble's analysis of available experimental data in the literature. The constants, a and b, are dependent on the ion and were tabulated by Criss and Coble in their original papers.

The reliable extension of potential-pH diagrams to high temperatures, where T<300°C, was accomplished by applying the "entropy correspondence principle" for ionic species to the thermodynamic equations above. For the case of ionic species, it is evident from the thermodynamic equations presented by Townsend, Lee, and Macdonald in their elevated temperature constructions that the free energy of an ionic species at temperature, T_2, can be expressed exclusively in terms of ionic entropies at temperatures T_1 and T_2 and the free energy for the ionic species at T_1 by applying the following approximation:

$$\int_{T_1}^{T_2} \overline{C}_p^{\circ}(T)\, dT \approx \frac{(T_2 - T_1)}{\ln (T_2 / T_1)} \int_{T_1}^{T_2} \frac{\overline{C}_p^{\circ}(T)}{T}\, dT$$

By substituting this approximation into the equation for the free energy at T_2, given above, and applying the thermodynamic relationship given for the entropy at T_2, the molar heat capacities are eliminated and the expression for the free energy at temperature T_2 is written as:

$$\overline{G}^{\circ}(T_2) = \overline{G}^{\circ}(T_1) - [T_2 S^{\circ}(T_2) - T_1 S^{\circ}(T_1)] + \frac{(T_2 - T_1)}{\ln (T_2 / T_1)} [S^{\circ}(T_2) - S^{\circ}(T_1)]$$

So, by this equation, the free energy at T_2 can be determined, given the entropies for the ionic species at T_1 and T_2. Accurate entropy values for ionic species can be estimated using the entropy correspondence principle discussed above, which allows for the determination of the free energy for the ionic species at elevated temperature, T_2.

2.4 Construction of Potential-pH Diagrams at Hydrothermal Conditions (T > 300°C)

Extension of potential-pH diagrams to very high subcritical and supercritical temperatures (T>300°C) requires a second approach. The construction of potential-pH diagrams at elevated temperatures is based upon the integration of the standard Gibbs free energy function over the desired temperature range for solid species and water, as standard state (e.g. unit activity) molar heat capacity functions are readily available for the temperature range of interest. For dissolved ionic species, which are almost never at unit activity, the thermodynamic functions must be extrapolated over this temperature range through the application of the Criss Coble entropy correspondence principal. However, this extrapolation method is based upon a model that is only valid for subcritical conditions. Furthermore, this extrapolation method can only be expected to generate reliable thermodynamic data for T<300°C. As temperature and pressure approach the critical point, the changes in the density and solvent properties of water render extrapolations based upon the Criss Coble entropy correspondence principle inapplicable to these conditions.

Thus, for T > 300°C, the complexity arises when attempting to determine the thermodynamic functions of ionic species under hydrothermal conditions. As with extensions to subcritical

temperatures below 300°C, the extension of the Gibbs energy function to near-critical and supercritical temperatures for solid species can be accomplished through direct integration of molar heat capacity functions, because such insoluble solid species are always at unit activity. For dissolved ionic species, however, these thermodynamic data are unavailable at elevated temperatures, either subcritical or supercritical. Moreover, for T > 300°C, these data may not be generated through simple extrapolations of ionic entropies to elevated temperatures, as accomplished through the Criss Coble correspondence. This is because the thermodynamic stability of dissolved ionic species is fundamentally affected by the changing density and solvent properties of the aqueous medium for hydrothermal conditions, where T > 300°C. Thus for dissolved ionic species in hydrothermal aqueous systems, it is necessary to determine thermodynamic functions using thermodynamic models modified to account for the changing density and solvent properties of the medium. These models give equations of state modified to account for the physical properties water in the near-critical and supercritical state [28].

Potential-pH diagrams at temperatures and pressures in the vicinity of the critical point of water first appeared in 1989, and were presented by Huang *et. al.* for iron alloys in supercritical water [24]. However these initial constructions under supercritical conditions were carried out using the "entropy correspondence principal" of Criss and Coble [5], the use of which is absolutely not justified for near critical and supercritical conditions. In their development of potential-pH diagrams for Fe-H_2O in supercritical water [25], Kriksunov and Macdonald addressed the problem of determining elevated temperature (subcritical and supercritical) thermodynamic data for ionic species by applying a more recent model developed by Helgeson, *et al.*, in the 1980's [29]. This model gives an equation of state that is valid for both subcritical and supercritical systems. In general, this equation of state is valid for supercritical systems because it splits the partial molal properties of an aqueous ion into solvation and non-solvation contributions:

$\overline{B}_j^\circ = \Delta\overline{B}_{n,j}^\circ + \Delta\overline{B}_{s,j}^\circ$ From Cline, (2000), Reference [28].

B represents an arbitrary state function. The subscript " n,j" represents the non-solvation contribution, and the subscript "s,j" represents the solvation contribution, for species "j". This equation of state, known throughout the literature as the Helgeson-Kirkham-Flowers (HKF) equation of state [29], determines thermodynamic functions of ionic species by considering both of these contributions: The solvation contribution is determined using a modified Born equation (Born, 1920) accounting for electrostatic interaction between ion and solvent. The non-solvation contribution, representing intrinsic properties of the ion in the solvent and the mechanical effects of the solvent on the ion, is determined through temperature-dependent and pressure-dependent state functions. Although it was originally developed with an emphasis on high-temperature and high-pressure aqueous geochemical systems, its application can be extended to supercritical water oxidation systems, as both applications deal with hydrothermal aqueous environments. This equation of state was used by Macdonald to calculate ΔG° for the appropriate reactions, assuming four solid species (Fe, FeO, Fe_2O_3, Fe_3O_4) and two ionic species (Fe^{2+} and Fe^{3+}).

The Helgeson model [29] was applied to the Fe-H_2O system over the temperature range, from 100°C to 500°C and pressures from 300 bar to 1,000 bar. All ionic species were assigned a molal-based activity of 10^{-6}. Water and solid species were assumed to have unit activity. The potential-pH diagrams derived using this model are presented in reference [25]. When the

potential-pH diagrams derived using this model are compared with those available in the literature for subcritical temperatures, where T < 300°C, computed using the entropy correspondence principal of Criss and Coble, the results are found to be in good agreement. Additionally, for Fe, the domain of thermodynamic immunity decreased significantly with increasing temperature for T > 300°C. However, the region of possible protection through the formation of passive oxide layers shifted to lower pH values with increasing temperature over 300°C. This is particularly relevant to the SCWO process, which maintains low pH values under highly oxidizing conditions, rendering passivity the only feasible means of corrosion mitigation. Macdonald also constructed the potential-pH diagram for Ni-H_2O, given in Figure 2-4 at T = 450°C and P = 500 bar [26, 27], by applying the Helgeson model to the Ni-H_2O system for these supercritical conditions. Currently, the data on the Ni-H_2O system is limited to these T and P conditions. Moreover, the diagram given Figure 2-4 lacks the key equilibria for several soluble ionic and insoluble passive oxide species (e.g. Ni_3O_4, Ni_2O_3, NiO_2), due primarily to a lack of thermodynamic data for these species under supercritical conditions.

2.5 Assessing Chemical/Electrochemical Conditions in SCWO Environments (Macdonald and Kriksunov)

Macdonald and Kriksunov have developed techniques for measuring pH, oxygen content, hydrogen content, and redox potential in supercritical aqueous environments [30, 31]. Measurement techniques were applied to high subcritical and supercritical aqueous solutions for temperatures up to 530°C. The standardization of pH and the development of a viable pH scale in supercritical water were addressed as a means of a providing reliable and accurate assessment of pH conditions in the supercritical regime. This is particularly important in light of all the work carried out over the past several decades in the construction of potential-pH diagrams at elevated temperatures and pressures, both subcritical and supercritical: The ability to conduct on-line monitoring of actual pH and redox parameters is essential in order to conduct reliable assessments of the chemical and electrochemical conditions in the SCWO process environment. The central issue in this research is the ability to assess whether or not electrochemical thermodynamic conditions are favorable from the standpoint of active-passive corrosion behavior. An overview of the work follows:

Knowledge of actual chemical and electrochemical thermodynamic parameters, such as pH, oxygen content, hydrogen content, and redox potential, is of particular importance for SCWO systems because the corrosion of constructional materials in the SCWO environments is invariably tied to acid attack under highly oxidizing conditions. YSZ (Yttria-Stabilized Zirconia) ceramic membrane based pH sensors and External Pressure Balanced Reference Electrodes (EPBRE) were implemented for measuring these chemical and electrochemical parameters in supercritical aqueous systems.

These researchers have recognized that the effective implementation of this method required establishing a pH scale for supercritical aqueous solutions. This pH scale is based upon a pH standard for aqueous solutions at supercritical conditions. The pH value at supercritical conditions is based upon the molal scale, whereby hydrogen ion, H^+, activity is computed with

respect to molal concentration (mol/kg), as opposed to molar concentration (mol/l), which is the basis for hydrogen ion activity under ambient conditions. This is necessary due to the large volume fluctuations with pressure under supercritical conditions. The pH scale is defined with respect to the pH of a standard solution in a similar manner to subcritical solutions: The pH of any test solution is determined by measuring the potential (E) of the cell comprised of a pH-sensitive electrode, which has been calibrated in some standard solution and a pH-independent reference electrode. However, under supercritical conditions, difficulties arise from the choice of standard solutions due to extreme fluctuations in fundamental properties of water with pressure, poor electrolyte dissociation, and low activity coefficients. Thus, specification of a universal standard solution under supercritical conditions becomes extremely difficult. This problem was addressed through the arbitrary definition of a scale based upon available estimates of dissociation constants and activity coefficients for .01 molal standard solutions of HCl and NaOH at some predetermined supercritical temperature and pressure. This allows for complete solubility and yields reliable model estimates for the dissociation constants and activity coefficients.

A complete understanding of pH scales and the methodologies for pH standardization under hydrothermal conditions requires some discussion of the physical chemistry of acid dissociation under these conditions and the implications on measured pH values in the near-critical and supercritical regime. Basically, the near-critical and supercritical states exhibit physical properties, such as density and dielectric constant, that change drastically as a function of small changes in either temperature or pressure. This results in drastic changes in the extent of acid dissociation with respect to temperature and pressure. Moreover, under supercritical conditions the extent of dissociation does not correlate directly with the stoichiometric acid concentration in the solution. Thus the physical properties of supercritical water effectively buffer pH values under these conditions, making pH scales completely dependent on temperature and pressure, as well as representative of different conditions of actual acidity for different T and P conditions. This has the following implications: For a given stoichiometric concentration of acid in a solution at ambient temperature and some given pressure, the pH of the solution increases as the temperature of the solution rises into the near-critical and supercritical regimes, at the fixed pressure. At a fixed supercritical temperature, increasing the pressure results in a falling pH value for a fixed stoichiometric acid concentration. This requires arbitrary definition of pH reference standards for each temperature and pressure. This topic is discussed in further detail Section 2.6.

For the case of 0.01 molal standard solution of HCl, the pH of this standard solution, heretofore designated by $pH_{st\ sol}$, is based upon hydrogen ion activity determined from model estimations through the following procedure: For solutions of HCl, the molal concentration of the hydrogen ion is determined by considering the HCl and H_2O dissociation reactions:

$HCl = H^+ + Cl^-$
$H_2O = H^+ + OH^-$

Solution of the system of equations including mass action constants, mass balance, and charge balance constraints associated with these reactions yields an expression containing the molal concentration of the hydrogen ion (m_{H+}) and its activity coefficient, γ.

For dilute solutions, activity coefficients are estimated using Debye-Huckel theory, the application of which is described in references [30, 31]. These equations yield solutions for the molal concentration and activity coefficient of the hydrogen ion, and the pH of the 0.01 molal standard solution of HCl, $pH_{st\ sol}$, is determined by these quantities.

By applying the Nernst equation to both the standard solution and the test solution, the pH scale is defined as follows:

$$pH = \frac{F}{2.303RT}(E_{ESP} - E_{meas}) + pH_{st.sol} + \frac{1}{2}\log\frac{a_{H2O}^{stsol}}{a_{H2O}}$$

Thus the pH scale is based upon a pH standard determined by hydrogen ion activity in the .01 molal standard solution as determined from the chemical equilibrium model above, where $pH_{st.sol}$ is defined as the negative log of the hydrogen ion activity in the standard solution. E_{meas} is the full cell potential measured in the test solution using the YSZ ceramic membrane pH sensors and external pressure balanced reference electrodes. E_{ESP} represents the effective standard potential, which is determined by a reference measurement of cell potential in the standard solution at the supercritical temperature and pressure. Knowledge of the activity of water, a_{H2O}, in the test solution and standard solution is also required.

Relative measurements of pH were conducted using the YSZ ceramic membrane pH sensors and external pressure balanced reference electrodes in supercritical aqueous solutions in a high temperature test cell described in references [30, 31]. This measurement is represented by the full cell potential response of the YSZ membrane pH electrode and external pressure balanced reference electrode to changes in actual solution pH. Data collected at temperatures of 400, 500, and 525-528°C and pressures of 4200 and 4500 psi are presented in references [30, 31]. A representative pH sensor response curve is given below. The test solution was varied over time between standard acid and base conditions at each temperature-pressure condition. Standard acid and base conditions consisted of the .01 molal HCl and NaOH solutions, respectively. One experiment was carried out using a supercritical aqueous solution incorporating a halogenated organic waste compound characteristic of SCWO organic waste. CCl_4 was hydrolyzed according to the reaction:

$$CCl_4 + 2H_2O = CO_2 + 4HCl$$

The production of HCl, according to this reaction, in the supercritical aqueous solution resulted in a change in solution chemistry from neutral to acidic. The full cell potential showed an immediate response to changes in the test solution pH, for all experiments, thereby demonstrating the viability of this method for monitoring pH in supercritical aqueous solutions. This relative tracking of changes in solution pH (as measured by the full cell potential) is rendered useful when the pH standard for supercritical water described previously is incorporated into the measurements, thereby establishing a viable pH scale. This pH scale may then be applied in the on-line monitoring of solution pH in an actual SCWO process environment at a particular temperature and pressure. In this manner, *in situ* pH data are generated and used

in assessing actual thermodynamic corrosion conditions at a specific location (e.g. specific temperature and pressure) in the SCWO process stream.

Monitoring of the redox parameters: oxygen content, hydrogen content, as well as redox potential, in addition to pH, in high subcritical and supercritical aqueous solutions is important for effective corrosion prevention and control in the SCWO process environment. A sensor for monitoring oxygen, hydrogen, and redox potential was implemented in high subcritical and supercritical aqueous solutions. This sensor is based on a combination of two electrodes structurally combined into one unit: an YSZ ceramic membrane pH electrode and a Pt electrode, which is sensitive to oxygen and hydrogen concentration and to pH. For both hydrogenated and oxygenated environments this sensor measures a potential, ΔE, which is expressed in terms of the thermodynamic fugacities of the dissolved oxygen and hydrogen gases. The hydrogen and oxygen fugacities may therefore be estimated based on the measured potential, independently from the solution pH:

$$\log f_{H_2} = \frac{2F(\Delta E - E^{\circ}_{YSZ})}{2.303RT} + \log a_{H2O}$$

$$\log f_{O_2} = \frac{4F(\Delta E - E^{\circ}_{YSZ} + E^{\circ}_{ox})}{2.303RT}$$

As with the measurements of YSZ sensor response to changes in pH, the response of the sensor to changes in dissolved oxygen and hydrogen concentration was also measured over time for both high subcritical and supercritical aqueous. Macdonald and Kriksunov present the data for the sensor's response to changes in oxygen and hydrogen concentration in references [30, 31], along with the derivations of equations presented above. The sensor was found to respond rapidly to changes in oxygen and hydrogen concentration, which corresponds to the redox potential of the solution. A representative sensor response curve is given below. An empirical calibration function, tying solution redox potential to oxygen and hydrogen concentration still needs to be established.

The integration of the proposed pH standard with reliable techniques for generating *in situ* pH data using the proposed YSZ sensor as a reliable means of responding to changes in the pH of high subcritical and supercritical aqueous solutions is a significant step in the development of reliable corrosion control methodologies. The application of this sensor toward monitoring the concentrations of dissolved oxygen and hydrogen is also an important development, however a reliable calibration function for correlating dissolved gas concentrations with overall redox potential is still needed. The development of methodologies for monitoring chemical and electrochemical conditions in SCWO process environments is important for effective corrosion control: Electrochemical conditions, particularly pH and redox potential, will determine whether thermodynamics favor active corrosion, passivity, or immunity. Thus, these methodologies could conceivably be applied in conjunction with elevated temperature potential-pH diagrams for determining corrosion conditions in the SCWO system.

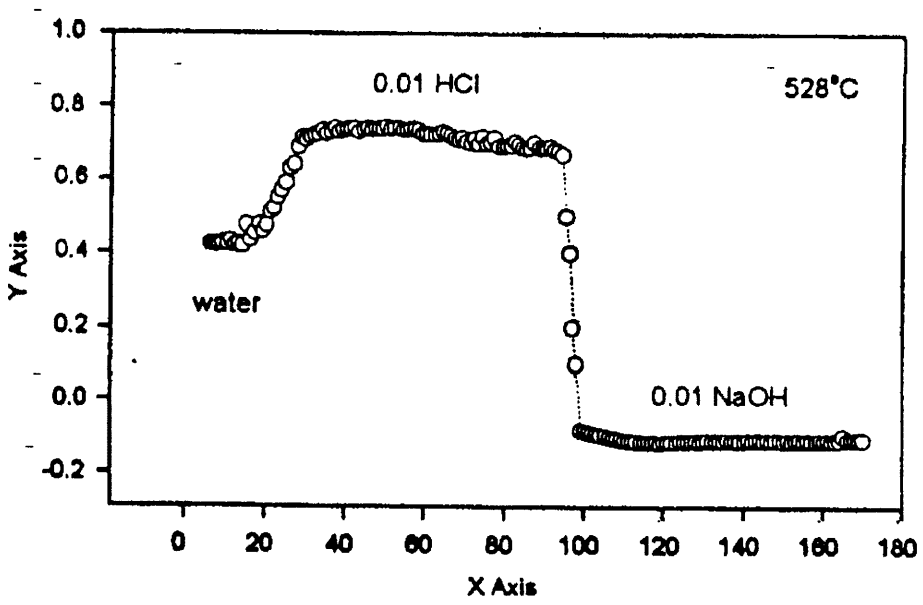

Figure 2-5: Response of YSZ pH sensor to changing solution chemistry, from acidic to alkaline. Sensor potential is indicative of relative changes in pH. From Macdonald, et al. (1995), Reference [30].

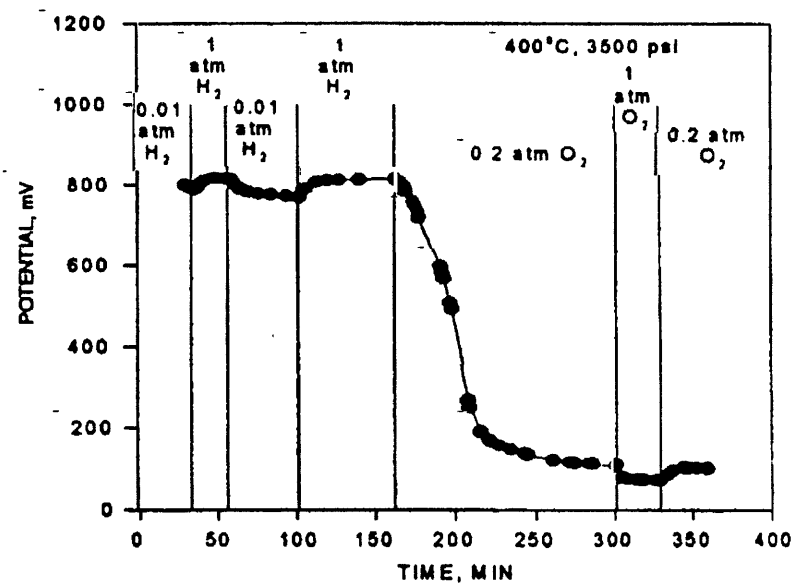

Figure 2-6: Response of YSZ redox sensor to changing partial pressure of oxygen and hydrogen. Sensor potential is indicative of relative changes in solution redox potential. From Macdonald, et al. (1995), Reference [30].

2.6 Physical Chemistry of Acid Dissociation in Supercritical Water – Implications on Supercritical pH Scales (Macdonald and Kriksunov)

Macdonald, *et al.*, has conducted extensive research on the physical chemistry of acid dissociation in supercritical water and the implications this has on chemical conditions and measured pH values in the supercritical state [31]. A full understanding of these concepts requires a brief review of the concept of acid strength in aqueous systems: An acid is defined as a proton (hydrogen ion, H^+) donor. The process of giving up hydrogen ions in aqueous systems is governed by dissociation reaction. Therefore, the strength of some species of acid (as opposed to actual solution acidity) is indicative of the extent to which it dissociates, and donates hydrogen ions to an aqueous solution. The actual acidity of a solution is defined, quantitatively, by the activity of the hydrogen ion in the solution, and the pH scale, for assessing acidity, is defined by $-\log(H^+)$. Thus, the acidity of a solution, measured by pH, is determined by considering the stoichiometric concentration of some species of acid, as well as the extent of the ionic dissociation reaction for that species of acid (e.g. strength of the acid) in the aqueous solution. For strong acids, such as HCl, in aqueous systems under normal ambient conditions, full ionic dissociation is always assumed, and solution acidity (pH) is determined by the stoichiometric concentration of HCl. However, for supercritical aqueous systems, the ionic dissociation of acids such as HCl is incomplete. So a strong acid in ambient solutions does not behave as a strong acid in supercritical solutions.

Incomplete ionic dissociation under supercritical conditions has the following implication [31]: While the pH of pure neutral water, which is defined by $pH = pK_w/2$, is equal to 7 under ambient conditions, this calculated molar scale pH for neutral supercritical water at $T = 528^{\circ}C$ and P= 300 bar is 10.4. This is because even pure neutral water dissociates to H^+ and OH^-, where K_w is the water dissociation constant: For ambient conditions the extent of water dissociation is such that the hydrogen ion activity, (H^+), gives a pH of 7. For the aforementioned supercritical conditions, the extent of the water dissociation reaction is significantly limited by the lower density and solvent (ionic dissociation) properties, thus resulting in lower hydrogen ion activity and correspondingly higher pH.

Thus, in general, for supercritical aqueous systems, a particular value for the pH, based on the molar scale, is indicative of conditions that are significantly more acidic, when compared with normal subcritical aqueous systems exhibiting that same pH value. (The word "normal", in this case, indicates T and P conditions that are well below the critical point.) That is to say, the "meaning" of a particular supercritical pH value is substantially different from the "meaning" of the same pH value, under ambient conditions. A plot of the calculated pH against several molal concentrations of stoichiometric HCl, m°_{HCl}, is shown in Figure 2-7. These calculated pH values were determined by these researchers from calculations of hydrogen ion activity based upon the model estimations discussed in section 2.5. For example, at $T = 525^{\circ}C$ and P = 345 bar, the calculated pH of the 0.01-m standard stoichiometric HCl solution is approximately 8.45. Hence, a pH of 8.45 under these conditions is representative of acidic conditions for this supercritical pressure and temperature, whereas this equivalent pH value under ambient conditions would indicate a weak base.

Clearly, the pH in the supercritical phase is influenced greatly by the degree of acid dissociation, and the extent of acid dissociation, and its resultant influence on pH, is a function of both pressure and temperature (Figure 2-8) – yet, the influences of these respective parameters on acid dissociation contradict one other. That is to say, at a fixed supercritical temperature, lowering of the pressure decreases the fluid density, which results in an increase in the calculated molar scale pH, as shown in Figure 2-9. However, at a fixed supercritical pressure, increasing the temperature likewise decreases the fluid density, resulting in a corresponding increase in the calculated molar scale pH (Figure 2-9). Most notably, these plots of calculated molar scale pH and acid dissociation as a function of temperature and pressure demonstrate how when solution temperatures are increased for a fixed 0.01 m HCl concentration, the pH values of the solution increase from the expected normal subcritical pH value of 2. Moreover, the extent of the increase in pH with respect to an increase in temperature becomes more drastic at lower pressures. This is a direct result of the influence of pressure on the fluid density, dielectric constant, and ionization constant in the supercritical phase: At a fixed supercritical temperature, higher supercritical pressures correspond to higher fluid densities and correspondingly higher values of the dielectric constant and ionization constant.

Under normal subcritical conditions it can always be assumed that, for a strong acid such as HCl, complete acid dissociation occurs. Therefore, as the stoichiometric concentration of an acid, namely HCl, is increased in the ambient solution, the activity of the hydrogen ion, H^+, increases in direct proportion, and the pH, defined by $-\log (H^+)$, decreases in a logarithmic manner. However, in the supercritical phase incomplete acid dissociation plays a dominant role in determining the actual degree of acidity in the solution: As the molal concentration of stoichiometric HCl rises, the degree of dissociation of HCl decreases. This is a direct implication of the density, dielectric, and ionization properties of water in the supercritical phase. Thus, for hydrothermal conditions, Macdonald, *et al.*, recognized the need for an independent reference standard for measurements of hydrogen ion activity. A reliable pH standard must take into account these fundamental differences in the properties of supercritical water, where acid dissociation decreases and increases as respective functions of temperature and pressure in the supercritical phase. This makes it necessary to incorporate an independent reference standard for each set of supercritical T and P coordinates.

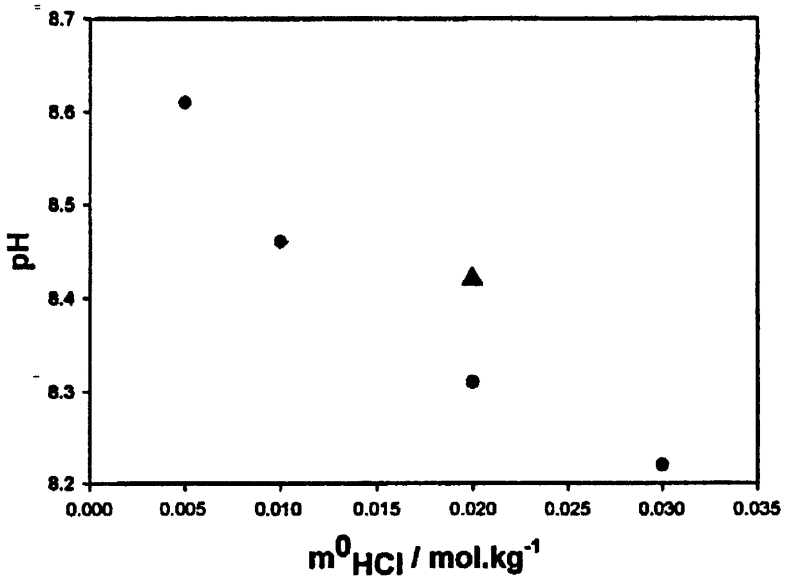

Figure 2-7: Calculated pH of standard supercritical HCl solutions for several stoichiometric concentrations of HCl at T = 525°C and P = 345 bar. From Macdonald, (2001), Reference [31].

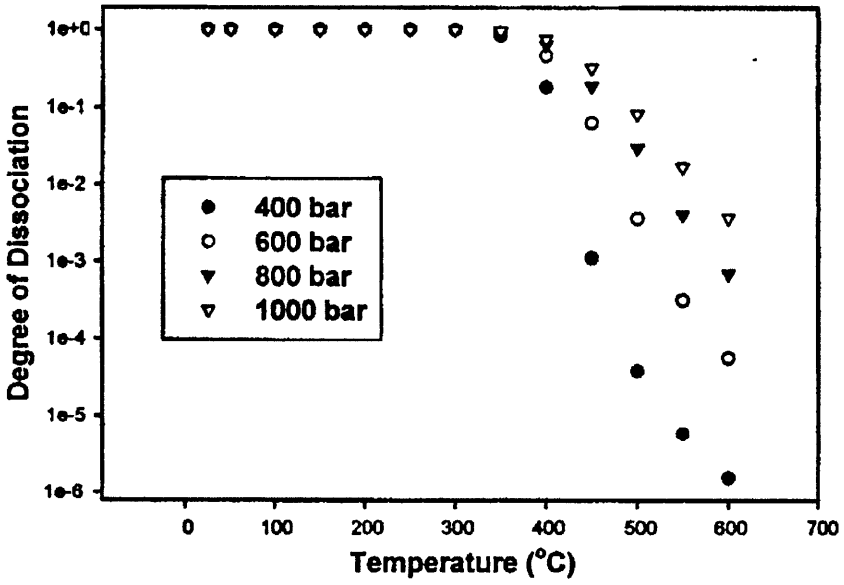

Figure 2-8: Calculated degree of dissociation for a 0.01 molal HCl standard solution as a function of temperature and pressure. From Macdonald, (2001), Reference [31].

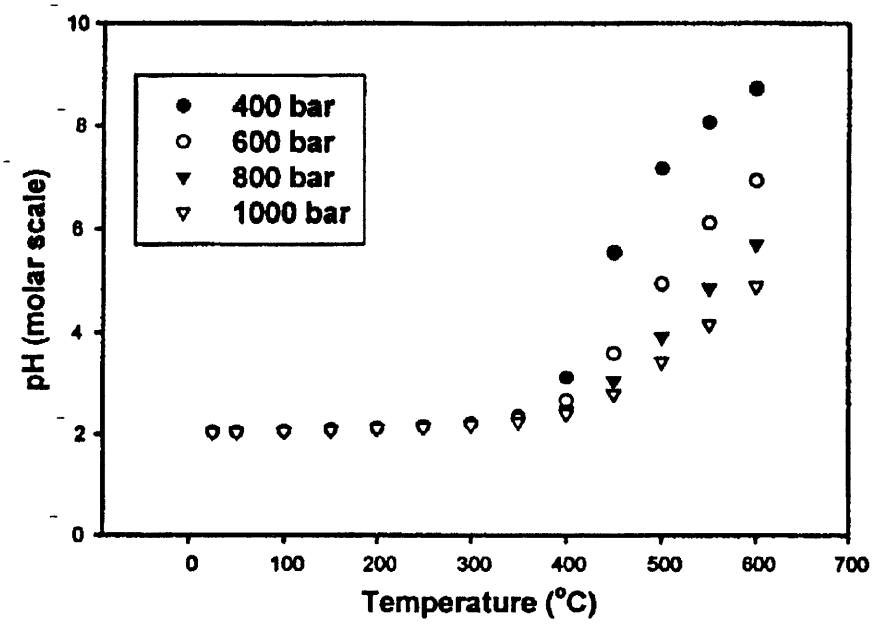

Figure 2-9: Calculated molar scale pH for a 0.01 molal HCl standard solution as a function of temperature and pressure. From Macdonald, (2001), Reference [31].

2.7 Electrochemical Kinetics

Thermodynamics will determine the conditions for phase stability. Thermodynamics will not determine the rate at which the system proceeds to its stable or equilibrium state. The problem of determining the rate at which a system proceeds to equilibrium is consigned to the realm of kinetics. The rates of electrochemical oxidation reactions which give rise to either active corrosion or passive formation of oxidized surface films are exclusively kinetic issues. Hence, a brief review of electrochemical kinetics is in order. A more detailed discussion of this topic is given in references [2, 3].

The rate of an electrochemical reaction is equivalent to the rate of electron transfer, or current flow, from anode (oxidation site) to cathode (reduction site). For a corrosion reaction, electrochemical current density, usually measured in A/cm^2, is directly proportional to the rate of dissolution of the metal per unit area, and therefore directly proportional to the rate of penetration into the metal surface. Electrochemical reactions, resulting in corrosion and/or passivation of the metal surface, will proceed when the metal surface is anodically polarized with respect to its environment. Polarization, η, is the potential change, E – e, from the equilibrium half-cell electrode potential, e, resulting from a half-cell electrochemical reaction at the surface of the metal. Both the cathode and the anode are located on the electrically conductive surface of the metal. Therefore, steady state conditions will result in a common corrosion potential on the metal surface, E. When this occurs both anode and cathode are polarized, and are therefore no longer at the equilibrium half-cell potentials. There is now a driving force for oxidation at the

anode and reduction at the cathode. This results in the flow of electrons through the metal from anode to cathode, which is manifested through the measurement of corrosion currents.

It is important to note that corrosion currents appear in both the active and passive states. However, due to the presence of the protective oxidized film, the passive dissolution rate is always several orders of magnitude less than the active dissolution rate. This is observed in the sharp drop-off in the corrosion current density as anodic polarization brings the corrosion potential at the metal surface up to a value where the passive film is stable. This behavior is observed in electrochemical polarization studies conducted for metals exhibiting active-passive behavior; for effective corrosion mitigation it is desirable to bring the surface potential of the metal into the passive state through anodic polarization. The resulting corrosion currents are orders of magnitude less than those that are characteristic of active dissolution. Highly oxidizing conditions, such as those encountered in SCWO, will often result in this very important kinetic transition. The maximum in the active corrosion current density before the drop-off in corrosion current to a value characteristic of the passive state occurs at a potential designated as the "primary passive potential". As anodic polarization brings the corrosion potential at the metal surface above this "primary passive potential" the passive film becomes stable, and the metal has transitioned to the state of passivity.

Details pertaining to instrumentation and experimental procedures for electrochemical polarization measurements are discussed in references [2, 3]. Briefly, these measurements may be carried out under controlled current (galvanostatic) conditions or controlled potential (potentiostatic) conditions. In order to derive electrochemical polarization curves for alloys exhibiting active-passive behavior, it is necessary to use potentiostatic instrumentation because on an anodic polarization curve for an alloy exhibiting active-passive behavior, current is a single-valued function of potential, however potential is not a single-valued function of current. In this manner, a potentiostat controls the open circuit potential between the test alloy, designated as the working electrode, and a reference electrode by automatically adjusting an applied current. This current, which is applied through an auxiliary electrode, polarizes the working electrode to the set potential, which is measured with respect to the reference. The open circuit potential, which is equal to the corrosion potential on the surface of the working electrode, is initially set in the active state. This potential is gradually stepped up to progressively higher set points, and the applied current that achieves this potential is recorded at each step. When the potential reaches a value characteristic of the primary passive potential, the measured applied current reaches a local maximum. As the potential is increased above this value, the applied current drops off significantly, and the current follows a curve characteristic of the passive behavior for the alloy under test.

Research pertaining to the kinetics of corrosion in SCWO systems may be classified into two categories: actual corrosion monitoring through electrochemical polarization experiments and theoretical prediction of SCWO corrosion based upon a chemical kinetic model. Both topics are important in developing a better understanding of active-passive behavior in the SCWO environment and explaining the regions of the SCWO process stream where constructional materials are most susceptible to attack. The review of these topics primarily follows the work of Kriksunov and Macdonald at Pennsylvania State University [26, 31, 32]. Earlier

experimentation, conducted by Huang, *et al.*, dealing with electrochemical polarization studies of corrosion for iron alloys in supercritical water is also addressed [33].

Oxidizing conditions can give rise to anodic polarization, and therefore an increase in the oxidizing power of the solution can bring the surface potential into the range required for passivity. This forms the basis for corrosion mitigation within the SCWO environment for most of the candidate constructional alloys, particularly stainless steels and nickel base alloys. Hence, it is desirable to have a thorough understanding of active-passive corrosion rates for these candidate alloys. In order to fully assess the active-passive corrosion behavior of candidate alloys in these environments, electrochemical polarization studies are necessary.

The electrochemical polarization experiments carried out by Huang, et al., in 1989 included the first electrochemical measurements of metal corrosion in supercritical water [33]. Electrochemical potentiostat measurements were performed for the corrosion of iron, carbon steel, and stainless steels in pure water, at temperatures and pressures ranging from ambient to supercritical. Measurements were carried out in a stainless steel high pressure, high temperature cell capable of sustaining the high temperatures and pressures required for bringing the electrolyte into the supercritical state. The iron base alloy test specimen served as the working electrode and the body of the cell served as the auxiliary electrode. A silver/silver chloride electrode was employed as a reference. His findings indicated a drop-off in corrosion currents, measured in both the active and passive regions, as the temperature approached the critical point.

Macdonald and Kriksunov have developed techniques for corrosion monitoring in near-critical and supercritical aqueous environments through electrochemical polarization studies at temperatures ranging from ambient to supercritical [26, 31]. These electrochemical polarization studies of nickel were carried out in deaerated .01 m NaOH, over a temperature range from 20–430°C and at a pressure of 345 bar. The polarization measurements were performed in a stainless steel, high-temperature/high-pressure test cell. The nickel working electrode and platinum counter electrode were placed in an alumina holder, which was then placed in the test cell. The cell was filled with electrolyte and brought up to the desired temperature and pressure. A silver/silver chloride external pressure balanced electrode was employed as the reference electrode.

These electrochemical polarization experiments carried out on nickel in high temperature solutions, both subcritical and supercritical, investigated the correlation between solution temperature and passivity range, as well as the correlation between solution temperature and corrosion current density in the passive state. These experiments demonstrated that both the potential range for passivity and the corrosion current density in the passive state are strongly dependent on the temperature of the solution. The potential range of passivity decreases steadily with rising temperature from 20°C to 400°C (Figure 2-10), because the stability of the metal oxides in solution is temperature dependent. This was attributed to an increase in the measured primary passive potential with temperature, as well as a decrease in the oxygen overvoltage. At all temperatures, the actual polarization curves indicate that the onset of transpassive dissolution occurs at sufficiently high potentials, however, there is not sufficient data to provide a clear indication that transpassive dissolution is a highly temperature dependent phenomenon, over the temperature range from 300°C to 400°C. Thus, the electrochemical polarization database must be

expanded significantly. This is important, because several researchers have credited general corrosion at high subcritical temperatures to transpassive dissolution of passive films.

Measurements of corrosion current in the passive region as a function of temperature at elevated pressures can shed light on corrosion mechanisms and kinetics in the SCWO process environment. Figure 2-11 shows how the corrosion current density in the passive region increases with temperature in the subcritical regime, reaches a maximum, and then decreases with temperature into the supercritical regime. Researchers have stated that the initial increase in passive current density is due to the effects of increasing temperature on the rate of ionic transport through the oxide film. Measurable corrosion currents appear in the passive region, where protective oxidized films are thermodynamically stable, because metal oxidation reactions in the passive state result in the transport of metal cations through the solid metal oxide/hydroxide film. For the case of solid metal oxide films, these ions then react with oxygen present in the electrolyte to form the solid metal oxide species that constitute the film. However, for this process to occur, there must be some small rate of passive oxide film dissolution, because a perfectly static and stable film that has a "zero" rate of dissolution would eventually prevent further oxidation of the bulk metal, resulting in a "zero" passive current density. Obviously, in practice, this never occurs. Thus, researchers have proposed that the passive current is also determined by the rate of dissolution of the passive oxide film. The rate of passive film dissolution may be proportional to the passive current density. Furthermore, Figure 2-11 shows how the passive current decreases from the maximum as temperatures become supercritical, a trend also exhibited by the calculated relative corrosion current density, which had been shown to reach a maximum in the vicinity of the critical point. Thus the decrease in the density and the decrease in the degree of acid dissociation of water, as temperatures rise above the critical point, may result in a drop-off in relative corrosion rates for both the active and passive states.

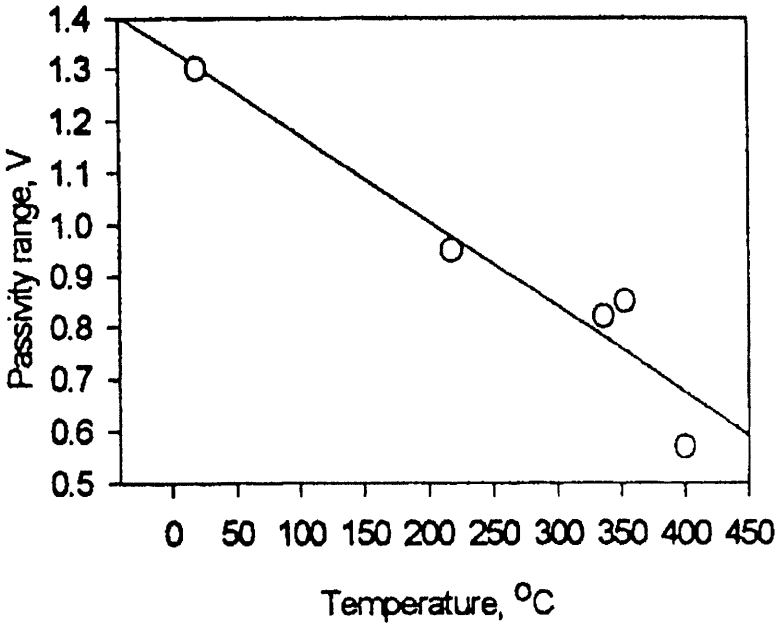

Figure 2-10: Passivity range determined from polarization studies of Ni in 0.01 m NaOH, plotted as a function of solution temperature. From Macdonald *et al.*, (1995), Reference [26].

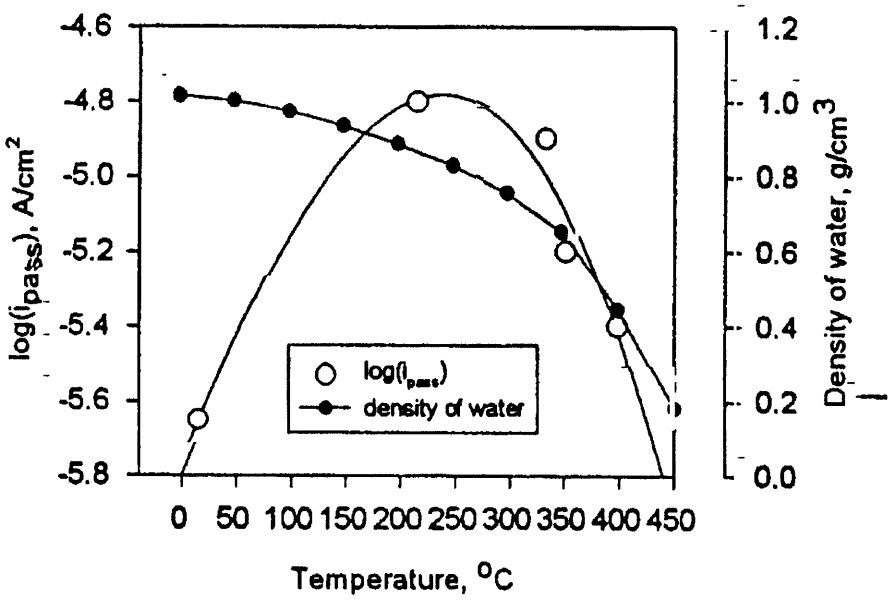

Figure 2-11: Passive corrosion current density for Ni in 0.01 m NaOH, plotted as a function of solution temperature. From Macdonald *et al.*, (1995), Reference [26].

2.8 A Chemical Kinetic Model of General Corrosion Under Hydrothermal Conditions (Macdonald)

L.B. Kriksunov and D.D. Macdonald addressed corrosion in SCWO systems using a theoretical approach and developed a phenomenological model for metal corrosion under hydrothermal conditions. The model seeks to explain the spatial distribution of corrosion damage in SCWO systems in terms of the temperature distribution within the reactor and preheater. Actual corrosion studies of candidate SCWO constructional materials have consistently shown that the most pronounced damage occurs at high subcritical conditions, in the vicinity of the critical point, and not in locations within the process stream where the conditions are exclusively supercritical, although these locations are still highly susceptible. This model provides a quantitative theoretical explanation of this phenomenon, based upon the competing effects between fundamental changes in the properties of water in the vicinity of the critical point and chemical kinetic influences. A detailed discussion of the properties of water at subcritical, near critical, and supercritical conditions is given in chapter 1. Coverage of this topic follows the work presented by Macdonald, *et al.*, in references [26, 31, 32]:

Aggressive species in SCWO processes are generated by the oxidation of organic waste, which is being destroyed in the supercritical aqueous solution. This occurs according to the following reaction:

$$C_aH_bX_c + (a + (b - c)/2)O_2 \rightarrow aCO_2 + [(b - c)/2]H_2O + cH^+ + cX^-$$

In the above reaction, $C_aH_bX_c$ represents a simple hydrocarbon and X represents the heteroatom, which is taken, in this case, to be a halogen such as Fluorine (F) or Chlorine (Cl). When the hydrocarbon oxidation reaction takes place, the halogen, X, converts to halide, X^-, and can persist as an acid in the fluid phase.

This model is based upon the chemical kinetics of the reaction for metal dissolution via oxidation reaction. The metal is assumed to have the same degree of contact with the process environment at all surface locations. That is to say, the model assumes a generalized corrosion morphology, and uniform degradation over the entire metal surface – localized effects are not considered. The model expresses the rate of the corrosion reaction, R, in terms of the concentrations of dissolved oxygen, O_2, and the hydrogen ion, H^+, which are designated throughout as the aggressive species.

$$R = k_c[C_o]^d[C_{H+}]^n$$

k_c is the rate constant for the corrosion reaction, and d and n are the kinetic orders of the reaction with respect to the molar concentrations, C, of dissolved oxygen and the hydrogen ion, respectively.

In order to develop the equations governing the chemical kinetics of the corrosion reation, the model makes the following key assumptions:

First, it assumes that when the SCWO system is operating in a steady state, the steady-state concentration of oxygen is a controlled process parameter. Therefore, the molal concentration of oxygen, m_{o_2}, is constant throughout the system. Hence, the dissolved oxygen concentration profile is fixed with respect to location in the system, and is therefore independent of temperature. This allows for the relative corrosion rate R/R° to be determined by temperature, density, and the molal concentration of H^+, m_{H+}, which is an aggressive species, and the molal concentration of oxygen, m_{o_2}, does not enter into the temperature dependent equation for the relative corrosion rate R/R°.

Secondly, in consideration of completely generalized corrosion morphology, the model assumes corrosion occurs as a result of completely non-localized acid attack, resulting in the following reaction for metallic corrosion:

$$Me + 2H^+ = Me^{2+} + H_2 \qquad \text{or} \qquad Me + 2HCl = MeCl_2 + H_2$$

Thus, H^+ and O_2 are the only designated aggressive species, and Cl^- induced localized attack (e.g. pitting) is not considered. Therefore, the dissolved oxygen concentration and Cl^- concentration do not enter into any of the temperature-dependent rate equations. Additionally, it is assumed, throughout, that the density of the HCl solution is equal to the density of water, ρ, throughout the entire subcritical and supercritical temperature ranges for the SCWO system. Therefore the molar concentration, C, is connected to the molal concentration, m, through the relationship $C_{H+} = \rho m_{H+}$. The molar concentration of H^+, C_{H+}, is replaced by the molal concentration of H^+, m_{H+}, in the rate equation due to the fact that molar concentration is a

volume based quantity, and large volume fluctuations occur in the system at high subcritical and supercritical conditions. Finally, it is assumed that the corrosion reaction at the metal surface follows first order reaction kinetics, and d = n = 1.

Given these key assumptions the following substitutions are made into the rate equation, given above:

$k_c = k_c^\circ \exp(-E/RT)$
$C_{H+} = \rho m_{H+}$
$d = n = 1$

The molal concentration of dissolved oxygen drops out of the equation by expressing the relative (or reduced) corrosion rate, R/R°, where R° represents the corrosion reaction rate at some reference temperature. When this is done, the temperature-independent molal concentration of dissolved oxygen cancels out. The end result is an equation expressing the relationship between the relative corrosion rate, R/R°, in terms of the molal concentration of H^+, density of water, and temperature:

$$\log (R/R^\circ) = \log [m_{H+}/m_{H+}^\circ] + 2 \log [\rho/\rho^\circ] + (-E/RT + E/RT^\circ)$$

Note that the molal oxygen concentration, m_{O_2}, has dropped out of the equation due to its temperature independence as a result of the steady-state assumption described above. The superscript $^\circ$ denotes the value of a variable at some reference temperature. This equation explicitly represents each of the important temperature dependent contributions to the relative corrosion rate in SCWO systems: The first term represents the contribution of the relative molal concentration of aggressive species, H^+, due to changes in the dissociation constants for the dissociations reactions:

$HCl = H^+ + Cl^-$
$H_2O = H^+ + OH^-$

The second term represents the contribution of the relative density of water to the molar concentrations of aggressive species, H^+ and O_2, due to the correlation between molar and molal concentrations given by $C_{H+} = \rho m_{H+}$. Finally, the third term represents the exponential effect of temperature on the reaction rate constant, which takes the form of the familiar Arrhenius dependence for kinetic processes.

The value of m_{H+} is determined by setting up the mass action, mass balance, and charge balance constraint equations for the HCl and H_2O dissociation reactions. These equations are combined into one expression containing m_{H+}, the mean molal activity coefficient, the molal dissociation constant of HCl, K_d, and of H_2O, K_w. The mean molal activity coefficient, $\gamma_\pm$, is estimated using Debye-Huckel theory, and substituted into the expression containing m_{H+}. A detailed description of these equations and the procedure for obtaining activity coefficients can be found in reference [32]. The final equation, used for the determination of m_{H+}, contains m_{H+}, ρ, K_w, and K_d, and is given as equation [21] in reference [32]. Data for K_w and K_d as a function of temperature were determined from the literature.

This equation was solved numerically for m_{H+}. Data for the molal dissociation constants, K_d and K_w as a function of density and temperature were obtained from literature sited in reference [32]. The molar concentrations of the hydrogen ion, C_{H+}, are determined from the molal concentrations, by applying $C_{H+} = \rho m_{H+}$.

A numerical solution for log (C_{H+}) versus temperature is shown in Figure 2-12. At subcritical temperatures below 300°C the decrease in the molar concentration of H^+, C_{H+}, with temperature is minimal. However, as the critical temperature is approached, above 300°C, the decrease in the hydrogen ion concentration with temperature becomes much more pronounced. Above the critical temperature, the decrease in C_{H+} is very large. These plots were made at pressures of 500 and 1000 bars for two molal HCl concentrations: $m_{HCl} = 0.01$ and $m_{HCl} = 0.1$. The Figure 2-12 model predicts that this one order of magnitude change in HCl concentration would have a minimal effect upon C_{H+} at supercritical temperatures. Thus, at supercritical temperatures, the concentration of aggressive species, H^+, is effectively buffered by the supercritical conditions. The rapid decrease in the concentration of aggressive species in solution with increasing temperature at temperatures near and above the critical point, as predicted by Figure 2-12, is caused by the combined effects of the decrease of the dissociation constant of the electrolyte, resulting in a decrease in acid dissociation with temperature, and the decrease in the solution density, ρ, with increasing temperature at temperatures near and above the critical point.

The relative corrosion rate, expressed in the model as log (R/R°), was determined based on the data for molal concentration of H^+, the density of water, and temperature through the equation derived for the relative corrosion rate. Plots of log (R/R°) versus temperature are shown in Figures 2-13 and 2-14 at pressures of 500 bars and 1000 bars, respectively. The value of log (R/R°) increases with increasing temperature below the critical point. However, in the vicinity of the critical point, it reaches a maximum, and then decreases with temperature in the supercritical regime. This is explained by the competing influences of the exponential dependence of the rate constant, k_c, on temperature and the rapid decrease in log (C_{H+}) in the vicinity of and above the critical point with temperature. Clearly, upon examination of Figures 2-12 through 2-14, the exponential increase in k_c with temperature has overwhelming influence on the increase in the relative corrosion rate with temperature at subcritical temperatures below approximately 300°C, due to the relatively small decrease in the concentration of H^+ with temperature over this subcritical temperature range.

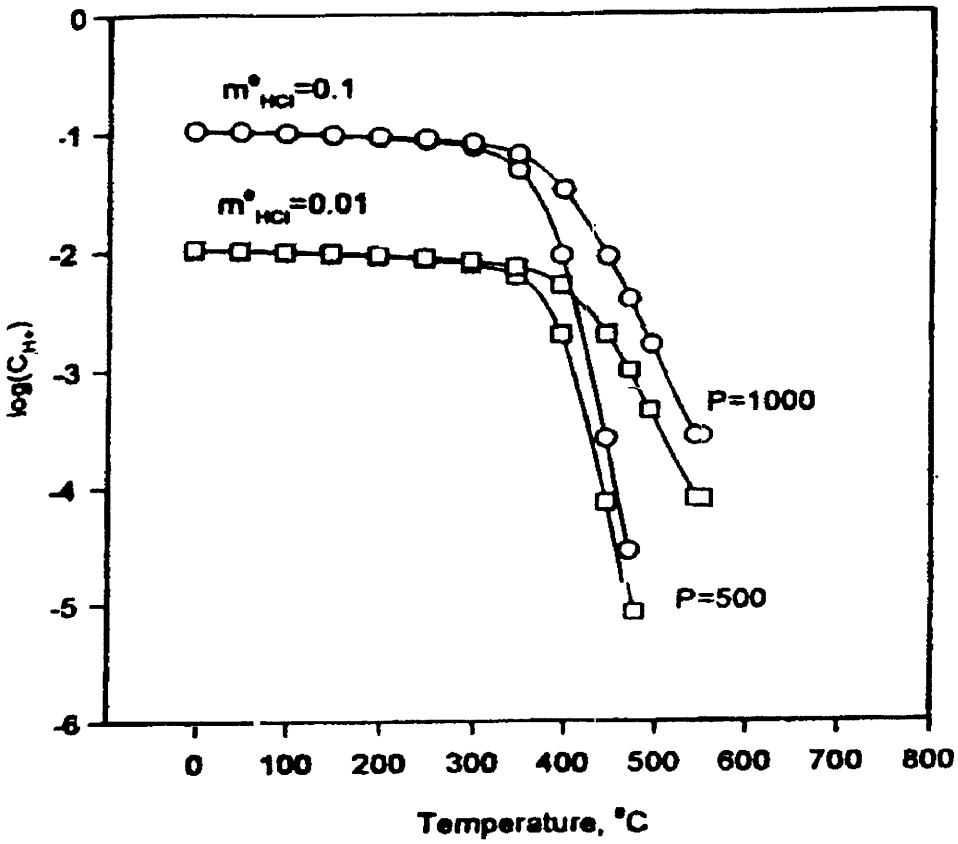

Figure 2-12: Molar concentration of hydrogen ion (C_{H+}) versus temperature for two molal concentrations of HCl, $m^{\circ}_{HCl} = 0.1$ and $m^{\circ}_{HCl} = 0.01$ at pressures, P = 500 bars and P = 1000 bars. From Macdonald, *et al.* (1995), Reference [32].

However, when the temperature exceeds 300°C, the drastic falloff in the density and ionic dissociation property of water as a function of temperature cause a correspondingly drastic falloff on the concentration of aggressive species, C_{H+}. This has a progressively greater influence on the relative corrosion rate with increasing temperature above 300°C, and at supercritical temperatures, cause the relative corrosion rate to fall rapidly with rising temperature. Effectively, the "non-polar dense gas" properties of supercritical water are preventing acids from fully dissociating, which, when with the lower density of the aqueous medium, prevents the rapid oxidation and dissolution of the metal. However, at a higher pressure (Figure 2-14), the density water is greater, and the effects of this rapid decrease in the relative corrosion rate are not as pronounced.

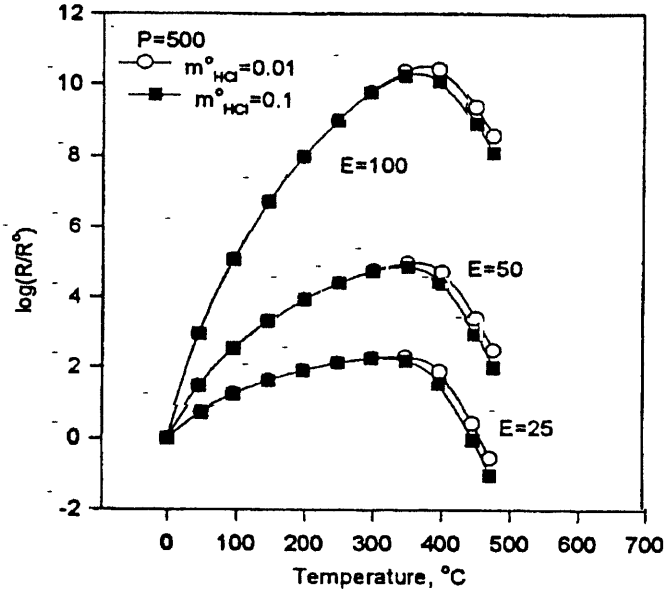

Figure 2-13: Relative corrosion rate (R/R°) vs. temperature for two molal concentrations of HCl, $m^{\circ}_{HCl} = 0.1$ and $m^{\circ}_{HCl} = 0.01$ at pressure, P = 500 bars and activation energies of corrosion, E = 25 kJ/mol, 50 kJ/mol, 100 kJ/mol. From Macdonald, *et al.* (1995), Reference [32].

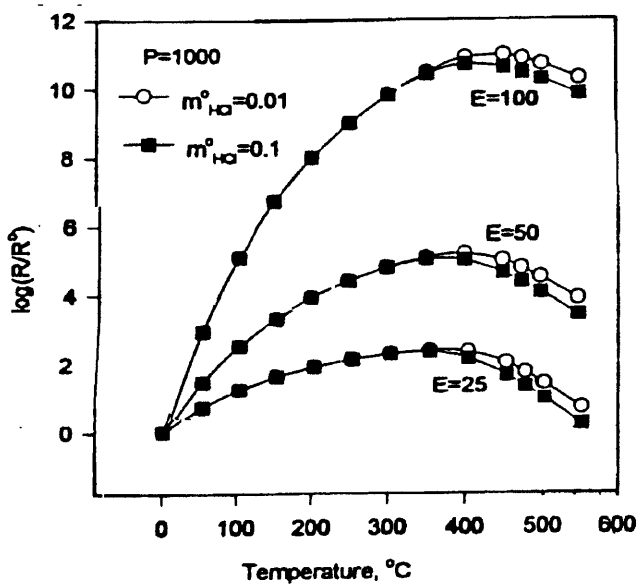

Figure 2-14: Relative corrosion rate (R/R°) vs. temperature for two molal concentrations of HCl, $m^{\circ}_{HCl} = 0.1$ and $m^{\circ}_{HCl} = 0.01$ at pressure, P = 1000 bars and activation energies of corrosion, E = 25 kJ/mol, 50 kJ/mol, 100 kJ/mol. From Macdonald, *et al.* (1995), Reference [32].

2.9 Summary

The goal of this section was to provide a comprehensive review of the key scientific principles that are relevant to the broad issue of corrosion control in supercritical water oxidation systems. These principles include the development of potential-pH diagrams at elevated temperatures and pressures, measurement and standardization of electrochemical parameters in supercritical aqueous environments, electrochemical polarization studies, and theoretical modeling based upon the chemical kinetics of the general corrosion reaction. The first two topics can be broadly classified as thermodynamic issues, whereas the later two may be broadly classified as kinetic issues. Active-passive behavior is intimately linked to both thermodynamics and kinetics. Successful corrosion mitigation requires a fundamental understanding of these issues in SCWO process environments. There are several important conclusions that should be drawn from the discussion of these scientific principles:

At this point it is appropriate to empathize that the terms "SCWO system" or "SCWO process" are meant to designate all components of the entire process for hazardous organic waste destruction, including feed streams, preheaters, transfer lines, cool down heat exchangers, and the actual SCWO reactor. Clearly, when viewed in this context, the SCWO process environment spans a temperature range extending from ambient well into the supercritical regime. Indeed, the most pronounced corrosion damage to constructional materials has been consistently shown to occur in the high subcritical regime through the exposure studies conducted at various laboratories. The theoretical basis for this corrosion performance was addressed, to a large extent, by the phenomenological models of Kriksunov and Macdonald. These simulations of the chemical kinetics for general corrosion reactions demonstrated that the competition between the effects of decreasing concentrations of aggressive species, H^+ and O_2, as a result of decreasing water density and acid dissociation, and the exponential (Arrhenius) increase in the corrosion reaction rate constant with temperature, result in a maximum relative corrosion rate in the vicinity of the critical point. The investigations demonstrating this behavior through actual exposure studies will be addressed in the following chapters.

There is still a lack of fundamental knowledge pertaining to the thermodynamic and kinetic issues discussed. The thermodynamic database is somewhat extensive for temperatures less than 300°C, although there is still a need for potential-pH diagrams specifically addressing alloy-water systems, and the possibility of passive protection through binary metallic oxides. The thermodynamic database for temperature in excess of 300°C is severely limited. There is still a significant need for electrochemical polarization studies of candidate metals and alloys over the entire SCWO temperature spectrum under various chemical conditions. Finally, effective monitoring of corrosion conditions requires significant research dedicated to the development of pH scales for hydrothermal aqueous systems and establishing a reliable calibration function correlating dissolved gas concentrations with overall redox potential.

REFERENCES – Chapter 2

1. M. Pourbaix, *Atlas of Electrochemical Equilibria in Aqueous Solutions*, Pergamon Press, New York, 1966.
2. D.A. Jones, *Principles and Prevention of Corrosion*, 2nd Edition, Prentice Hall, Upper Saddle River, NJ, 1996.
3. M.G. Fontana, *Corrosion Engineering*, 3rd Edition, McGraw-Hill, New York, 1986.
4. M. Pourbaix, *Atlas of Electrochemical Equilibria in Aqueous Solutions*, NACE, Houston, 1974.
5. C.M. Criss, J.W. Coble, J. Amer. Chem. Soc., 86 (1964), pp. 5385 and 5390.
6. H.E. Townsend, "Potential-pH Diagrams at Elevated Temperature for the System Fe-H_2O," Corrosion Science, 10 (1970), pp. 343-358.
7. R.J. Biernat, R.G. Robins, Electrochem. Acta, 17 (1972), p. 1261.
8. D. Lewis, J. Inorg. Nucl. Chem., 33 (1971), p. 2121.
9. R.L. Cowan, R.W. Staehle, J. Electrochem. Soc., 118 (1971), p. 557.
10. D.D. Macdonald, G.R. Sherman, P. Butler, Atomic Energy of Canada Ltd., Report Nos. 4136 through 4139 (1972).
11. D.D. Macdonald, P. Butler, Corrosion Science, 13 (1973), p. 259.
12. D.D. Macdonald, Corrosion Science, 16 (1976), p. 461.
13. D.D. Macdonald, B.C. Syrett, Corrosion, 35 (1979), p. 471.
14. J.B. Lee, "Elevated Temperature Potential-pH Diagrams for the Cr-H_2O, Ti-H_2O, Mo-H_2O, and Pt-H_2O Systems," Corrosion, 37 (8) (1981), pp. 467-481.
15. H.S. Betrabet, W.B. Johnson, D.D. Macdonald, W.A.T. Clark, "Potential-pH Diagrams for the Tantalum-Water System at Elevated Temperatures," in Equilibrium Diagrams, *Proc. Int. Symp. Electrochem. Soc.*, eds. R.P. Frankenthal, J. Kruger, (Pennington, NJ: The Electrochemical Society, 1984), p. 83.
16. G.J. Theus, P.L. Daniel, S.L. Harper, C.M. Chen, D. Cubicotti, T.O. Passell, "Computer-Calculated Potential-pH Diagrams to 300°C – Applications to Corrosion in Power Plant Generating Systems," in Equilibrium Diagrams, *Proc. Int. Symp. Electrochem. Soc.*, eds. R.P. Frankenthal, J. Kruger, (Pennington, NJ: The Electrochemical Society, 1984), p. 95.
17. J.T.N. Atkinson, "Development of High-Temperature Pourbaix Diagrams," in Equilibrium Diagrams, Proc. Int. Symp. Electrochem. Soc., eds. R.P. Frankenthal, J. Kruger (Pennington, NJ: The Electrochemical Society, 1984), p. 175.
18. P. Duby, "Graphical Representation of Equilibria in Aqueous Systems at Elevated Temperatures," in High-Temperature High-Pressure Electrochemistry in Aqueous Solutions, NACE-4 (Houston, TX: NACE, 1976), p. 353.
19. "Diagrams of Chemical and Electrochemical Equilibria," Proc. NATO Advanced Research Workshop, eds. M. Pourbaix, A. Pourbaix, Brussels, Belgium, 1981 (Brussels, Belgium: CEBELCOR, 1982), p. 296.
20. D. Cubiccotti, Corrosion Science, 44 (1988), p. 875.
21. D. Cubiccotti, J. Nucl. Mater., 167 (1989), p. 241.
22. D. Cubiccotti, J. Nucl. Mater., 201 (1993), p. 176.
23. D.B. Mitton, P.A. Marrone, and R.M. Latanision, "Interpretation of the Rationale for Feed Modification in SCWO Systems," J. Electrochem. Soc., 143 (3) (1996), p. L59.

24. S. Huang, K. Daehling, T.E. Carleson, P. Taylor, C. Wai, A. Propp, "Thermodynamic Analysis of Corrosion of Iron Alloys in Supercritical Water," in Supercritical Fluid Science and Technology, eds K.P. Johnston, J.M.L. Penninger, ACS Symposium Series 406 (Washington DC: ACS, 1989), p. 276.
25. L.B. Kriksunov and D.D. Macdonald, "Potential-pH diagrams for Iron in Supercritical Water," Corrosion, 53 (8) (1997), p. 605.
26. L.B. Kriksunov and D.D. Macdonald, "Corrosion Testing and Prediction in SCWO Environments," *Proceedings of the ASME Heat Transfer Dividison*, Heat Transfer Division (Am. Soc. Mech. Eng.), Vol. 317-2 (1995), pp. 281-288.
27. D.D. Macdonald, *et al.*, "Supercritical water oxidation studies: understanding the chemistry and electrochemistry of SCWO systems", Pennsylvania State University Final Report to the US Army Research Office, Grant Nos. DAAL 03-92-G-0397 and DAAH 04-93-G-0150, February, 1997.
28. J.A. Cline, "Experimental and *Ab* Initio Investigations into the Fundamentals of Corrosion, in the Context of Supercritical Water Oxidation Systems," PhD thesis in Chemical Engineering, Massachusetts Institute of Technology, Cambridge, MA, (2000).
29. H.C. Helgeson, K.D.H. Kirkham, G.C. Flowers, American Journal of Science, 281 (1981), p.1249
30. L.B. Kriksunov and D.D. Macdonald, "Understanding Chemical Conditions in Supercritical Water Oxidation Systems," *Proceedings of the ASME Heat Transfer Division*, Heat Transfer Division (Am. Soc. Mech. Eng.), Vol. 317-2 (1995), pp. 271-279.
31. L.B. Kriksunov and D.D. Macdonald, "Probing the chemical and electrochemical properties of SCWO systems," Electrochimica Acta, 47 (2001), pp. 775-790.
32. L.B. Kriksunov and D.D. Macdonald, "Corrosion in Supercritical Water Oxidation Systems: A Phenomenological Analysis," J. Electrochem. Soc., 142 (12) (1995), p. 4069.
33. S. Huang, K. Daehling, T.E. Carleson, P. Taylor, C. Wai, A. Propp, "Electrochemical Measurements of Corrosion of Iron Alloys in Supercritical Water," in Supercritical Fluid Science and Technology, eds K.P. Johnston, J.M.L. Penninger, ACS Symposium Series 406 (Washington DC: ACS, 1989), p. 276.
34. L.B Kriksunov and D.D. Macdonald, *Proceedings of the 1st International Workshop on Supercritical Water Oxidation*, Jacksonville, FL, (1995) (Lake Bluff, IL: WCM Forums, 1995).
35. L.B. Kriksunov, C. Liu, and D.D. Macdonald, "Oxygen, hydrogen, and redox potential combination sensors for supercritical aqueous systems," *Proc. 1st International Workshop on Supercritical Water Oxidation*, Amelia Island Plantation, FL, (1995).
36. L.B. Kriksunov and D.D. Macdonald, "Understanding corrosion in high subcritical and supercritical aqueous environments," *Proc. 1995 Summer National Meeting of AIChE*, Boston, MA, (1995).
37. J.W. Johnson, E.H. Oelkers, H.C. Helgeson, Computers and Geosciences, 18 (1992), p. 899.
38. J.C. Tanger, H.C. Helgeson, Amer. J. Sci., 281 (1988), p. 19.
39. E.L. Shock, H.C. Helgeson, Geochem. Cosmochim Acta, 52 (1988), p. 2009.

Chapter 3

Corrosion Phenomena and Materials Performance in SCWO Process Environments

3.1 Overview

The various corrosion phenomena that have been observed and studied in SCWO process environments, both real and simulated, will be addressed in this chapter. These modes of attack can be understood in the context of thermodynamics, kinetics, and active-passive behavior. For example, electrochemical polarization studies, which provide actual measurements of active-passive corrosion rates as a function of corrosion potential at elevated temperatures, can indicate the extent of passive film stability for particular metals and alloys at elevated temperatures. This can help to explain the observed temperature-dependent transitions in corrosion morphology. Also, the selective dissolution of certain metallic elements observed during alloy C-276 exposure studies can be rationalized on a thermodynamic basis. Finally, the kinetic models of general corrosion, developed by Macdonald, which account for decreasing acid dissociation and decreasing water density as a function of temperature, for hydrothermal conditions, explain why degradation is far less extensive in regions of the process exposed to supercritical temperatures. Thus, the topics covered in the previous chapter form a necessary framework for understanding and affecting corrosion phenomena and ultimately, materials performance.

This chapter also presents an overview of materials performance in SCWO process environments. Many of the studies addressed in this section assess corrosion behavior by conducting material exposure studies in simulated SCWO feeds, as opposed to actual SCWO process streams, which produce corrosive species through oxidation of actual organic feeds, although both of these methodologies have been utilized. With respect to studies of material corrosion behavior in simulated feeds – these simulated feeds incorporate all of the most aggressive aspects of actual SCWO feeds: High temperatures and pressures, highly acidic and oxidizing conditions, and for most studies, significant chloride concentrations. Several studies of corrosion have also been carried out in feeds containing sulfates or phosphates, as opposed to chloride. However, studies of corrosion behavior in non-chlorinated feeds are less extensive because non-chloride species are generally not as aggressive. For simulated SCWO feeds, aggressive species are added directly to aqueous streams and are not generated through the oxidation of hydrocarbons.

3.2 Experimental Design

A number of different experimental designs have been employed specifically for studying the corrosion performance of candidate SCWO constructional materials. These bench-scale experimental setups differ significantly from the more generic SCWO process flowsheets and designs, which were originally developed to test the SCWO concept for waste treatment, and were not developed specifically for studying the corrosion performance of constructional materials. As the need for detailed studies of the corrosion behavior of candidate constructional materials became evident, bench-scale experiments were designed specifically to study this issue under chemically aggressive conditions at high temperatures and pressures. Some experiments were designed for simulated SCWO feeds, while others were designed to test corrosion performance under actual SCWO process conditions. The general SCWO process design is discussed in Chapter 1. Other bench scale experiments have been designed specifically to study the reaction kinetics and mechanisms for hydrolysis and oxidation of hydrocarbons in supercritical water. Such studies are beyond the scope of this review. Hence, the reader is referred to references [1-3] for descriptions of these experiments.

The experimental design employed by Cline and Mitton, *et al.*, is given in references [4-6]. This experimental apparatus was specifically designed as a "cooling-tube experiment" for investigating the effects of key SCWO process variables on the corrosion performance of Hastelloy C-276 tubing. This experimental work was prompted by the failures of Hastelloy C-276 coiled preheater heat exchanger tubing that occurred during the supercritical hydrolysis and oxidation reaction kinetics experiments mentioned above. The apparatus employed 3 feed streams: 2 containing deionized water, and one containing dilute aqueous hydrochloric acid. A detailed description of this apparatus, along with schematics, can be found in references [4-6]. Dilute hydrochloric acid pressurized at room temperature was mixed with deionized water after it was pressurized and preheated to 500°C in a 4:1 (water to acid) ratio such that the pH of the acidic test solution was 2.0, when measured under ambient conditions. Atmospheric oxygen in the feed solution served as the only source of O_2 for maintaining oxidizing conditions. Pressure throughout the system was maintained at 24.6 MPa (246 bar) (3600 psig). Preheating, mixing, and transfer of the test fluid to the test section all occurred in autoclave components that were insulted. The cooling-tube test specimen consisted of a test section of C-276 alloy tubing. Thus, the pressure tube test section formed the non-insulated component of the reactor autoclave, which allowed for the analysis of corrosion along the length of tube to be carried out over a range of temperature: from the supercritical to the subcritical, by virtue of the ambient cooling of the tube along its length. Two different diameters of C-276 tubing was tested: 1/16'' and 1/8'' outer diameter, with .010'' and .035'' wall thickness, respectively. The tubes were welded and solution annealed. The tube test specimens sustained the full system pressure of 246 bar (3600 psig). Thus the C-276 alloy, from which the tubes were constructed, was subjected to the tensile stress conditions associated with tubular pressure vessels, and was therefore susceptible to stress corrosion cracking (SCC), as a potential mode of attack. The solution entered the test section from the transfer line at a supercritical temperature of 395°C, and was cooled along the length of the test section by exposure of the test section to ambient air. Seven thermocouples were placed

at measured locations along the test section to monitor temperatures at each of these locations. Temperature, as measured by the thermocouples, decreased as a function of position along the test section to a subcritical value of 292°C, measured by the seventh thermocouple at the low-temperature end of the test section. After passing through the test section, the flow was cooled to room temperature and sent through a back-pressure regulator, where it was depressurized, and then proceeded to effluent storage, for chemical analysis.

The apparatus employed by Kritzer, *et al.*, shown in Figure 3-1 is also based on the pressure tube test specimen concept. A detailed description of this apparatus is given in references [7-9]. This apparatus was employed in studies of the corrosion performance of Alloy 625 in oxidizing aqueous solutions containing chlorides (HCl in the feed stream) or sulfates (H_2SO_4 in the feed stream). This design utilizes pressure tube test specimens for reasons similar to those described above: The experiments were able to cover an extended range of temperature from room temperature up to his maximum experimental temperature of 500°C. As in the experiments carried out by Mitton, *et al.*, the test specimen served as the test section component of the autoclave, and was therefore subjected to the full system pressure, thereby subjecting the specimen to stress conditions, similar to those described above. The tubes were 1000 mm (39.4'') long, with 14.3-mm (0.56'') outer diameters and 8.5-mm (0.33'') inner diameters. The tube specimens were solution annealed. Studies of the corrosion performance of Alloy 625 in aqueous solutions of hydrochloric acid also incorporated test coupons that were placed inside the test tube specimens. Unlike the experimental design utilized by Mitton, *et al.*, temperature variation along the length of the actual tube test section was accomplished by electrical heating of the actual pressure tube test specimen, and each heating block (preheater and heater) was equipped with several thermocouples. The length of each of the two heating blocks was 200-mm (7.9''), and therefore the actual test section was only a fraction of the full 1000-mm tube length. The ends of the tube, which were outside of the heating zone, were maintained at room temperature by two water-cooled Cu blocks. System Pressure was maintained at 38 MPa. Experiments were run for up to 800 hours. Hydrogen peroxide (H_2O_2) was used as the O_2 source. This was accomplished by decomposition of the H_2O_2 into O_2 and water in the low temperature section of the apparatus, after pressurization. H_2O_2 and HCl (or H_2SO_4) were part of the same feed solution.

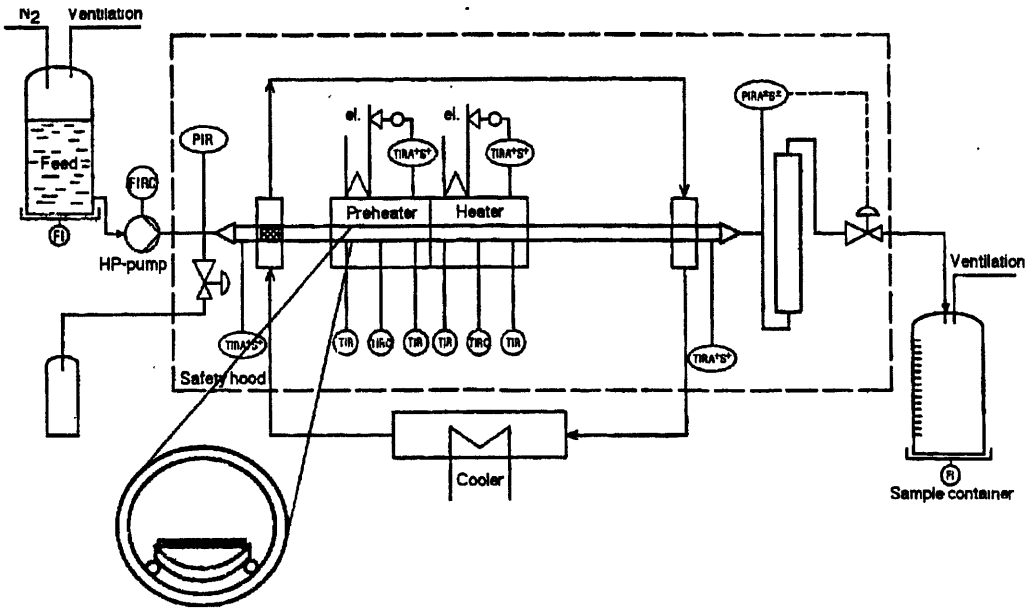

Figure 3-1: Experimental apparatus for corrosion studies of Alloy 625 utilizes pressure-bearing tubes as test specimens. Total test section length: 400 mm = 200 mm preheater section + 200 mm heater section. From Kritzer, *et al.* (1998), Reference [7].

An experimental SCWO reactor design often employed for testing the corrosion of coupon specimens employs a reactor vessel consisting of two tubes arranged in a coaxial configuration, with two separate coaxial streams. Generally, the purpose of this design scheme is to minimize corrosion through the use of a "floating type" corrosion resistant inner ceramic (Al_2O_3) tube within an outer pressure-bearing alloy tube. The outer alloy tube serves the exclusive purpose of bearing the full system pressure. The pressure-bearing outer alloy tube does not come into contact with any corrosive species. A chemically inert annular stream of deionized H_2O flows through the outer alloy tubing and over the outer surface of the inner ceramic tubing at the same pressure and flow rate as the corrosive aqueous SCWO reactant stream, flowing through the inner ceramic tube. Therefore, the pressure exerted by this inert annular stream of deionized H_2O on the inner ceramic tube cancels the internal pressure exerted inside the inner ceramic tube by the SCWO reactant stream. The result is that the corrosion resistant inner ceramic tube is not subjected to any significant tensile stress. This design concept was introduced by Casal, *et al.* as a possible alternative for the design of a SCWO system with acceptable overall corrosion resistance [10]. An example of this design scheme, employed by Konys, *et al.* in their studies of alloy corrosion [11] is given in Figure 3-2.

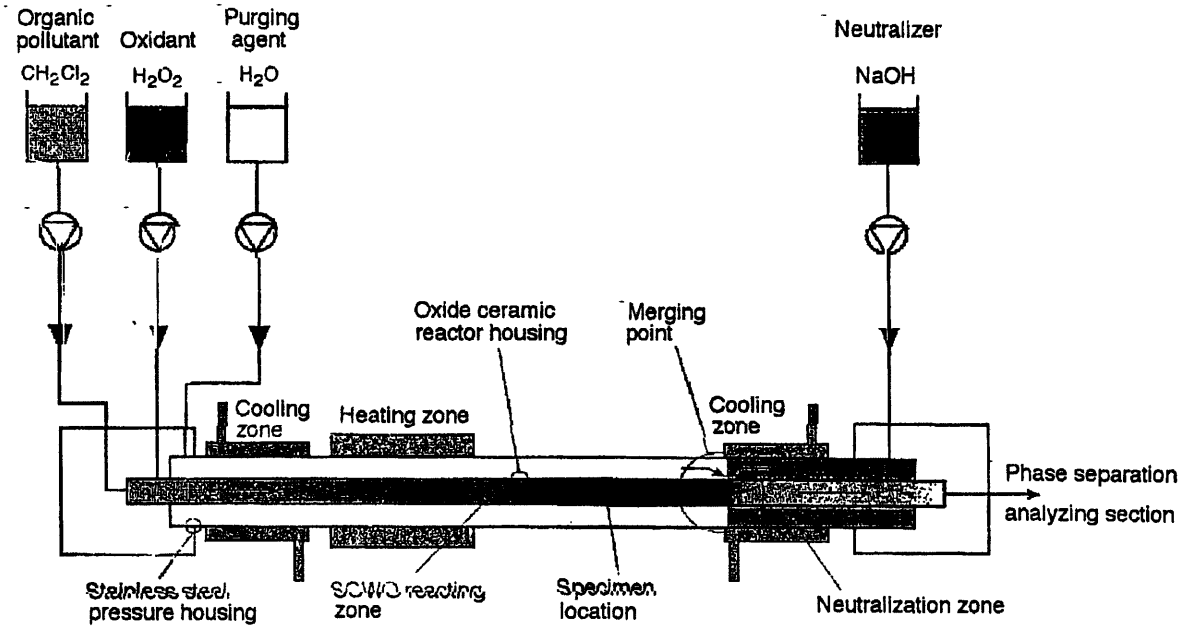

Figure 3-2: Schematic of the SUWOX III reactor utilized to study alloy corrosion under real SCWO conditions. The reactor employs a stainless steel pressure-bearing outer tube and a corrosion resistant inner tube fabricated from Al_2O_3. The tubes are place in a coaxial configuration, with an annular stream of deionized H_2O flowing through the outer stainless steel tube and over the outer surface of the inner ceramic tube. The annular stream of deionized H_2O is maintained at the same pressure and flow rate as the SCWO reactant stream, flowing inside the ceramic tube. Thus, the pressure on the outside of the inner ceramic shell cancels the internal pressure of the reactant stream so that the inner ceramic shell is not subjected to significant tensile stresses. From Konys, *et al.* (1999), Reference [11].

The experiments carried out by Kritzer, *et al.* to study "transpassive dissolution" of Alloy 625, chromium, nickel, and molybdenum in high-temperature solutions containing oxygen and hydrochloric acid did not employ pressure tube test specimens. Instead, coupons of each element and alloy were placed inside a reactor with the design scheme similar to the one discussed above, consisting of a corrosion-resistant ceramic inner tube inside an outer pressure-bearing alloy tube. Deionized water was flowed between the inner alumina tube and the outer nickel alloy tube. Other aspects of the experimental design were similar to those described above. A detailed description of this experiment can be found in reference [12]. The experimental design employed by Boukis, *et al.*, in the study of the corrosion of high-performance ceramics also utilized this coaxial reactor design [13].

At this point, it is appropriate provide a detailed explanation of the chemical conditions employed as part of the experimental design for studies of corrosion behavior and material performance in SCWO process environments, both real and simulated. In the absence of external control of feed stream pH through the addition of neutralizing agents (e.g. caustic species) to acidic influents, the SCWO of hydrocarbons containing chlorine heteroatoms will give rise to the formation of hydrochloric acid (HCl) in high temperature aqueous solutions under conditions that are highly oxidizing. With respect to the degradation of the process unit, these high temperature oxidizing HCl solutions are considered to be representative of the most aggressive conditions arising from the SCWO of organic waste compounds. This is because, under normal circumstances, the dissociation of HCl in high-temperature solutions results in dissolved ionic species H^+ and Cl^-. H^+ is clearly an aggressive species due to the effects of acid attack under highly oxidizing conditions; such conditions preclude any possibility of thermodynamic immunity to corrosion for even the mot noble metals. The presence of chloride (Cl^-) anions in solutions at high oxidizing potentials can cause localized destruction of passive oxidized films, giving rise to localized effects such as pitting and stress corrosion cracking (SCC). The formation of other acids, including H_2SO_4, H_3PO_4, in SCWO process streams can also result in general corrosion of constructional alloys. This is known to occur for sulfuric acid (H_2SO_4) solutions. However, the high temperature sulfate and phosphate solutions formed by the dissociation of both of the respective acids generally do not result in localized phenomena, such as pitting and SCC. This is likely due to the fact that sulfate and phosphate anions do not readily attack the passive film in preferred locations. For these reasons, the vast majority of studies related to material corrosion in simulated SCWO process streams and virtually all studies dealing with localized effects such as SCC and pitting involve chloride containing solutions.

3.3 Pitting

Stainless steels and nickel-base alloys, under highly oxidizing conditions at subcritical temperatures, are susceptible to pitting. Pitting is highly localized degradation, resulting in the formation of pits, which penetrate rapidly into the metal. Pits are often of small surface area, and hence, difficult to detect. In most cases, this form of environmental degradation is attributed to localized penetration of the passive film. Hence, conditions must be sufficiently oxidizing to allow for the metal to be maintained in a state of passivity. Usually, localized penetration of the passive film is due to chloride (Cl^-) attack, and pit initiation generally requires a high chloride concentration at the surface of the passive film in a preferred location. The Cl^- anion concentration increases at the passive surface as the potential increases to a critical value, E_{pit}, by redox reaction. This is thought to result from the electrostatic attraction of the Cl^- anion to the positively charged surface. At sufficiently high chloride concentrations in preferred locations, the passive film is degraded at these preferred locations until the metal surface is directly exposed to the oxidizing environment, thereby allowing for active anodic dissolution of the metal at the preferred location. Once the passive film has been penetrated and pitting initiates, high chloride concentrations inside the newly forming pit prevent the metal from reforming insoluble passive oxidized compounds at this location, thereby allowing aggressive species to oxidize the

exposed metal inside the pit to form soluble metal ionic species, resulting in further penetration into the surface. Thus the exact mechanism of pitting, though still not completely understood, is completely different from the mechanism for general corrosion: In general corrosion, aggressive species, including dissolved oxygen and hydrogen ions, are cathodically reduced directly at the metal surface, and localized penetration of a passive film does not occur. However, pitting does generally does involve acid attack in preferred locations, once chlorides have induced localized destruction of the passive film – Pitting corrosion is often suppressed in alkaline solutions [14]. Therefore, for localized pitting to occur the following conditions must be met: sufficiently oxidizing conditions that favor passivity, low pH values, high chloride concentrations, and high temperatures. A complete background on pitting phenomena is given in references [15–19].

The theoretical kinetic models proposed by MacDonald and Kriksuov [20] do not take this form of attack into consideration. As previously discussed in Section 2.8, the chemical kinetic equations used by MacDonald are based upon the general corrosion reaction, whereby the hydrogen ion, H^+, and dissolved oxygen, (O_2), are cathodically reduced at the metal surface, for acidic oxygenated solutions. These models do not consider halogen anions, such as Cl^-, to be an aggressive species. However, the SCWO constructional materials are clearly susceptible to this form of attack: Highly oxidizing conditions, low pH values, high temperatures, and high chloride concentrations, due to the production of HCl by the supercritical oxidation of many organic hydrocarbons, all make SCWO constructional materials extremely susceptible to pitting, particularly in regions of the preheater, where temperatures fall in the range of 150°C to 250°C [21–31]. Localized pitting was only observed in acidic aqueous solutions containing chlorides. In the absence of chlorides, localized pitting was not observed, and either dealloying or general corrosion at higher temperatures were the predominant forms of attack. Kritzer, *et al.* has observed that for alloy 625 in oxygenated chloride-containing solutions, the localized pitting morphology transitions to a general corrosion morphology as temperatures exceed 250-300°C. Kritzer, *et al.* has proposed that as temperatures exceed 250°C, non-localized breakdown of the passive film initiates due to the onset of "transpassive dissolution" of the chromium(III) oxide layer, and localized pitting gives way to general corrosion as the primary mode of attack for oxygenated HCl solutions. General corrosion and the proposed "transpassive" breakdown of passive chromium(III) compounds will be discussed in subsequent sections. It should be noted that, at these higher temperatures, chlorides were still found to affect the rate of this general corrosion: In the absence of chlorides, localized pitting was not observed and general corrosion was somewhat suppressed for many solutions, but high temperature general corrosion morphologies were similar for oxidized solutions of HCl, H_2SO_4, and HNO_3 [32–35]. For non-oxygenated HCl solutions, pitting was rarely observed [22, 36].

3.4 Dealloying

Dealloying is the preferential dissolution of one or more elemental components in an alloy, due to the greater susceptibility of these elements to corrosion. For a susceptible alloy immersed in a chemically aggressive environment, certain elemental components are often more active, electrochemically, compared with other elements. Thus, the more active elemental components are in galvanic contact with the more noble elemental components, and preferential anodic

dissolution of the more active elements can occur, which gives rise to dealloying. Dealloying can also occur when thermodynamics favor the formation of insoluble "passive" oxide or hydroxides for one or more elements, with active dissolution being favored for other elemental components. Mitton, *et al.* observed this later form of dealloying for Hastelloy C-276 tubing at high subcritical temperatures for simulated SCWO feeds containing chlorides [37, 38, 39]. A more extensive background on dealloying is given in references [15 and 16].

Bramlette, *et al.*, first recognized the issue of dealloying as a potential contributor to the environmental degradation of SCWO system constructional materials in 1990 [40]: The selective dissolution of chromium and molybdenum in Alloy 625 and the selective dissolution of chromium, molybdenum, and tungsten in C-276 were sited as potential corrosion issues. Rice, *et al.*, confirmed this in 1993 through experiments investigating the destruction of Navy wastes using SCWO technology [41]. The effluent analysis conducted during these experiments suggested selective dissolution of chromium for non-chlorinated feed solutions and selective dissolution of the base element, nickel, for chlorinated feeds. Subsequent research confirmed this behavior: Mitton, *et al.*, carried out extensive metallographic analysis of failed C-276 preheater tubes from methylene chloride (CH_2Cl_2) hydrolysis and oxidation kinetics experiments in 1995. This analysis revealed that the corroded inner layer of the C-276 preheater tubing was enriched in chromium and tungsten, yet depleted in nickel, iron, and molybdenum [37, 38, 39].

3.5 Stress Corrosion Cracking

When brittle failure of an alloy occurs under constant tensile stress in a corrosive environment, stress corrosion cracking (SCC) is often said to have occurred. For a component to be susceptible to SCC, it is generally thought that three conditions must be simultaneously present: a corrosive environment, an alloy susceptible to attack in that environment, and a component of constant tensile stress. A specific environment is not required for SCC to occur, and alloys that are highly susceptible in one type of corrosive environment may be completely resistant in another, as many alloys are not universally susceptible to chemical attack in all corrosive environments. Most importantly, the component of constant tensile stress need not be very large. SCC can occur when the tensile stress is less than the yield stress for the alloy. Thus, SCC can be viewed as resulting from the synergistic effects of corrosion in a chemically aggressive environment and mechanical stress. The phenomenon of SCC in chemically aggressive environments at elevated temperatures and pressures will be examined in the context of supercritical water oxidation systems. A description of the SCWO process is given in Chapter 1.

The SCWO of hydrocarbons produces acid under highly oxidizing conditions. For most of the organic wastes targeted for destruction by SCWO, and assuming a significant degree of acid dissociation, the process gives rise to the ionic species, H^+ and generic anion X^-. The SCWO of chlorinated hydrocarbons results in solutions of HCl, and the anion, X^-, takes the form of chloride, Cl^-. Both the hydrogen ion (H^+) and chloride anion (Cl^-), produced by the hydrocarbon oxidation reaction, may be regarded as aggressive species. This is reasonable because conditions are always sufficiently oxidizing such that the metal will undergo either passivation or active corrosion; thermodynamic conditions preclude any possibility of metallic immunity. When

oxidation reactions result in passivity, the passive layer generally consists of one or more insoluble metal oxides or hydroxides. Chlorides (Cl^-) are thought to contribute to the localized instability of these passive insoluble compounds, resulting in the breakdown of the passive film at these preferred locations. Higher temperatures may result in greater passive film instability at preferred locations and correspondingly greater susceptibility to SCC. Thus, stainless alloys (e.g. Ni-Cr and Fe-Cr alloys), which are largely dependent on solid Cr(III) compounds for passive protection, exhibit extremely high susceptibility to SCC in high-temperature, high-pressure acidic chloride-containing solutions, particularly under highly oxidizing conditions, where redox potential approaches the upper "transpassive" limit, and passive films are less stable. Thus, SCWO pressure tubing constructed from stainless alloys is extremely susceptible to SCC.

For an alloy component subjected to the three conditions discussed above, the initiation of SCC cracks at the alloy surface in contact with the corrosive environment becomes a possibility: For the case of SCWO, it is generally thought that these cracks may initiate at grain boundaries, which appear to serve as a channel, allowing the aggressive species in solution to contact the alloy deeper and sooner [42]. For acidic, chlorinated, feed streams, under oxidizing conditions, the aggressive species in solution are: H^+, chlorides (Cl^-), and O_2. As the aggressive species penetrate down the grain boundary channel, they are believed to become highly concentrated within the channel, as corrosion products form on the surface. Therefore, the rate of corrosion within the channel becomes rapid with respect to the surface, allowing the aggressive species to penetrate further. Therefore, it is anticipated that the local chemistry in the channel becomes increasingly acidified and chlorinated. These local conditions are characterized by a local pH and local chloride concentration, which are substantially more aggressive than the conditions of the feed stream solution. Once the local pH and Cl^- concentration reach some critical value, an SCC crack will initiate. Please consult references [42–44] for further background on SCC in SCWO systems.

The propagation of SCC cracks, after crack initiation occurs due to a combination of the stress concentration at the crack front and chemical embrittlement [45]. For the case of SCWO systems, this chemical embrittlement involves active corrosion reactions between the alloy and the aggressive species at the crack front, which have become highly concentrated inside the crack, as discussed above. Furthermore, it is assumed that any passive films have been breached locally. The stress concentration at the crack front helps to promote this chemical embrittlement, and as the crack penetrates further into the alloy, the magnitude of the stress concentration, as given by the stress intensity factor, K_I, increases with the length of the crack. Therefore, higher stress intensities will further promote chemical embrittlement, which causes the crack to propagate further. The synergistic effects of the chemical embrittlement promoted by higher stress intensity factors with increasing crack length, are what cause the crack to propagate under a static tensile stress that is usually less than the yield stress for the alloy. Just as in the case of fracture and fatigue, rapid crack propagation and ultimate failure will occur when the stress intensity factor at the crack front reaches some critical value. A more detailed description of the mechanical aspects of SCC crack propagation is given in references [45, 46, 47].

The corrosion associated with SCC is a localized form of attack and alloys are generally more susceptible to SCC than pure metals. The localized chemical attack associated with SCC results

in brittle failure. Hence, alloys with higher yield strengths will have a greater susceptibility to SCC. SCC can be either transgranular or intergranular, but the crack will always follow a macroscopic path that is normal to the tensile component of the stress, where the cracking has occurred. Passivity is generally a prerequisite for SCC, and the zones of susceptibility to SCC are generally on the boundaries of the passive region on the anodic polarization curve for the alloy. The boundaries of the passive region on the anodic polarization curve represent the regions of potential in which the passive films exhibit instability, and passive film instability is what results in passive film breakdown at preferred locations, resulting in susceptibility to localized attack. Moreover, chlorides are known to contribute to the localized instability of the passive film, and can therefore be viewed as contributing to the passive film breakdown at these preferred locations, in a manner analogous to that observed with pitting. Therefore, just as with pitting, it is ultimately the breakdown in the passive film at preferred locations that can potentially give rise to SCC. A more extensive background on the electrochemical aspects of SCC is given in reference [15 and 16].

Clearly, in SCWO systems, the first two conditions of a corrosive environment and susceptible alloys are immediately met for virtually all candidate constructional alloys. The third condition of constant tensile stress is met for SCWO system components by virtue of the high operating pressures that are required for bringing the aqueous feed streams into the supercritical state. The entire SCWO process is closed cycle, and hence all SCWO system components, including preheaters, transfer lines, reactor, cool-down heat exchanger, and so forth, must contain the corrosive aqueous feed streams under these high pressures. Therefore, the alloys from which these components are constructed are subjected to the third condition of static tensile stress, which is roughly equivalent to the hoop stresses that are generated in pressure vessels. It is noteworthy that stresses within the tubing often fall slightly above or below some nominal value, due to the large volume fluctuations that occur. Therefore, the exact value of the tensile stress experienced by component tubing materials is generally regarded as randomly fluctuating within the vicinity of this nominal value. Furthermore, as the system is brought online and offline for operation and/or experimentation, the stress in the tubing fluctuates between zero and that characteristic of the full operating pressure, as described above. Hence, as the number of operational cycles increases, there is likely to be an impact on the rate of crack penetration into the tube wall. However, detailed studies as to the impact of these issues on SCC in SCWO systems have yet to be addressed.

It has been repeatedly observed by numerous researchers that the worst localized corrosion in SCWO systems tends to occur in the heat exchangers, which includes the preheater and the cool down heat exchanger [42]. In these components temperatures range from ambient to the operating supercritical temperature for oxidation of organic waste. Therefore, throughout substantial sections of the heat exchanger component tubing, temperatures are high but subcritical, thereby making these components highly susceptible to failure by localized attack. This is due to the combined effects of high concentrations of aggressive species, H^+, Cl^-, and O_2 at subcritical conditions (as opposed to supercritical conditions where the lower densities and ionic dissociation constants conspire to drastically lower the concentrations of aggressive species [20]) and the exponential (Arrhenius) increase in the corrosion reaction rate constant with temperature. This results in a set of chemical conditions that are most favorable for sustaining ionic reactions at high rates for high temperatures under subcritical conditions. The

phenomenological model of Macdonald, *et al.*, describes in a quantitative manner, how the aggressiveness of acidic aqueous solutions will increase with temperature for temperatures below the critical point, subsequently reaching a maximum in the vicinity of the critical point, and then dropping off significantly with temperature above the critical point, for a fixed pressure [20].

Unlike general corrosion, localized corrosion is difficult to detect and quantify, as only a very small amount of material is consumed before the process component tubing is compromised. SCC is generally considered to be a localized form of corrosion due to the very small quantities of material that are consumed in the degradation process. SCC is a particularly insidious and dominant mode of attack in SCWO system heat exchanger components, which experience high subcritical temperatures, and has frequently resulted in premature failures of heat exchanger tubing due to the highly localized nature of the corrosion and brittle failure mechanism. Among the potential modes of degradation, SCC appears to be the most likely to result in catastrophic failure of a SCWO system component. Thus, the mitigation and prevention of SCC in SCWO system components represents a particularly crucial objective for SCWO research and development, as the prevention of catastrophic failure has important safety implications.

Nickel-base alloys and other high nickel materials, which have been extensively characterized for corrosion performance in SCWO systems, and have been utilized as constructional materials for bench-scale and pilot-plant SCWO reactors, have been studied in detail for susceptibility to localized attack, particularly SCC. The database on the performance of this class of alloy in simulated SCWO feed streams is far more extensive than for other alloy classes, from the standpoint of SCC as well as other forms of corrosion. Previous research has suggested that these alloys may not be able to withstand the very aggressive SCWO feed streams due to significant weight losses and localized forms of attack that occur in aggressive environments. However, these nickel-base alloys remain a primary candidate constructional alloy for SCWO systems. There are several reasons for this: There tends to be a substantially more extensive amount of research on the high temperature corrosion performance for this class of alloy than for others, as high-nickel alloys are frequently designed for severe service applications. Secondly, this class of alloy, to a large extent, has outperformed other classes of alloys and ceramic materials with respect to corrosion performance in simulated SCWO environments. This has prompted the need for more extensive research into the corrosion performance of nickel-base alloys under such aggressive environments, focusing particular attention on the localized forms of attack described above.

SCC in SCWO systems seems to occur only in system components, where temperatures are high yet subcritical. The main reactor, which experiences only supercritical temperatures does not appear to be highly susceptible, although the potential for SCC in this region cannot be ruled out. SCC requires susceptible metallic components immersed in chemically aggressive environments under a state of constant tensile stress. Therefore, all components must be deemed susceptible, as all components, including the main reactor, meet these three conditions. Significant challenges still remain in the development of a system that is less susceptible to catastrophic failure by SCC. At this point it appears unlikely that a single alloy exists that is resistant to SCC in these systems: This is because virtually all alloys are known to exhibit some form of corrosion under these extremely harsh environmental conditions.

3.6 General Corrosion / Wastage

The phenomenon of general corrosion or wastage is commonly defined by relatively uniform dissolution of the metal or alloy over a large surface area. Ideally, for a metal with a perfectly uniform composition completely immersed in a corrosive environment with corrosion conditions constant over the entire perfectly uniform surface, general corrosion of the alloy would involve the removal of roughly the same amount of material at all locations on the surface. However, such ideal conditions are never encountered in practice, and SCWO process streams are no exception. Accordingly, general corrosion always involves some degree of variation in the extent of dissolution over the surface of the metal or alloy. However, as opposed to localized phenomena such as pitting and SCC, general corrosion involves some degree of material loss over the entire surface, and this is generally accompanied by a measurable decrease in the thickness of the part or component under attack. For metal in the active state, where passive films do not form and thermodynamics favor the stability of dissolved metal cationic species, general corrosion is the expected mode of attack, provided that no coatings or galvanic couples exist. For alloys, it is very important to distinguish between general corrosion and dealloying, because dealloying can result in significant mass loss, without a corresponding decrease in part thickness, as one or more noble or passivated elements will not dissolve, leaving the original dealloyed surface, with a dealloyed layer that is depleted in one or more elements extending into the part.

For a pure metal maintained in the passive state, where oxidized surface films are thermodynamically and kinetically stable, significant mass loss due to general corrosion would not be expected. However for alloys in high-temperature chemically aggressive aqueous environments, such as those encountered in SCWO process streams, the extent of corrosion and the corrosion mechanism are highly dependent on passive film stability. In regions of the process stream where thermodynamics clearly favor the stability of passive oxide films, only localized effects have been observed. However, there have been convincing reports of generalized corrosion morphologies for alloy 625 (Kritzer, *et al*) in regions of the process stream exposed to near-critical temperatures, and, in accordance with these observations, the stability of the protecting passive films have been called into question – For general corrosion to initiate in these environments one of the following events has to occur: First, the passive oxide film may be dissolved over a significant surface area, as a result of "transpassive breakdown". Second, the solid metal oxides may remain stable and insoluble, but the properties of these compounds may change in such a way that the film is rendered ineffective in preventing significant general corrosion. Third, preferential dissolution (dealloying) of elements composing a majority of the weight percentage of the alloy may facilitate removal of the remaining thermodynamically stable solid insoluble "skeletal framework" by some form or erosion. At this point, it is appropriate to emphasize that in high-temperature subcritical solutions, chemical reactions are accelerated, and the transformation of a solid, thermodynamically unstable metal or metal oxide/hydroxide into a dissolved, thermodynamically stable ionic species will occur rapidly. Therefore, if conditions in the aqueous environment change, such that solid species (metals or oxides) are rendered thermodynamically unstable, the high-temperature conditions will facilitate rapid dissolution of these solids. Hence, simultaneous "kinetic stability" along with thermodynamic instability of

solid species is highly unlikely at the elevated temperatures and pressures encountered in SCWO feeds.

Many metals and alloys can exhibit high resistance to corrosive solutions under highly oxidizing conditions provided that anodic polarization is sufficient to bring the surface potential into the passive range. As discussed previously, the oxidized surface films characteristic of the passive state are stable over a limited range of potential. Anodic polarization curves for metals and alloys exhibiting active-passive behavior show a large decrease in the corrosion current density of several orders of magnitude as anodic polarization brings the surface potential above the primary passive potential. This sudden drop in the corrosion current density, as the surface potential passes the primary passive potential, indicates the onset of passivity. The state of passivity will persist over an extended range of potential until an upper limit is reached, at which point, the passive film becomes unstable, and "transpassive breakdown" of the film commences, and corrosion currents increase back up to levels characteristic of active dissolution. Transpassive dissolution of protective oxide films occurs only in the presence of the strongest oxidizers. Several researchers, namely Kritzer, *et al.*, have proposed that transpassive dissolution of solid Cr(III) compounds accounts for the temperature dependent transition from a localized corrosion morphology to one indicative of general corrosion, at high subcritical temperatures [22, 48, 49]. In particular, general corrosion of alloy 625 was reported at temperatures in excess of 300°C. However, there has been no conclusive proof that at these high subcritical temperatures the conditions are sufficiently oxidizing to favor transpassive breakdown. Moreover, the proposed transpassive dissolution phenomenon would occur only in the context of hydrothermal conditions, assuming fixed values for pH and oxygen fugacity. This would clearly indicate that transpassive dissolution is a highly temperature dependent phenomenon. While it is well known that solid oxides/hydroxides become less stable at higher temperatures and higher oxidizing potentials, it has not been proven that a temperature increase within the near-critical regime will destabilize solid Cr(III) compounds. A discussion of transpassive dissolution, specifically in the context of alloy 625 corrosion performance is given in Section 3.10.

The electrochemical polarization experiments carried out by Macdonald, *et al.*, on nickel in high temperature solutions, both subcritical and supercritical, investigated the correlation between solution temperature and passivity range, as well as the correlation between solution temperature and corrosion current density in the passive state. These experiments demonstrated that both the potential range for passivity and the corrosion current density in the passive state are strongly dependent on the temperature of the solution. The details of these electrochemical polarization studies are discussed in Chapter 2. As discussed previously, the potential range of passivity decreases steadily with rising temperature from 20°C to 400°C, because the potential range of stability of the metal oxides in solution is temperature dependent. This was attributed to an increase in the measured primary passive potential with temperature, as well as a decrease in the oxygen overvoltage. At all temperatures, the onset of transpassive dissolution occurs at sufficiently high potentials, however, there is not sufficient data to provide a clear indication that transpassive dissolution is a highly temperature dependent phenomenon, within the near-critical regime.

Furthermore, for the case of the nickel base alloys and stainless steels used in SCWO research, the passive surface films that provide the primary means of protection are known to be primarily solid chromium (III) compounds (CrOOH, Cr_2O_3). The composite potential-pH diagram for Ni, Fe, Cr, Mo constructed by Mitton, *et al.*, shows that in the absence of neutralizing agents, highly acidic (low pH) and moderately oxidizing conditions favor the stability of insoluble chromium (III) compounds and soluble Ni^{2+}, Fe^{2+}, and Mo^{3+}. The cooling tube experiments carried out by these researchers on alloy C-276 have indicated that the primary mode of attack at high subcritical temperatures in the range from approximately 320°C to the critical temperature, are dealloying and SCC. General corrosion was not observed for this alloy at these high subcritical temperatures. Consequently, the results of these cooling tube experiments are rationalized through thermodynamic arguments, which explain that preferential dissolution of Ni, Fe, and Mo occurs because potential-pH conditions favor the thermodynamic stability of solid chromium (III) compounds and dissolved ionic species, Ni^{2+}, Fe^{2+}, and Mo^{3+}. Clearly, these experiments show the predominant mode of attack in the high-subcritical regime to be dealloying, as opposed to the general corrosion reported by Kritzer for alloy 625. It is conceivable that the general corrosion of alloy 625 reported by Kritzer could have arisen from rapid dealloying of Ni as this element composes roughly 60% of alloy 625 by weight. This would be corroborated by the measured concentration of dissolved Ni in the effluent: For acidic, oxygenated solutions of HCl, the relative concentration of Ni in the effluent was effectively 100%, and that of Cr was close to 0%. Clearly, Ni was preferentially dissolved in these studies, and there is very little direct evidence supporting the contention that the observed general corrosion of alloy 625 occurred as a direct result of "transpassive dissolution" of solid Cr(III) compounds. This issue will be revisited in Section 3.10.

3.7 Iron-Base Alloys / Stainless Steels

Stainless steels are the only iron-base alloys that have been considered for application to SCWO process environments: Carbon and low-alloy steels generally have relatively low corrosion resistance and would never withstand the aggressive SCWO process streams. Stainless steels contain moderate to substantial weight percentages of chromium. In general, these chromium additions serve to induce passivity under the acidic and highly oxidizing conditions associated with SCWO. Most of the stainless steels considered for SCWO research fall into the category of austenitic stainless steels, which are widely used in industry for chemically aggressive environments. Austenitic stainless steels contain nickel in addition to the substantial weight percentages of chromium. The nickel additions serve to improve corrosion resistance, which is achieved through the formation of a thin, hydrated, oxidized, chromium-rich, passive surface layer. This passive film is susceptible to pitting, SCC, and crevice corrosion via chloride attack, however molybdenum additions can improve resistance to these effects. In general, the higher the weight percentages of secondary alloying elements, particularly chromium, the greater the corrosion resistance under acidic and oxidizing conditions, particularly in the presence of chlorides.

For the highly aggressive feed streams associated with the destruction of most aqueous organics, particularly those containing high chloride concentrations, most stainless steels are not likely to

exhibit acceptable resistance to corrosion. However, preliminary results have indicated that an iron-base alloy containing high weight percentages of chromium (50% Cr) could possibly perform reasonably well in moderately aggressive environments, although a more significant amount of research is required to confirm this behavior.

The iron-base alloys subjected to the exposure studies carried out in various laboratory-scale SCWO systems are displayed in Table 3-1, along with the weight percentages of the various alloying elements. Note that this list also includes alloys with iron weight percentages less than 50 percent (e.g. Ducrolloy)

Table 3-1: Fe-Base Alloys

Alloys	316-L	F255	20CB3	2205	Ducrolloy
Cr	16-18	24-27	19.55	22.5	50.2
Mo	2-3	2-4	2.13	3.3	
W	-	-			
Co	-	-			
N	-	0.1-0.25		0.18	
C	0.08	0.04	0.02	0.02	
Nb	-	-			
Fe	Bal.	Bal.	Bal.	Bal.	44
Ni	10-14	4.5-6.5	33.55	5.7	
Si	1	1.0	0.36	0.4	
Mn	2	1.5	0.62	0.7	
P	0.045	0.04	0.014	0.025	
S	0.03	0.03	0.0001	0.0002	
Cu	-	1.5-2.5	3.3	0.19	
Other	-	-		0.0008Al	5Al 0.3Ti $0.5Y_2O_3$

The majority of the experimentation dealing with the behavior of stainless steels in simulated SCWO process environments has focused on AISI Type 316-L. However, early experimentation with the SCWO of sludge wastes at a maximum test temperature of 425°C also addressed the behavior Alloy 20CB3 and Alloy 2205: Thomas, et al., reported pitting and crevice corrosion for 316-L in both the subcritical and supercritical regions. For these same conditions, he reported a high susceptibility to pitting for Alloy 20CB3 and reasonable resistance, with the exception of crevice corrosion at attachment points, for Alloy 2205 [50]. AISI Type 316-L stainless steel has been included in a number of additional experiments, primarily as a baseline material. In general, results have suggested that this alloy may be able to withstand innocuous feed streams, where the processing is restricted to low halogen, moderate pH solutions [51]. Several researchers, including Boukis, *et al.*, and Mitton, *et al.*, and subsequently Tebbal, *et al.*, addressed the performance of 316-L in high temperature subcritical and supercritical water within a restricted pH range: This alloy was exposed to deionized water within the temperature range 300-500°C. The overall performance of this alloy within this environment was reasonable,

however localized forms of attack, such as pitting, intergranular corrosion or crevice corrosion have been observed [52, 53]. For feed streams with pH values ranging from 2 to 11, the performance of 316-L was reasonable, with general uniform corrosion rates as low as 0.035 mmpy [52]. However SCC was observed for chlorinated feeds and higher pH values (pH>12) [51]. Mitton, *et al*, later addressed the corrosion performance of Alloys 316-L and Ferralium 255: Alloy 316-L was exposed to a highly chlorinated organic feed stream (0.3 weight % chloride) at 600°C. This alloy demonstrated significant general corrosion, with weight losses on the order of 50 mmpy, and SCC. Ferralium 255 revealed a much lower rate of general corrosion (18 mmpy). However degradation was anisotropic, and more pronounced in the ferrite phase [54, 55]. Konys, et al. recently addressed the performance of Ducrolloy, a relatively new iron-chromium alloy containing 50% Cr and 44% Fe. The results for this alloy indicate good corrosion resistance for chlorinated acidic conditions and exposure times up to 400 hours [56].

The results seem to indicate that certain iron-base alloys may exhibit reasonable performance in relatively innocuous feed streams, where pH values are maintained within a restricted range, and chloride concentrations are relatively low. Moreover, the data seem to confirm the general argument by many researchers that corrosion resistance in acidic high temperature environments, with significant halide concentrations, improves for alloys with higher chromium content. However, it should be emphasized that there is only a limited amount of data for the corrosion performance iron-base alloys in simulated SCWO process environments, and further experimentation is required to confirm these results.

3.8 Nickel-Base Alloys

Nickel-base alloys are widely used in industrial applications requiring corrosion resistance at high temperatures and pressures and are therefore frequently used as constructional materials in SCWO systems. Pure nickel has inherently low active corrosion rates in acidic solutions. When alloyed with elements such as copper, molybdenum, and tungsten, the active corrosion rate is even lower. Highly oxidizing conditions, however, result in a substantial increase in active corrosion rates at low pH values. This problem is resolved to a considerable extent through alloying with large weight percentages of chromium. In highly oxidizing acidic solutions, nickel alloys containing significant weight percentages of chromium (typically 10 – 30 wt. %) exhibit passivity and dramatically improved corrosion resistance in these solutions, due to the presence of chromium. The chromium in these nickel-base alloys forms a chromium-rich, passive oxide film under sufficiently oxidizing conditions. Furthermore, the addition of molybdenum to nickel-base alloys containing chromium results in substantially improved resistance to pitting corrosion in aqueous solutions containing chlorides, which cause pitting corrosion due to localized attack of the passive film. Molybdenum additions also result in improved resistance to stress corrosion cracking (SCC). Chromium is considered to be an essential alloying element for nickel-base alloy constructional materials in SCWO systems, and most of the candidate nickel-base alloys contain large percentages of chromium, due to the highly oxidizing conditions of these environments. Molybdenum is also considered an important alloying element for nickel-base alloy constructional materials in SCWO systems, although not all nickel-base alloys tested in SCWO exposure studies have contained it. The presence of iron in nickel-chromium-iron-

molybdenum alloys can potentially reduce the corrosion resistance when the weight percentages of iron exceed several percent for fixed concentrations of nickel chromium and molybdenum. Large percentages of iron (~30%) with nickel and chromium results in decreased resistance to general corrosion, pitting corrosion, crevice corrosion, and SCC compared with nickel-chromium-molybdenum alloys, where the iron weight percentages are less than a few percent. However, such alloys are still more resistant to these forms of attack than stainless steels.

The nickel-base alloys subjected to the exposure studies carried out in various laboratory-scale SCWO systems are displayed in Table 3-2, along with the weight percentages of the various alloying elements [57]. Note that this list also includes alloys with nickel weight percentages less than 50 percent (e.g. alloy G30).

Table 3-2: Ni-Base Alloys

Alloys	625	C-276	C-22	HR-160	G30	I-686
Cr	20-23	14.5-16.5	22	28	30	20.4
Mo	8-10	15-17	13	1	5.5	16.42
W	-	3-4.5	3	1	2.5	4.06
Co	1	2.5	2.5	30	5	0.04
N	-	-	-	-	-	
C	0.1	0.01	0.01	0.05	0.03	0.01
Nb	3.15-4.15	-	-	1	1.5	0.08
Fe	5	3	3	3.5	15	1.03
Ni	58	56	56	37	43	57.42
Si	0.5	0.08	0.08	2.75	1	0.02
Mn	0.5	0.5	0.5	0.5	1.5	0.23
P	0.015	-	-	-	-	0.006
S	0.015	-	-	-	-	0.001
Cu	-			-	2	0.01
Other	0.4Al 0.4Ti	0.35V	0.35	0.5Ti	-	0.22Al 0.04Ti

For reasons discussed above, nickel-base alloys containing both chromium and molybdenum are generally the most resistant to hydrochloric acid. Due to the presence of chlorides in aqueous solutions and the resulting susceptibility to localized effects, including pitting and SCC, aqueous solutions of HCl are considered to be among the most aggressive from a corrosion standpoint. In actual SCWO process streams, the presence of chloride heteroatoms in the organic waste compound will lead to the formation hydrochloric acid (HCl) as a product of the oxidation reaction in the high-temperature aqueous solution. Chlorides are often found in many of the organic waste compounds that have been sited as candidates for possible destruction by SCWO. Therefore numerous researchers have investigated the corrosion performance of nickel-base

alloys containing high weight percentages of chromium in high temperature subcritical and supercritical aqueous solutions containing hydrochloric acid and dissolved oxygen. Iron-base alloys containing high weight percentages of chromium (~50 % Cr) also have exhibited reasonable corrosion performance under certain conditions. However, the results for these alloys are only of a preliminary nature, and the database is somewhat limited, in comparison to the extensive amount of research carried out on the corrosion performance of nickel-base alloys. Furthermore, as discussed previously the presence of high weight percentages of iron in nickel-chromium-iron-molybdenum alloys can potentially reduce the corrosion resistance. Therefore, based on the current state of knowledge of alloy performance in simulated SCWO process environments, the most promising class of alloys are the nickel-base alloys containing high weight percentages of chromium and molybdenum.

Over the previous decade, an extensive amount of data has been collected on the corrosion performance of nickel-base alloys in simulated SCWO process environments, and the database for this class of alloy is more extensive than for others. Chemical conditions in virtually all of these simulated SCWO process environments were moderately to highly oxidizing. Hence, feed stream solutions generally contained significant amounts of dissolved oxygen. A majority of these studies were carried out using chlorinated acidic feed streams over high subcritical and supercritical temperature ranges, however several studies have dealt with non-chlorinated feeds, particularly aqueous solutions containing sulfuric acid (H_2SO_4).

The earlier research into the corrosion behavior of potential SCWO constructional materials indicated a level of susceptibility that was unacceptably high for most of the candidate nickel-base alloys. This earlier work also shed light on localized phenomena, including the selective dissolution of certain elemental components as well as SCC. The earliest studies conducted by Bramlette, et al., tested the corrosion performance of various nickel base alloys, including Alloy 625 and C-276 during the destruction of DOE surrogate wastes at Sandia National Laboratory in 1990 [40]. These experiments revealed dealloying in the nickel-base alloys, with preferential dissolution of chromium and molybdenum. The subsequent studies conducted by Barner, *et al.*, in 1992 focused primarily on the high nickel, high chromium alloys, as well as titanium for lower temperatures [58]. Barner, *et al.*, reported high levels of corrosion for alloys 625, C-276, 556, C22, C276, MC-3, and G-30. At lower temperatures, titanium was found to exhibit reasonable performance. Downey, et al., reported unacceptable levels of corrosion for nickel alloys C-22, C-276, 625, 825 and HR-160 when tested in both chlorinated and non-chlorinated acidic chemical agent simulant feed solutions [59]. Latanision, et al., reported general corrosion and localized attack, including pitting and SCC for both Alloy 625 and C-276 in a workshop on SCWO systems held at MIT in 1993 [60]. Rice, *et al.*, conducted experiments in 1993 investigating the destruction of Navy wastes using SCWO technology [41]. Although these experiments were not specifically designed for investigating corrosion behavior, the effluent analysis shed light on the specific problem of selective dissolution of alloying elements. The effluent analysis conducted during these experiments suggested selective dissolution of chromium for non-chlorinated feed solutions, and selective dissolution of the base element, nickel, for chlorinated feeds. In 1995-1996 Mitton, *et al.* reported similar results from a failure analysis of C-276 preheater heat exchanger coils that were part of a bench-scale SCWO system designed for experimentation with the kinetics of methylene chloride (CH_2Cl_2) oxidation and hydrolysis [37, 38, 39]. The preheater tube failure occurred by SCC, and the analysis of the

failure site revealed severe depletion of nickel, which occurred as a result of exposure to the acidic chlorinated feed. The fluid temperature where the cracking and the most severe corrosion occurred was estimated to be high, yet subcritical. The details of these investigations are discussed in Section 3.9.

By 1995, a very significant pattern of SCWO corrosion performance started to emerge: The presence of the most severe corrosion in regions at high subcritical temperatures up to a level near the critical point, with a significant decrease in corrosion above the critical point at supercritical temperatures up to approximately 600°C. Important findings were presented at the first International Workshop on SCWO, held in 1995: Hong, et al., reported the following: The overall rate of general corrosion was determined to be on the order of 4500 mils per year, for nickel-base alloys in chlorinated acidic environments [61]. This same researcher also presented data indicating that alloys 625, C-22, and 686 exhibit a temperature dependent pattern of corrosion resistance, where the general corrosion rate decreases in the supercritical regime between 400 and 600°C, with a significant increase above 600°C. However, this same study indicated that within the same supercritical temperature range, the corrosion rate of alloy C-276 increased with increasing temperature. The 1995 experiments of Boukis, *et al.* were carried out using the pressure tube experimental concept described previously: Pressure tube test specimens were constructed from alloys 625, 686, C-276, Nicrofer 5923 and 6025, and alloy 214 and exposed to chlorinated acidic feed streams. General corrosion along with SCC and pitting was found to occur in locations where the fluid temperature was near the critical point: in the preheater and cooling sections of the test tubes. In the supercritical regime, general corrosion was much slower and localized effects were not as pronounced [62]. In a separate study, this same researcher reported transgranular SCC for high chloride concentrations (18000 ppm), and without the addition of oxygen, exclusively within the subcritical temperature zone (300°C) after exposure for only 46 hours. Only general corrosion was observed in the subcritical zone for chloride concentrations of 1800 ppm, without the addition of oxygen [52]. Hong, et al., reported both transgranular and intergranular SCC of alloy 625 at subcritical temperatures. However, no cracking was observed at supercritical temperatures [63]. Later studies have also identified the most pronounced corrosion within the high subcritical temperature regime. The 1998 experiments of Kritzer, et al., several of which dealt specifically with the corrosion behavior of alloy 625 in chlorinated acidic solutions, confirmed this pattern: Pitting and general corrosion were severe at moderate to high subcritical temperatures and only slight intergranular attack was observed in the supercritical region [22, 23]. Additionally, it has been observed that the upper temperature limit for severe corrosion depends on the pressure, due to the impact of pressure on the density of the solution in the vicinity of and above the critical point, where higher pressures and densities favor more extensive corrosion [21, 22, 64]. Thus, at higher pressures the upper temperature limit for severe corrosion is shifted to slightly higher values, and corrosion in the supercritical regime can be more extensive, because higher pressures result in higher densities, and correspondingly higher concentrations of aggressive species.

Notwithstanding the large quantity of data pointing to the most severe corrosion occurring in regions at high subcritical temperatures, there have been numerous observations of moderate corrosion in regions at supercritical temperatures: At the first workshop on SCWO systems held at MIT in 1993 cracking was reported at supercritical temperatures after extended exposure times [60]. Early studies have reported observations of SCC and pitting of alloy 625 exposed to a

mixed methylene chloride (CH_2Cl_2) / isopropyl alcohol feed solution neutralized with NaOH after extended exposure to supercritical conditions (300 hours at 580°C) [60]. Moreover, early research carried out by Norby in 1993 suggested no apparent pattern in the temperature dependent location of localized corrosion for alloy 625 [65]. Mitton, *et al.* reported the following in 1999: When exposed to a highly chlorinated acidic feed at a supercritical temperature of 600°C for a short duration of 66.2 hours, alloy HR-160 (30% Co) exhibited reasonable performance based on weight loss measurements. However, severe grain boundary corrosion was observed in regions where the surface oxide layer was locally disrupted [66]. Research conducted by Konys, *et al.* in 1999 focused on the corrosion performance of alloys 625, 686, 602CA, 214, and G-30 in feed solutions containing a one-to-one mixture of methylene chloride (CH_2Cl_2) simulated organic waste and hydrogen peroxide (H_2O_2) oxidant [67]. These experiments were conducted at only one supercritical temperature and pressure: 420°C and 400 bar. Subcritical conditions were not addressed. Even under these supercritical conditions, only alloy G-30 exhibited successful corrosion resistance.

The investigations into the corrosion performance of nickel-base alloys in simulated SCWO process environments seem to indicate that none of these alloys will be capable of withstanding the most aggressive SCWO feed streams over all temperature ranges. In general, the results indicate localized corrosion over high subcritical temperature ranges, and general corrosion for both high subcritical and, to an extent, supercritical temperature ranges, particularly for temperatures in excess of 600°C. The preponderance of evidence seems to indicate that the most severe corrosion occurs in locations where temperatures are high but subcritical. These observations seem to apply overwhelmingly to localized effects such as pitting, dealloying, and SCC. However, SCC has also been observed in supercritical regions, for extended exposure times. The most significant general corrosion is likewise observed primarily in high temperature subcritical regions. At this point, it is appropriate to emphasize that significant corrosion, both localized and non-localized, can and will occur in the supercritical regions of the process stream, although for a given pressure, the regions exposed to high subcritical temperatures appear to susceptible to most severe corrosion.

For localized corrosion phenomena, such as pitting and SCC, the primary cause seems to be feed streams containing high chloride concentrations. Chlorinated feeds may also give rise to the selective dissolution of the base element, nickel, as discussed previously. Significant weight loss is the result of dealloying and/or general corrosion. A decrease in the tube wall thickness is almost exclusively a result of general corrosion, however general corrosion is observed when the selective dissolution of large weight-percentages of susceptible component elements in a dealloyed layer can lead to subsequent removal of the remaining "skeletal" dealloyed layer by mechanical forces, particularly erosion. SCC and pitting are highly localized effects that do not give rise to significant mass loss or decrease in wall thickness because they do not involve the dissolution of large quantities of metal. Dealloying, which is discussed in a previous section, is the selective dissolution of elemental components. Therefore, the dissolution of significant quantities of nickel for chlorinated feed streams or possibly chromium for non-chlorinated feed streams will contribute to the measured weight loss. However dealloying alone may not impact tube wall thickness measurements if the dealloyed layer remains mechanically intact. For metals and alloys under a state of passivity under highly oxidizing conditions, general corrosion is often caused by non-localized breakdown of the passive oxidized surface layers at high subcritical and

supercritical temperatures. Kritzer, *et al.* has proposed that "transpassive dissolution" of passive oxidized films at high subcritical and supercritical temperatures may account for this [22, 48, 49]. The details of these studies will be covered in the next section.

The most extensive SCWO related corrosion studies in high-temperature, high-pressure aqueous environments containing hydrochloric acid (HCl) and dissolved oxygen (O_2) have been performed on alloys 625 and C-276. Alloys 625 and C-276 have been the most thoroughly investigated reactor materials for SCWO, due their well-known resistance to common corrosive environments. In recent years Kritzer, *et al.* has carried out detailed studies of the corrosion behavior of alloy 625. Mitton, *et al.* has focused much attention on Alloy C-276.

3.9 Corrosion Performance of Alloy C-276 (Mitton, *et al.*)

The studies of Hastelloy C-276 corrosion in simulated SCWO process environments by Mitton, *et al.* were prompted by the failure of preheater tubing in an experimental SCWO system, based on a plug-flow reactor design concept. Three preheater tubes failed prematurely over the course of a series of experiments performed in this plug-flow reactor (PFR) SCWO system that was designed for methylene chloride (CH_2Cl_2) hydrolysis and oxidation experiments in subcritical and supercritical water. The original objective of these experiments was to study the kinetics of CH_2Cl_2 decomposition under these oxidative and nonoxidative hydrolysis conditions, and did not pertain to the study of corrosion. However, a detailed analysis of these preheater tube failures provided valuable information pertaining to the susceptibility of SCWO heat exchanger components to localized effects, particularly SCC. Mitton, *et al.*, carried out the in-depth failure analysis of the preheater tubing in 1996 at MIT, and the results of this failure analysis are summarized herein [42, 43].

Reference [1] gives a schematic of the experimental plug-flow reactor. The coiled preheater tubing and main reactor of the experimental apparatus were heated in a fluidized sand bath. The sand bath temperature was varied between 450°C and 600°C, depending on the experiment. Two separate preheater coils were employed in the system; one for a pressurized aqueous feed solution of CH_2Cl_2, and another for a pressurized O_2 and deionized water solution. Each preheater coil had a length of approximately 300 cm, with 275 cm of that length submerged in the sand bath. The preheater tubing had an inner diameter of 0.108 cm and a wall thickness of 0.025 cm, and was constructed from welded, drawn, solution-annealed Hastelloy C-276. Both of the feed solutions entered their respective preheater coils at ambient temperature. The solutions were then heated to a specified operating temperature in the preheater, and were then mixed and fed to the main reactor. Therefore the fluid temperature varied along the length of the preheater coil between ambient temperature and the supercritical temperature of the main reactor, which had a value close to the sand bath temperature. Hydrolysis conditions existed in the CH_2Cl_2 feed preheater coil for all experiments carried out using this system. The decomposition of CH_2Cl_2, by either hydrolysis or oxidation reactions proceeded to completion in the main reactor at temperatures that were always supercritical and maintained within a few degrees of the sand bath temperature. The aqueous solution containing the hydrolysis/oxidation reaction products coming from the main reactor, heretofore referred to as the effluent, was brought back to room

temperature in a cool-down heat exchanger, and collected for subsequent chemical analysis. Ambient CH_2Cl_2 feed concentrations at the entrance to the preheater tubing ranged from 0.006 M to 0.038 M. After accounting for subcritical hydrolysis in the preheater, the effects of decreasing fluid density with increasing fluid temperature, and dilution, CH_2Cl_2 concentrations, where fluid entered the main reactor from the preheater, were calculated to range from 0.0002 to 0.0006 M. The residence times of the fluid inside the preheater tubing were calculated to be 7 to 17 seconds. All experiments were performed at an operating pressure of 246 bar.

The three preheater coils that failed prematurely over the course of the hydrolysis and oxidation experiments were all CH_2Cl_2 feed preheater coils. None of the coils carrying the dissolved O_2 and deionized water solution failed. For each of the failed CH_2Cl_2 feed preheater coils, severe corrosion, resulting in through-wall failure, was observed. In each of the three cases, the failure occurred in a region between 7 and 29 cm downstream of the point at which the tubing entered the sand bath. The operating life of the tubes until failure ranged from 45 hours to 104 hours of use at the operating temperatures, as set by the sand bath temperature. The pH of the effluent collected from the cool-down heat exchanger, when measured at ambient temperature, ranged between 1.5 and 2.5. These pH levels were a result of the formation of HCl from the hydrolysis of CH_2Cl_2. The ambient HCl concentrations in the effluent ranged from 4 to 25 mM. Therefore, the three failed preheater coils contained acidic chlorinated aqueous feed solutions at high subcritical temperatures in the vicinity of the failure site, under hydrolysis conditions.

Each of the CH_2Cl_2 feed preheater tubes failed by developing an intergranular crack (Figure 2). In the vicinity of the failure site, an elemental analysis of the inner diameter of the tube wall exhibited significant dealloying of Ni, Fe, and Mo, leaving the dealloyed layer rich in chromium. Based on the operating lives of the tubes until failure, a minimum crack propagation rate of 21.4 to 39.8 mm/year was estimated. This crack propagation rate is well within the normal range for SCC. While failure did not occur in the cool down heat exchanger, some crack development was observed within the first 20 mm of the length of the heat exchanger, where the temperature was high but subcritical. The elemental analysis of the inner wall of the tube at this location again revealed dealloying of Ni, Fe, and Mo, as well as chromium enrichment, as was observed in the case of the preheater failure sites. There was no significant corrosion at the preheater inlet, which was at ambient temperature. Furthermore, the preheater exit (going to the main reactor) and the inlet to the cool-down heat exchanger (coming from the main reactor), both of which were exposed to high HCl concentrations, due to the extent of the hydrolysis and/or oxidation reaction(s), displayed little damage and low corrosion rates. At both of these locations, temperatures were supercritical. These observations all corroborate with numerous accounts of the most severe corrosion occurring in SCWO heat exchangers in locations at high subcritical temperatures, with damage in locations/components at supercritical temperatures being of a more limited nature.

The preheater tubing exhibited cracking only in locations where it also exhibited dealloying. This was an important observation, in light of the studies conducted by Kelly, *et al.*, which established a strong link between dealloying and SCC for some systems based on electrochemical impedance studies [68]. These studies proposed a dealloyed film-induced cleavage model of SCC. Elemental analysis of the inner diameter of the tube wall in the region of the failure site revealed selective dissolution of nickel, iron, and molybdenum, and enrichment

of chromium. In this model, a crack originates in a dealloyed surface layer, and reaches a crack-tip velocity sufficient to be injected into the underlying metal, which has not yet undergone dealloying. Therefore, the selective dissolution of nickel is likely to have contributed to the cracking.

Mitton, *et al.*, has carried out additional research in the form of instrumented tube experiments in order to provide a more controlled assessment of alloy C-276 corrosion [42, 43, 44, 69]. The results of these experiments seem to indicate that, for alloy C-276, exposed to chlorinated feeds, the dealloying and SCC phenomena are closely linked. Figure 3-3 shows the extent of degradation, for both dealloying and SCC, as a function of temperature. These experiments clearly confirm that cracking occurs in regions which experience significant dealloying at high subcritical temperatures: The depth of cracking and dealloying generally tracked one another as a function of temperature over the entire high subcritical temperature regime. As the temperature in the cooling tube test specimen approached the critical point, the cracking and dealloying phenomena became well established. This graph clearly demonstrates that serious degradation did not occur either in the supercritical regime or in the subcritical regime, for temperatures less than approximately 310°C. These results are in agreement with the conclusions reached from the failure analysis of the C-276 preheater tubing.

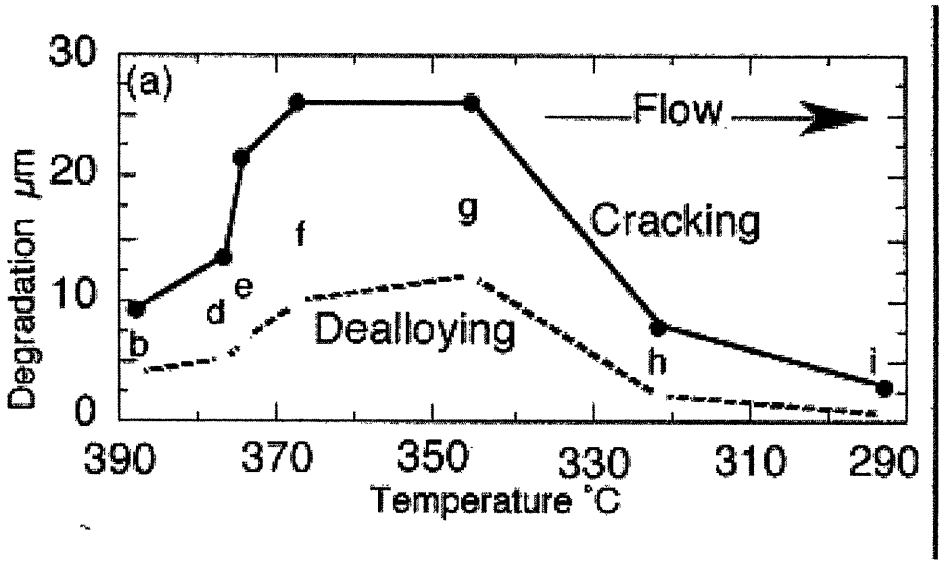

Figure 3-3: Results from the instrumented C-276 cooling tube experiments conducted by Mitton, et al. Depths of cracking and dealloyed layer are plotted as a function of temperature. From Mitton, *et al.* (2001), Reference [42].

The following conclusions may be drawn from the studies of alloy C-276. Clearly, the regions of the process stream that are exposed to high subcritical temperatures experience the most severe corrosion, in the form of dealloying and correspondingly high susceptibility to failure by SCC. However, significant corrosion also occurs at supercritical conditions. Moreover, the severity of corrosion in the supercritical state should be expected to increase with higher supercritical pressures. This is a direct implication of the isothermal compressibility of supercritical water, whereby increases in the supercritical pressure at constant temperature result in correspondingly higher fluid densities, and correspondingly higher ionic dissociation constants, resulting in higher concentrations of attacking species. Another important observation was that the most heavily dealloyed regions of the process tubing experienced the greatest susceptibility to cracking, to an extent that the depth of the dealloyed region and the crack penetration depth tracked one another.

3.10 Corrosion Performance of Alloy 625 (Kritzer, *et al.*)

Kritzer, *et al.*, has carried out extensive investigations into the corrosion behavior of alloy 625 in high-temperature, high-pressure oxygenated HCl solutions and sulfuric acid (H_2SO_4) solutions. These experiments were designed to examine the overall corrosion behavior of alloy 625 as a function of solution temperature. A review of corrosion phenomena for alloy 625 in the context of SCWO systems can best be presented through a review of these investigations.

Kritzer, *et al*, carried out an in-depth study of the corrosion behavior of Alloy 625 pressure tube specimens under SCWO conditions. An acidic oxidizing environment was achieved through the use of solutions containing O_2, HCl, sodium chloride (NaCl), and sodium hydroxide (NaOH). The latter two species were used as a means of controlling pH. Intergranular corrosion (IGC), pitting, and general corrosion were observed. Several conditions resulted in transgranular stress corrosion cracking (TGSCC). The severity of all types of corrosion decreased significantly as the fluid temperature passed above the critical temperature of water. Because overall variation in tube pressure was under 8%, the variation in the severity of overall corrosion was viewed primarily as resulting from the increasing temperature of the fluid along the length of the tube test section.

Thus, temperature-dependent corrosion phenomena for Alloy 625 in acidic oxygenated HCl solutions are classified into the four categories, each one covering a specific temperature regime: Below approximately 130°C, only slight intergranular corrosion (IGC) was observed. From ~130° to 250°C Cl^--induced pitting was observed along with slight IGC. In this regime, the pits were relatively deep (maximum depths between 270 μm and 1300 μm) with a hemispherical shape. The pits were located in an otherwise unattacked surface. Corrosion products inside the pits were enriched in Cr and Mo. When temperatures exceeded 240°C to 340°C (depending on experimental conditions: higher pH values shifted the temperature onset of these phenomena to lower levels) the corrosion morphology changed significantly, from one characterized by a large density of deep pits located on an otherwise unattacked surface, to one characterized by

"shallow" pits covering 100% of the surface - the shallow pits essentially intruded upon one another in such a manner that penetration occurred over the entire surface, with the depth of penetration reaching a maximum at the bottom of the aforementioned "shallow" pits. This was indicative of a more "general" corrosion morphology, where the surface was attacked at all locations.

The results, overall, seem to indicate that for temperatures below the critical point, the severity of the general corrosion, in comparison to localized effects, increases with increasing temperature. That is to say, at subcritical temperatures below approximately 250°C corrosion seems to be limited to a localized pitting morphology and general corrosion is not significant. However above 250-300°C the corrosion morphology is no longer exclusively local, and general corrosion is observed through measurements of decrease in wall thickness and mass loss in these high subcritical regions, although localized effects are still significant, as numerous studies have shown. Above the critical point, pitting and general corrosion levels are far less severe for supercritical temperature below approximately 600°C. Above this temperature, significant general corrosion has been observed.

A crucial issue in this research is the temperature-dependent transition from a localized corrosion morphology, characterized by relatively deep pits dispersed on an otherwise unattacked surface, to a generalized corrosion morphology, characterized by "shallow pits", which cover 100% of the surface. This transition is rationalized by the so-called "transpassive dissolution" of solid chromium(III) compounds to form soluble chromium(VI) species, known as "hexavalent chromium". This occurs according to the following generalized reaction scheme for transpassive dissolution:

$$\text{solid chromium(III)} \rightarrow \text{aqueous chromium(VI)}$$

Solid Cr(III) compounds are known to provide passive protection of stainless alloys under normal conditions, and it is the existence of such compounds that make high chromium stainless alloys the materials of choice for a variety of applications requiring acceptable resistance to corrosion in aggressive environments. However, the behavior of these compounds in aggressive environments at hydrothermal conditions is not well understood. Numerous researchers have maintained that alloys high in chromium are necessary for adequate corrosion control in SCWO process environments. Yet, it is well known that such alloys are highly dependent on chromium(III) compounds for passive protection. If Cr(III) compounds are susceptible to transpassive dissolution to form soluble hexavalent chromium in highly oxidizing solutions under hydrothermal conditions, then it is likely that alloys high in Cr may not be appropriate constructional materials for certain sections of the SCWO process unit.

The "transpassive dissolution" phenomenon is likely to be a major concern for stainless alloys. However, there is not yet sufficient data to prove that this is the specific phenomenon responsible for the observed general corrosion of alloy 625 at near-critical temperatures. Furthermore, it is highly unlikely that this behavior can be "generalized" for all stainless alloys. Kritzer, *et al.* contends that as the temperature of the solution increases, for some concentration of oxidizer and acidic pH, the transpassive potential of the Cr(III) drops in the high subcritical regime, whereas the actual oxidizing potential of the solution rises, due to increasing O_2 solubility as a function of

increasing temperature. This transpassive potential is determined by the upper oxidation potential limit of the stability field for the solid Cr(III) compound. Therefore, at some temperature, designated as the "inversion temperature", the oxidizing potential of the solution is equal to the transpassive potential of the solid Cr(III) compound. At higher subcritical temperatures (e.g. > ~300°C) the transpassive potential falls below the solution's oxidizing potential, and Cr(III) compounds break down in a transpassive state to form soluble Cr(VI) species, or hexavalent chromium. This concept is illustrated in Figure 3-4. Kritzer has maintained that this type of behavior can be generalized to other nickel-based alloys and stainless steels. However, given the unpredictability of alloy corrosion behavior in hydrothermal aqueous mediums, this is certainly not the case. Clearly, adequate resolution of this issue requires substantial research devoted to the thermodynamics (E-pH diagrams) and active-passive corrosion behavior of Cr in aqueous systems, under hydrothermal conditions, as well as additional exposure studies of Cr and Cr-containing stainless alloys at specific measurable oxidation potentials.

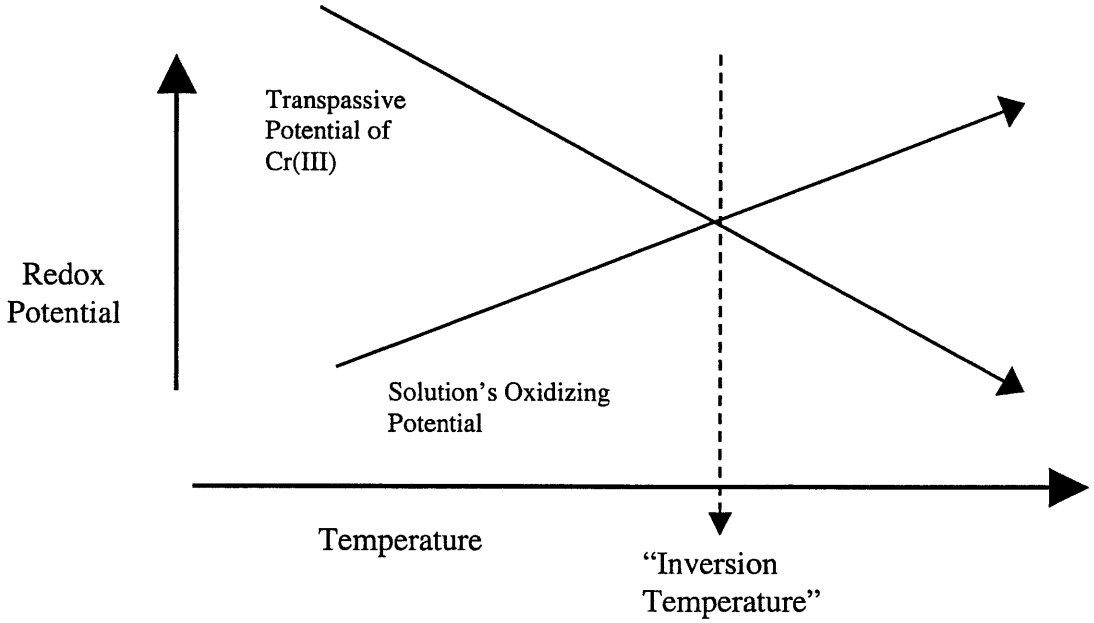

Figure 3-4: Schematic of the concept of the inversion temperature, where the solution's oxidizing potential is equal to the transpassive potential of the solid Cr(III) compounds, which provide passive protection for stainless alloys. Kritzer contends that the inversion temperature is the temperature at which the corrosion morphology transitions from one characterized by localized pitting to general corrosion, and that this temperature-dependent morphology transition is therefore attributed to the "transpassive breakdown" of solid Cr(III) compounds to form soluble hexavalent Cr ionic species.

3.11 Passive Protection of High Chromium Alloys by Solid Chromium(III) Compounds - Recent Developments

In recent years, research efforts in the area of materials performance have been more focused on the effects of chromium (Cr) on corrosion behavior in SCWO environments. In 1999, Konys, *et al.* [56] reported that alloy G-30, containing 30% Cr, exhibited reasonable performance for supercritical solutions of HCl. However, as previously mentioned, these studies only addressed one supercritical temperature and pressure (420°C and 400 bar). Additional experimentation that year by these same researchers compared the corrosion performance of alloy G-30 and Ducrolloy, a Cr-Fe alloy containing 50.2 wt.% Cr and 44 wt. % Fe, at the same temperature and pressure for the same chloride bearing solution. The alloy G-30 samples revealed limited corrosion and mass loss, whereas the Ducrolloy samples revealed virtually no mass loss under these conditions. Thus, the performance of these alloys revealed the beneficial effect of Cr for these supercritical conditions. Evidently, at this temperature and pressure, Cr formed a Cr_2O_3 oxide layer that remained stable under these conditions. This Cr_2O_3 layer was said to be responsible for passive protection of the Ducrolloy sample from significant mass loss. Furthermore, this oxide layer was effective in preventing dealloying of Fe for the Ducrolloy samples. It was concluded that the high weight percentages of Cr in Ducrolloy were responsible for its comparatively good corrosion resistance due to the formation of this Cr_2O_3 oxide. This study also revealed the beneficial effects of preoxidation for the high Cr Ducrolloy. However, this same year, Wagner, *et al.* [70] conducted experiments comparing the corrosion performance of alloy 625 to that of a pure Cr specimen in an attempt ascertain the effects of Cr on corrosion performance. The data indicate that, for a chlorinated feed, at 500°C and 465 bar, Cr is detrimental to alloy performance, due to the instability of Cr(III) compounds under these specific conditions supercritical conditions. Thus, it should be noted that the studies claiming the beneficial effects of Cr were conducted at a lower supercritical temperature and pressure (420°C and 400 bar), whereas the studies claiming detrimental effects of Cr were conducted at a significantly higher supercritical temperature and pressure (500°C and 465 bar). Furthermore, the former study compared alloy G-30, a 43% Ni and 15% Fe alloy, to Ducrolloy, an alloy with 44% Fe and 0% Ni - there is no conclusive proof that higher Cr content, alone, is responsible for improved corrosion resistance at these conditions.

The latest research activities into alloy corrosion behavior under SCWO conditions, presented at the NACE 2002 conference proceedings, have gone further in addressing the effects of Cr and other alloying elements on alloy performance. Konys, *et al*, focused his recent experiments on the performance of nickel-base alloys containing high weight percentages of Cr and other alloying elements, such as Tungsten (W), in chloride-containing solutions at a pressure of 400 bar and temperatures between 110°C and 410°C [71]. Unfortunately, most of his reported data ignore the subcritical regime and again focus primarily on analyzing corrosion behavior at supercritical temperatures. This study concludes that Ni-Cr alloys with 30% Cr exhibit optimal performance at supercritical temperatures ranging from T_c to 410°C. Higher weight percentages of Cr in Ni-base alloys were reported to result in greater mass loss for reasons that were not entirely clear. The best performance over the entire range of temperatures from 110° to 410°C was exhibited by ternary Ni-base alloys containing 30% Cr and 5-10 % W. These researchers

hypothesized that tungsten (W) may play a role in reducing the degree of solubility of the solid Cr(III) compounds, CrOOH and Cr_2O_3. The recent experiments by these researchers only addressed Ni-base alloys and did not address the performance of Ducrolloy. Experiments conducted by Sue, *et al.* measured the mass loss of pure Fe, Ni, and Cr samples in supercritical water at 400°C and 250, 300, and 400 bar [72]. The Cr samples exhibited no significant mass loss over a 24-hour exposure time. These data were corroborated by model estimations of the solubility for solid Cr(III) compounds in supercritical water at these conditions. These calculations indicated that solid Cr(III) compounds exhibited a very low solubility for these conditions. Hara, *et al.* reported transpassive dissolution of solid Cr(III) compounds formed on pure Cr test specimens at high subcritical temperatures (~350°C) and supercritical temperatures in excess of 500°C [73]. However this same study indicated that increasing Cr content in both Ni-Cr and Fe-Cr alloys resulted in improved corrosion resistance.

A convincing study was presented by Watanabe, *et al.* investigating the effects of oxidizer concentration on corrosion of Ni-base and Fe-base alloys in supercritical solutions containing sulfuric acid (H_2SO_4) at 400°C and pressures of 300 bar and 600 bar [74]. This study is particularly important because it is the second study that has attempted to rationalize corrosion behavior on a thermodynamic basis, by directly computing potential-pH diagrams for Fe, Cr, and Ni at these supercritical conditions. Furthermore, this is the first study to attempt this for supercritical conditions. His data demonstrate that for these supercritical conditions and low to moderate oxygen concentrations (3ppb and 8ppm), the alloy with the highest weight percentage of chromium, MC alloy (44% Cr, Bal. Ni) exhibited the smallest overall mass loss, while the alloy with the smallest weight percentage of Cr, Alloy B-2 (0.8% Cr, 27.1% Mo, Bal. Ni) exhibited the greatest overall mass loss. Even more intriguing, at high oxygen concentrations (800ppm), iron-base alloys exhibited a dramatic decrease in mass loss, indicating the possibility of passive protection by insoluble iron oxide under highly oxidizing conditions at this temperature and pressure. Potential-pH diagrams were constructed for Cr, Ni, and Fe at a temperature of 400°C and 300 bar. These diagrams were based on thermodynamic data generated by the SUPCRT92 software, which computes thermodynamic functions based on the HKF equation of state [] for hydrothermal systems, as discussed in Section 2.4. The pH scales are applicable to the given supercritical conditions (Ref. Section 2.6), and based on calculations of H_2SO_4 dissociation in the medium at 400°C and 300 bar, the pH at these supercritical conditions is estimated to be 3.27. Therefore, based on the current state of knowledge, the diagrams should be valid for these supercritical conditions. The diagram for Cr indicates that Cr_2O_3 is stable at this temperature and pressure for low pH values and moderate oxidizing potentials. The diagram indicates that very high oxidizing potentials result in dissolution of Cr and Cr(III) compounds to form $HCrO^{4-}$. The diagram for Fe indicates the stability of Fe_2O_3 at high oxidizing potentials over large ranges of pH. The diagram for Ni only shows the stability of soluble Ni^{2+} for pH values ranging from 0-5 at moderate to high oxidizing potentials. Thus, this study concludes that Cr plays a vital role in passive protection for Ni alloys, provided that the oxidizing power of the solution allows for the thermodynamic stability of Cr(III) compounds, such as Cr_2O_3. At high oxidizing potentials, Cr(III) compounds will dissolve in a transpassive state as $HCrO^{4-}$. Such moderate oxidizing potentials require that oxygen concentration be kept under a specified limit. It also suggests the possibility of passive protection of iron base alloys, through the formation of insoluble Fe_2O_3 under highly oxidizing conditions, over significant

ranges of pH. It should be noted that this study was limited to solutions containing sulfuric acid, and therefore did not consider the effects of chlorides on corrosion behavior.

3.12 Ceramics and Ceramic Liners

Ceramic materials have traditionally been known for good resistance against common corrosive environments. Thus, ceramics have been recommended as a candidate constructional material for SCWO systems. This has prompted a limited amount of research into the corrosion behavior of ceramic materials and ceramic coatings on metal substrates in simulated SCWO process environments. In acidic aqueous solutions containing dissolved oxygen and chlorides, non-oxide ceramics were quickly dissolved or disintegrated due to a transformation into the corresponding oxides. However, alumina (Al_2O_3) and zirconia (ZrO_2) based materials were found to be resistant under limited conditions: Boukis, *et al.*, performed corrosion screening tests on various high-performance oxide and non-oxide ceramics in supercritical water containing oxygen and hydrochloric acid (HCl) [62]. His results indicated that only several oxide ceramics, Al_2O_3 and ZrO_2, demonstrated reasonable performance in acidic chlorinated supercritical water. Discoloration was observed for certain Al_2O_3 samples and weight loss was negligible for all Al_2O_3 and ZrO_2 samples. Disintegration of ceramics B_4C, TiB_2, Y_2O_3 and Y-TZP and severe weight loss, often in excess of 90%, for SiC and Si_3N_4-based ceramics was observed under these same environmental conditions. M. Schacht, *et al*, subsequently examined, in detail, the corrosion behavior of alumina ceramics in acidic aqueous solutions at high temperatures and pressures [76]. His data indicated that alumina ceramics exhibited a high solubility at subcritical temperatures of 240–290°C in sulfuric acid. In HCl solutions, dissolution of grains was observed. Additional research pertaining to the corrosion behavior of ceramics and ceramic coatings can be found in references [77 and 78].

3.13 Summary

In general, studies of corrosion performance have not been able to successfully identify corrosion resistant materials for SCWO feeds. This is indicative of the extremely harsh oxidizing conditions present in SCWO process streams. Hence, these studies should be viewed as contributions to the materials performance database for SCWO process environments; these studies should not be viewed as attempts to "discover" a corrosion resistant material. Indeed, the thermodynamics of metals in aqueous systems under hydrothermal conditions, discussed in Chapter 2, precludes the existence of a universally corrosion resistant alloy for SCWO processes: Conditions are far too oxidizing for metallic immunity to remain a possibility, even if feed stream pH is controlled through the addition of neutralizing agents. Virtually all materials will undergo some aspect of corrosion given sufficient exposure time. Hence, the mitigation of corrosion in SCWO systems remains an enormous challenge, and this challenge will not be adequately met by proper selection of materials, without regard to conditions in the process environment.

References – Chapter 3

1. J.W. Tester, J.A. Cline, Corrosion 99, Paper No. 252, NACE, Houston, TX (1999).
2. J.W. Tester, J.A. Cline, "Hydrolysis and Oxidation in Subcritical and Supercritical Water: Connecting Process Engineering Science to Molecular Interactions," Corrosion, 55 (11) (1999), p. 1088.
3. P.A. Webley, J.W. Tester, H.R. Holgate, "Oxidation Kinetics of Ammonia and Ammonia-Methanol Mixtures in Supercritical Water in the Temperature Range 530°C to 700°C at 246 bar," Ind. Eng. Chem. Res., 30 (8) (1991), p. 1745.
4. J.A. Cline, "Experimental and *Ab* Initio Investigations into the Fundamentals of Corrosion, in the Context of Supercritical Water Oxidation Systems," PhD thesis in Chemical Engineering, Massachusetts Institute of Technology, Cambridge, MA, (2000).
5. R.M. Latanision, D.B. Mitton, S-H Zhang, J.A. Cline, M.S. Quintana, N. Caputy, "Corrosion Mechanisms in Supercritical Water Oxidation Systems for Hazardous Water Disposal," *Proceeding 1997 Tri-Service Conference on Corrosion*, Wrightsville Beach, NC, (1997) (Naval Surface Warfare Center: Office of Naval Research, 1997).
6. D.B. Mitton, S-H Zhang, M.S. Quintana, J.A. Cline, N. Caputy, P.A. Marrone, R.M. Latanision, "Corrosion Mitigation in SCWO Systems for Hazardous Waste Disposal," Corrosion 98, Paper No. 414, NACE, Houston, TX (1998).
7. P. Kritzer, N. Boukis, E. Dinjus, "Corrosion of Alloy 625 in Aqueous Solutions Containing Chloride and Oxygen," Corrosion, 54 (10) (1998), p. 824.
8. P. Kritzer, N. Boukis, E. Dinjus, "Corrosion of Alloy 625 in High-Temperature, High-Pressure Sulfate Solutions," Corrosion, 54 (9) (1998), p. 689.
9. P. Kritzer, N. Boukis, E. Dinjus," "The corrosion of alloy 625 (NiCr22Mo9Nb; 2.4856) in high-temperature, high-pressure aqueous solutions of phosphoric acid and oxygen. Corrosion at subcritical and supercritical temperatures," Mater. Corros., 49 (1998), p. 831.
10. V. Casal, H. Schmidt, "SUWOX—a facility for the destruction of chlorinated hydrocarbons," Journal of Supercritical Fluids, 13 (1998), pp. 269–276.
11. J. Konys, S. Fodi, J. Hausselt, H. Schmidt, V. Casal, "Corrosion of High-Temperature Alloys in Chloride-Containing Supercritical Water Oxidation Systems," Corrosion, 55 (1) (1999), p. 45.
12. P. Kritzer, N. Boukis, E. Dinjus, "Transpassive Dissolution of Alloy 625, Chromium, Nickel, and Molybdenum in High-Temperature Solutions Containing Hydrochloric Acid and Oxygen," Corrosion, 56 (3) (2000), p. 265.
13. N. Boukis, P. Kritzer, M. Schacht, E. Dinjus, "The Initiation of Material Corrosion in Semicritical and Supercritical Aqueous Hydrochloric Acid Solutions," Corrosion 99, Paper No. 256, NACE, Houston, TX (1999).
14. W.F. Bogaerts, A.A, Van Haute, M.J. Brabers, "Relative Critical Potentials for Pitting Corrosion of 304 Stainless Steel, Incoloy 800 and Inconel 600 in Alkaline High-Temperature Aqueous Solutions," J. Nucl Mater., 115 (1983), pp. 339-342.
15. D.A. Jones, *Principles and Prevention of Corrosion*, 2nd Edition, Prentice Hall, Upper Saddle River, NJ, 1996.
16. M.G. Fontana, *Corrosion Engineering*, 3rd Edition, McGraw-Hill, New York, 1986.
17. H.H. Strehblow, "Breakdown of Passivity and Localized Corrosion: Theoretical Concepts and Fundamental Experimental Results," Mater. Corros., 35 (1984), pp. 437-448.

18. G. Cragnolino, "A Review of Pitting Corrosion in High-Temperature Aqueous Solutions," in: H. Isaacs (Ed.), *Advances in Localized Corrosion, International Corrosion Conference Series*, NACE, Houston, TX (1990), pp. 413-431.
19. B. Baroux, "Further Insights on the Pitting Corrosion of Stainless Steels," in: P. Marcus, J. Oudar (Eds.), *Corrosion Mechanisms in Theory and Practice*, Marcel Dekker, New York (1995), pp. 265-309.
20. L.B. Kriksunov and D.D. Macdonald, "Corrosion in Supercritical Water Oxidation Systems: A Phenomenological Analysis," J. Electrochem. Soc., 142 (12) (1995), p. 4069.
21. P. Kritzer, N. Boukis, E. Dinjus, "Factors Controlling Corrosion in High-Temperature Aqueous Solutions: A Contribution to the dissociation and Solubility Data Influencing Corrosion Processes," Journal of Supercritical Fluids, 15 (1999), pp. 205-227.
22. P. Kritzer, N. Boukis, E. Dinjus, "Corrosion of Alloy 625 in Aqueous Chloride and Oxygen Containing Solutions," Corrosion, 54 (10) (1998), p. 824.
23. N. Boukis, P. Kritzer, "Corrosion Phenomena on Alloy 625 in Aqueous Solutions Containing Hydrochloric Acid and Oxygen," Corrosion 97, Paper No. 10, NACE, Houston, TX (1997).
24. T. Fujii, "Electrochemical Study on the Corrosion Behavior of Metals and Alloys in Aqueous Solutions at High Temperatures and Pressures," Trans. Nat. Res. Inst. Met., 18 (1976), p. 101.
25. W.F. Bogaerts, A.A. Van Haute, M.J. Brabers, "Pitting Behaviour of Austenitic Stainless Steels at Elevated Temperatures," *International Congress on Metallic Corrosion* 7, Rio de Janeiro, Brasil (1978), p. 526.
26. P.E. Manning. D.J. Duquette, "The Effect of Temperature (25°–289°C) on Pit Initiation in Single Phase and Duplex 304L Stainless Steels in 100 ppm Cl^- Solution," Corrosion Science, 20 (1980), p. 597.
27. J. Hickling, N. Wieling, "Electrochemical Investigations of the Resistance of Inconel 600, Incoloy 800, and Type 347 Stainless Steel to Pitting Corrosion in Faulted PWR Secondary Water at 150°C to 250°C," Corrosion, 37 (1) (1981), p. 147.
28. M. Karaminezhaad-Ranjbar, J. Mankowski, D.D. Macdonald, "Pitting Corrosion of Inconel 600 in High-Temperature Chloride Solution Under Controlled Hydrodynamic Conditions," Corrosion, 41 (2) (1985), p. 197.
29. J.R. Park, Z. Szklarska-Smialowska, "Pitting Corrosion of Inconel 600 in Aqueous Chloride Solutions at 60 to 280°C," *Proceedings of the 2nd International Symposium on Environmental Degradation of Materials in Nuclear Power Systems – Water Reactors*, Monterey, CA (1985), p. 456.
30. J.R. Park, Z. Szklarska-Smialowska, "Pitting Corrosion of Inconel 600 in High-Temperature Water Containing $CuCl_2$," Corrosion, 41 (1985), p. 665.
31. W.F. Bogaerts, C. Bettendorf, "Electrochemistry and Corrosion of Alloys in High-Temperature Water," EPRI-Report NP-4705, Electric Power Research Institute, Palo Alto, CA, (1986).
32. A.M. Olmedo, M. Villegas, M.G. Alvarez, "Corrosion Behaviour of Alloy 800 in High-Temperature Aqueous Solutions: Electrochemical Studies," J. Nucl. Mater., 229 (1996), p.102.
33. P. Kritzer, "The Corrosion of Alloy 625 Under Hydrothermal Conditions," FZKA 6168, Forschungszentrum Karlsruhe GmbH, Karlsruhe, Germany (1998).
34. P. Kritzer, N. Boukis, E. Dinjus, "The Corrosion of Nickel-Base Alloy 625 in Oxidizing Sub- and Supercritical Aqueous Solutions of HNO_3," J. Mater. Sci. Lett., (1999).

35. P. Kritzer, N. Boukis, E. Dinjus, "Investigations of the Corrosion of Reactor Materials During the Process of SCWO," *Proceeding of the 6th Meeting on Supercritical Fluids*, Nottingham, UK (1999), p. 433.
36. J.F. Hall, A.S. O'Neill, "Pitting of Alloy 600 Steam Generator Tubes Under Heat Transfer Conditions," *Proceeding of the 3rd International Symposium on Environmental Degradation of Materials in Nuclear Power Systems – Water Reactors*, Traverse City, MI (1987), p. 437.
37. D.B. Mitton, P.A. Marrone, and R.M. Latanision, "Interpretation of the Rationale for Feed Modification in SCWO Systems," J. Electrochem. Soc., 143 (3) (1996), p. L59.
38. R.M. Latanision, D.B. Mitton, S-H Zhang, J.A. Cline, N. Caputy, T.A. Arias, A. Rigos, "Corrosion and Corrosion Mechanisms in Supercritical Water Oxidation Systems for Hazardous Waste Disposal," *Proceedings of the 4th International Symposium on Supercritical Fluids*, Sendai, Japan Vol. C (1997), p. 865.
39. D.B. Mitton, S-H Zhang, M.S. Quintana, J.A. Cline, N. Caputy, P.A. Marrone, R.M. Latanision, "Corrosion Mitigation in SCWO Systems for Hazardous Waste Disposal," Corrosion 98, Paper No. 414, NACE, Houston, TX (1998).
40. T.T. Bramlette, *et al.*, "Destruction of DOE/DP Surrogate Wastes with Supercritical Water Oxidation Technology," (Report SAND90-8229, Sandia National Laboratories, 1990).
41. S.F. Rice, R.R. Steeper, C.A. LaJeunesse, "Destruction of Representative Navy Wastes Using Supercritical Water Oxidation," (Report SAND 94-8203 UC-402, Sandia National Laboratories, 1993).
42. R.M. Latanision, D.B. Mitton, N. Eliaz, "Stress Corrosion Cracking in Supercritical Water Oxidation Systems for Waste Destruction," *Chemistry and Electrochemistry of Stress Corrosion Cracking: A Symposium Honoring the Contributions of R.W. Staehle*, ed. R.H. Jones, TMS (2001), p. 597.
43. D.B. Mitton, S-H Zhang, K.E. Hautanen, J.A. Cline, E-H Han, R.M. Latanision, "Evaluating Stress Corrosion and Corrosion Aspects in Supercritical Water Oxidation Systems for the Destruction of Hazardous Waste," Corrosion 97, Paper No. 203, NACE, Houston, TX (1997).
44. R.M. Latanision, D.B. Mitton, "Stress Corrosion Cracking in Supercritical Water Systems" (Publisher Unknown – Source obtained with permission from and through private communication with the authors.)
45. R.E. Reed-Hill, R. Abbaschian, *Physical Metallurgy Principles*, 3rd Edition, PWS Publishing Company, Boston, MA, 1994.
46. F.A. McClintock, A.S. Argon, *Mechanical Behavior of Materials*, Addison-Wesley Publishing Company, 1999.
47. D. Broek, *Elementary Engineering Fracture Mechanics*, Martinus Nijhoff Publishers, The Hague, The Netherlands, 1984.
48. P. Kritzer, N. Boukis, E. Dinjus, "Review of the Corrosion of Nickel-Based Alloys and Stainless Steels in Strongly Oxidizing Pressurized High-Temperature Solutions at Subcritical and Supercritical Temperatures," Corrosion, 56 (11) (2000), p. 1093.
49. P. Kritzer, N. Boukis, E. Dinjus, "Transpassive Dissolution of Alloy 625, Chromium, Nickel, and Molybdenum in High-Temperature Solutions Containing Hydrochloric Acid and Oxygen," Corrosion, 56 (3) (2000), p. 265.
50. A.J. Thomas E.F. Gloyna, "Corrosion Behavior of High Grade Alloys in the Supercritical Water Oxidation of Sludges," University of Texas at Austin Technical Report CRWR 229 (1991).

51. S. Tebbal, R.D. Kane, Corrosion 98, Paper No. 413, NACE, Houston, TX (1998).
52. N. Boukis, R. Landvatter, W. Habicht, G. Franz, *First International Workshop on Supercritical Water Oxidation*, Jacksonville, Florida, Feb. (1995).
53. D.B. Mitton, J.C. Orzalli, R.M. Latanision, *12th ICPWS*, Begell House, New York, NY (1995), p. 638.
54. D.B. Mitton, S-H Zhang, E-H Han, K.E. Hautanen, R.M. Latanision, *Proc. 13th ICC*, Melbourne, Australia (1996).
55. D.B. Mitton, Y.S. Kim, J.H. Yoon, S. Take, R.M. Latanision, Corrosion 99, Paper No. 257, NACE, Houston, TX (1999).
56. J. Konys, S. Fodi, A. Ruck, J. Hausselt, Corrosion 99, Paper No. 253, NACE, Houston, TX (1999).
57. D.B. Mitton, J-H Yoon, R.M. Latanision, "An Overview of Corrosion Phenomena in SCWO Systems for Hazardous Waste Destruction," Corrosion Engineering (Korean Journal), 49 (3) (2000), p. 130.
58. H.E. Barner, C.Y. Huang, T. Johnson, G. Jacobs, M.A. Martch, W.R. Killilea, "Supercritical Water Oxidation: An emerging technology," Journal of Hazardous Materials, 31 (1992), p. 1.
59. K.W. Downey, R.H. Snow, D.A. Hazelbeck, A.J. Roberts, *Innovations in Supercritical Fluids, Science and Technology*, ACS Symposium Series, 608, ACS, Washington, DC (1995), p. 313.
60. R.M. Latanision, R.W. Shaw, Co-Chairs, *Corrosion in Supercritical Water Oxidation Systems*, Summary of a Workshop Held at MIT May 6-7, 1993 Report No. MIT-EL 93-006, (1993).
61. G.T. Hong, D.W. Ordway, V.A. Ziberstein, "Materials Testing in Supercritical Water Oxidation Systems," *1st Int. Workshop on Supercritical Water Oxidation*, Jacksonville, Florida (1995).
62. N. Boukis, G. Franz, C. Friedrich, W. Habicht, K. Ebert, "Corrosion Screening Tests With Ni-Base Alloys in Supercritical Water Containing Hydrochloric Acid and Oxygen," *Proceedings of the ASME Heat Transfer Division*, Heat Transfer Division (Am. Soc. Mech. Eng.), Vol. 335-4 (1996), p. 159.
63. G.T. Hong, D.W. Ordway, V.A. Ziberstein, Corrosion 95, Paper No. 558, NACE, Houston, TX (1995).
64. P. Kritzer, N. Boukis, E. Dinjus, "The corrosion of alloy 625 (NiCr22Mo9Nb; 2.4856) in high-temperature, high-pressure aqueous solutions of phosphoric acid and oxygen. Corrosion at subcritical and supercritical temperatures," Mater. Corros., 49 (1998), p. 831.
65. B.C. Norby, "Supercritical Water Oxidation Benchscale Testing Metallurgical Analysis Report," Idaho National Engineering Laboratory Report, EGG-WTD-10675 (1993).
66. D.B. Mitton, Y.S. Kim, J.H. Yoon, S. Take, R.M. Latanision, "Corrosion of SCWO Constructional Materials in Chloride-Containing Environments," Corrosion 99, Paper No. 257, NACE, Houston, TX (1999).
67. J. Konys, S. Fodi, J. Hausselt, H. Schmidt, V. Casal, "Corrosion of High-Temperature Alloys in Chloride-Containing Supercritical Water Oxidation Systems," Corrosion, 55 (1) (1999), p. 45.
68. J.R. Scully, D.C. Silverman, M.W. Kendig, eds., ASTM STP 1188 (West Conshohocken, PA: ASTM, 1993), p. 94.

69. R.M. Latanision, D.B. Mitton, S-H Zhang, J.A. Cline, M.S. Quintana, N. Caputy, "Corrosion Mechanisms in Supercritical Water Oxidation Systems for Hazardous Water Disposal," *Proceedings 1997 Tri-Service Conference on Corrosion*, Wrightsville Beach, NC, (1997) (Naval Surface Warfare Center: Office of Naval Research, 1997).
70. M. Wagner, *et al*, Corrosion 99, Paper 255, NACE, Houston, TX (1999).
71. J. Konys, C. Schroer, *et al*, "Corrosion Investigation on Binary and Ternary Ni-Cr Alloys in SCWO Systems," Corrosion 2002, Paper 02359, NACE, Houston, TX (2002).
72. K. Sue, *et al*, "Relationship Between Corrosion Rate and Metal Oxide Solubility in Supercritical Water," Corrosion 2002, Paper 02354, NACE, Houston, TX (2002).
73. N. Hara, *et al*, "Corrosion Resistance of Fe-Cr and Ni-Cr Alloys in Oxidizing Supercritical HCl Solution," Corrosion 2002, Paper 02358, NACE, Houston, TX (2002).
74. Y. Watanabe, K. Shoji, T. Adschiri, K. Sue, "Effects of Oxygen Concnetration on Corrosion Behavior of Alloys in Acidic Supercritical Water," Corrosion 2002, Paper 02355, NACE, Houston, TX (2002).
75. H. Yakuwa, *et al*, "Effect of Cr and Mo Contents on the Corrosion Properties of Ni-Base Alloys in the Supercritical Water Including Chloride," Corrosion 2002, Paper 02361, NACE, Houston, TX (2002).
76. M. Schacht, N. Boukis, E. Dinjus, "Corrosion of Alumina Ceramics in Acidic Aqueous Solutions at High Temperatures and Pressures," Journal of Materials Science, 35 (2000), p. 6251.
77. K. Garcia, R. Mizia, "Corrosion Investigation in Supercritical Water Oxidation Process Environments," *Proceedings of the ASME Heat Transfer Dividison*, Heat Transfer Division (Am. Soc. Mech. Eng.), Vol. 317-2 (1995), p. 299.
78. M. Drews, M. Williams, M. Barr, "The Corrosion of Sol-Gel Coated Type 316 SS in Chlorinated SC Water," Ind. Eng. Chem. Res., 39 (2000), p. 4772.
79. D.B. Mitton, N. Eliaz, J.A. Cline, R.M. Latanision, "Assessing Degradation Mechanisms in Supercritical Water Oxidation Systmes," Corrosion 2001, Paper 01352, NACE, Houston, TX (2001).
80. D.B. Mitton, H. Kim, J. Zhang, N. Eliaz, C.R. Sydnor, R.M. Latanision, "An Examination of the Corrosion Phenomena of Potential Constructional Materials for SCWO System Fabrication," Corrosion 2002, Paper 02353, NACE, Houston, TX (2002).
81. R.M. Latanision, "Corrosion Science, Corrosion Engineering, and Advanced Technologies," Corrosion, 51 (4) (1995), p. 270.
82. D.B. Mitton, J.C. Orzalli, R.M. Latanision, "Corrosion Studies in Supercritical Water Oxidation Systems," *The Supercritical Fluid Science and Technology Symposium at the AIChE Annual Meeting*, San Francisco, CA (1994).
83. J.C. Orzalli, "Preliminary Corrosion Studies of Candidate Materials for Supercritical Water Oxidation Reactor Systems," (S.M. thesis, MIT, Cambridge, MA, 1994).

Chapter 4

Discussion

4.1 Supercritical Water Oxidation

Supercritical Water Oxidation (SCWO) is a promising technology for destroying hazardous organic wastes. SCWO systems provide high destruction efficiencies for organics within short residence times. In the United States potential targets for destruction by SCWO include rocket fuels, explosives, organics present in low-level liquid radioactive wastes, and chemical warfare agents.

SCWO technology is capable of providing rapid and complete oxidation of hydrocarbons by capitalizing on the properties of water above its critical point. The critical point for pure water is 374°C and 221 bar. As the critical point is approached, key physical properties including density and dielectric constant, change drastically, correlating directly with drastic changes in solvation properties: Accordingly, low-density supercritical water acts as a non-polar dense gas with solvation properties approaching those of a low-polarity organic. Thus, as a solvent, supercritical water exhibits high solubilities for non-polar organic compounds and non-condensable gases. Conversely, inorganic solubility decreases rapidly with temperature, as the critical point is approached. Therefore supercritical water is an ideal medium for spontaneous and fast oxidation of most organic compounds. The products of the SCWO reaction are primarily H_2O and CO_2. However, heteroatoms present in hydrocarbons will give rise to the formation of acids and inorganic salts. The formation of acids under highly oxidizing conditions at high temperatures and pressures will result in severe corrosion of the process unit.

4.2 Corrosion Mitigation in SCWO Systems

Corrosion may ultimately be the most important factor in determining whether SCWO technology can be successfully implemented for industrial and government applications. The consensus of the first International Workshop on Corrosion in SCWO Systems held at MIT in 1993 was that the existence of a constructional material capable of withstanding the most aggressive feeds and applicable to all sections of a SCWO system, under all conceivable conditions was extremely unlikely. Today that consensus still holds. Hence, effective corrosion mitigation in SCWO systems will likely require an eclectic approach, utilizing advanced materials combined with advanced methodologies. Currently, the SCWO database for nickel-

base alloys is the most extensive, and while success with these alloys has been extremely limited, it is likely that no other class of commercially available alloys will come closer to exhibiting reasonable corrosion behavior in simulated SCWO feed streams. Moreover, it is most likely that the proper choice of constructional materials alone will not provide sufficient protection from corrosion – Methodologies for precise control of environmental conditions in SCWO process streams will almost certainly be required. Additional alternatives for corrosion mitigation may include corrosion resistant liners and coatings, as well as alternative reactor designs. For this reason, the corrosion behavior of ceramic materials in simulated SCWO feeds has been addressed.

Corrosion control in SCWO environments is gained only through the existence of stable passive oxidized films. Alloys contain several metallic elements, and thus, if the alloy is maintained in a state of passivity by the environmental conditions, the solid compounds making up the passive layer are likely to be composed of one metallic oxide/hydroxide. This is likely to be the case for many of the stainless alloys, which have been investigated for corrosion performance in simulated SCWO environments. The composite potential-pH diagram for Ni, Fe, Cr, and Mo at 300°C, constructed by Mitton, *et al.*, in 1996 (Figure 2-3), depicts a region of thermodynamic stability for insoluble CrOOH and soluble Ni, Fe and Mo. Within this shaded region, thermodynamic conditions favor the active corrosion of Ni, Fe, and Mo, and the insoluble CrOOH surface layer provides the only means of passive protection for alloys composed of these elements. These thermodynamic arguments explain the preferential dissolution of Ni, Fe, and Mo at low pH values under oxidizing conditions. This data corroborates with the results presented by Kritzer, *et al.*, for alloy 625 exposed to chlorinated acidic feeds, demonstrating selective dissolution of Ni at low pH values, with minimal dissolution of Cr and Mo (Chapter 3). Thus, the preferential protection of certain alloying elements by the insoluble compounds containing these elements is most likely related to dealloying in simulated SCWO feeds. It is likely that if aggressive SCWO feed streams are not neutralized, most commercially available alloys, including Ni-based alloys, will not demonstrate acceptable corrosion resistance over the long term. Thus, it is likely that feed stream modification will be necessary combined with proper selection of advanced alloys for specific temperature regimes.

It is likely that a unique SCWO system/process design may be required for each class of organic compounds. Such a design would incorporate particular constructional material(s) and unique control of environmental parameters (e.g. pH, redox potential, and halide concentration). Such unique designs would be required due to the existence of different heteroatoms in each class of organic compounds – In particular, consideration must be given to halogenated hydrocarbons versus non-halogenated hydrocarbons. The SCWO of halogenated hydrocarbons may require a design that allows for more direct control of feed chemistry and incorporates particular classes of alloys or corrosion resistant liners: In many of the halogenated hydrocarbons, heteroatoms such as Cl, will react to form chroride (Cl^-) anions. For non-halogenated hydrocarbons, S and P heteroatoms will oxidize to form sulfates (SO_4^{2-}) and phosphates (PO_4^{3-}), respectively. If a system and/or process is designed to withstand feeds containing sulfates and/or phosphates, it is certain that this identical system/process will not be capable of accommodating chlorinated feeds, as chlorides are known to attack passive oxidized films in preferred locations. For this reason the majority of SCWO research has been focused on solutions containing chlorides. Conversely, a design optimized for the processing of chloride-containing solutions may not be

able to withstand oxidizing solutions containing sulfuric acid. Overall, the design of SCWO processes, with respect to corrosion mitigation, will require that the effects of aggressive species arising from the oxidation of each class of organic compound on the process unit be considered independently.

It has been demonstrated, by numerous researchers, through studies of the corrosion performance of various alloys in simulated feeds, that the regions of the process stream where constructional alloys are most susceptible to corrosion experience temperatures that are high, yet subcritical. At temperatures above the critical point overall degradation is not nearly as extensive when compared with regions experiencing high subcritical temperatures. Nevertheless, regions of the process stream experiencing exclusively supercritical temperatures (e.g. the main reactor) are still highly susceptible. Furthermore, it is possible that materials, which demonstrate more successful resistance to corrosion at high subcritical temperatures, may prove to be less successful at supercritical temperatures. Thus, it is likely that materials of construction for the heat exchanger(s) and the main reactor will differ, because these respective components experience primarily high subcritical and supercritical temperatures.

4.3 Recommendations / Future Work

It is imperative that future research carried out with the goal of mitigating and controlling corrosion phenomena in SCWO process environments should include, but should not be limited, to the following:

- There is a need for potential-pH diagrams at elevated temperatures and pressures, extending well into the supercritical regime. The thermodynamic database for subcritical temperatures less than 300°C is fairly extensive, although there is still a need for potential-pH diagrams specifically addressing alloy-water systems, and the possibility of passive protection through the formation of binary metallic oxides. The thermodynamic database for temperatures in excess of 300°C is severely limited, and the need for potential-pH diagrams for metals and alloys in aqueous systems at near-critical and supercritical temperatures and pressures is substantial.

- Recently, there has been a significant amount of research devoted to the construction of stability diagrams for metals and alloys in the presence of realistically modeled aqueous solutions [1]. Such "real-solution" thermodynamic models could consider the effects of anionic species, and can be generalized to include the effects of various other active species. These real-solution stability models expand on the work of Helgeson *et al*, and combine the HKF equation of state [2, 3, 4], which has been successfully applied to regular subcritical and hydrothermal systems, with a solution non-ideality model. These comprehensive "real-solution" models would be extremely useful in determining the thermodynamic conditions for corrosion, especially given the susceptibility of construction materials to localized attack by chlorides. Traditional potential-pH diagrams, even those based upon the HKF equation of state, do not take into consideration the localized degradation of passive films by chlorides.

- There is still a very significant need for electrochemical polarization studies of candidate metals and alloys over the entire spectrum of SCWO temperatures and pressures for a range of pH values and chloride concentrations. These polarization studies are required to provide a controlled assessment of active-passive behavior for elemental metal and alloys. Only then will it be possible to determine the extent to which certain alloying elements are capable of providing passive protection for various pH, temperature, and pressure conditions.

- In order to implement effective methodologies for precise control of environmental conditions in SCWO process streams, such that critical environmental parameters can be "fine tuned" in such a way to effectively control corrosion, it will be absolutely necessary to have reliable techniques for monitoring and measuring pH and redox potential over the entire SCWO temperature spectrum. This requires significant research dedicated to the development of pH scales and pH standards for hydrothermal aqueous systems and establishing reliable calibration functions correlating dissolved gas concentrations with overall redox potential for subcritical, near-critical, and supercritical conditions.

- Subsequent exposure studies seeking to assess the corrosion behavior of metals and alloys in hydrothermal systems should, in general, have a well defined strategy for controlling "degrees of freedom" in such a way that the phenomena exhibited by candidate alloys can be more readily explained by fundamental physicochemical and/or electrochemical processes, both thermodynamic and kinetic. Such "degrees of freedom" would include temperature, pressure, dissolved gas concentrations, redox potential, alloy composition, alloy phase stability, trace elements, pH, anion concentration, fluid dynamics within the process stream, etc, etc. Tight control over these variables, through intelligent experimental design, will naturally lead to materials and methodologies that could substantially reduce environmental degradation in SCWO systems. Corrosion in SCWO systems will never be "eliminated", but it can be successfully mitigated.

References – Chapter 4

1. A. Anderko, S.J. Sanders, R.D. Young, "Real-Solution Stability Diagrams: A Thermodynamic Tool for Modeling Corrosion in Wide Temperature and Concentration Ranges," Corrosion, 53 (1) (1997), p. 43.
2. H.C. Helgeson, K.D.H. Kirkham, G.C. Flowers, American Journal of Science, 281 (1981), p.1249
3. J.W. Johnson, E.H. Oelkers, H.C. Helgeson, Computers and Geosciences, 18 (1992), p. 899.
4. E.L. Shock, H.C. Helgeson, Geochem. Cosmochim Acta, 52 (1988), p. 2009.